CONTRACT NO. N00014-70-C-0095 AND MOD. NO. P.001
REPORT NO. GDCA-DDB 71-001

FILM BOILING HEAT TRANSFER AND DRAG REDUCTION

GENERAL DYNAMICS
Convair Aerospace Division

87

Unclassified

Security Classification

DOCUMENT CONTROL DATA - R&D

(Security classification of title, body of abstract and indexing annotation must be entered when the overall report is classified)

1. ORIGINATING ACTIVITY (Corporate author)	2a. REPORT SECURITY CLASSIFICATION
General Dynamics, Convair Aerospace Division San Diego, California	Unclassified
	2b GROUP

3. REPORT TITLE

Film Boiling Heat Transfer and Drag Reduction

4. DESCRIPTIVE NOTES (Type of report and inclusive dates)

Final Report

5. AUTHOR(S) (Last name, first name, initial)

Gay, Archibald

6. REPORT DATE	7a. TOTAL NO. OF PAGES	7b. NO. OF REFS
April 1971	67	12

8a. CONTRACT OR GRANT NO.	9a. ORIGINATOR'S REPORT NUMBER(S)
N00014-70-0095 & MOD. P001 b. PROJECT NO. NR 097-380/8-15-69 (473) c. d.	GDCA DDB 71-001 9b. OTHER REPORT NO(S) (Any other numbers that may be assigned this report)

10. AVAILABILITY/LIMITATION NOTICES

Qualified requesters may obtain copies of this report from DDC.

11. SUPPLEMENTARY NOTES	12. SPONSORING MILITARY ACTIVITY
	ONR, Washington, D. C.

13. ABSTRACT

Preparations were made for turbulent film boiling tests of a heated flat plate model in the California Institute of Technology high speed water tunnel. The model and most of the support instrumentation has been assembled. The model dimensions are 24.0 inches long x 4.730 inches span x 1.5 inches deep. The high heat flux anticipated to maintain film boiling with forced convection is produced by cartridge heaters embedded in the copper body of the model. The heater power controllers are designed to provide independent control of the heater banks in six chordwise zones. The controllers are of the Triac Thyristor type with a total power capability of 0-150 Kw. Design and fabrication of the major components for the tunnel installation, such as model hydrofoil shields and an adapter for force balance connection has been completed at the California Institute of Technology. (U)

Approximate analyses of the two-phase forced-convection boundary layer flow was carried out for both laminar and turbulent flows. The analyses indicate considerable skin friction drag reduction in both flow regimes. This reduction is typically around 90 percent for water flow around a surface heated to 1000 - 2000° F. (U)

DD FORM 1 JAN 64 1473

Unclassified

Security Classification

14. KEY WORDS	LINK A		LINK B		LINK C	
	ROLE	WT	ROLE	WT	ROLE	WT
Two-Phase Forced-Convection Boundary Layer Flow						
Film Boiling Forced-Convection Boundary - Layer Flow						

INSTRUCTIONS

1. ORIGINATING ACTIVITY: Enter the name and address of the contractor, subcontractor, grantee, Department of Defense activity or other organization *(corporate author)* issuing the report.

2a. REPORT SECURITY CLASSIFICATION: Enter the overall security classification of the report. Indicate whether "Restricted Data" is included. Marking is to be in accordance with appropriate security regulations.

2b. GROUP: Automatic downgrading is specified in DoD Directive 5200.10 and Armed Forces Industrial Manual. Enter the group number. Also, when applicable, show that optional markings have been used for Group 3 and Group 4 as authorized.

3. REPORT TITLE: Enter the complete report title in all capital letters. Titles in all cases should be unclassified. If a meaningful title cannot be selected without classification, show title classification in all capitals in parenthesis immediately following the title.

4. DESCRIPTIVE NOTES: If appropriate, enter the type of report, e.g., interim, progress, summary, annual, or final. Give the inclusive dates when a specific reporting period is covered.

5. AUTHOR(S): Enter the name(s) of author(s) as shown on or in the report. Enter last name, first name, middle initial. If military, show rank and branch of service. The name of the principal author is an absolute minimum requirement.

6. REPORT DATE: Enter the date of the report as day, month, year; or month, year. If more than one date appears on the report, use date of publication.

7a. TOTAL NUMBER OF PAGES: The total page count should follow normal pagination procedures, i.e., enter the number of pages containing information.

7b. NUMBER OF REFERENCES: Enter the total number of references cited in the report.

8a. CONTRACT OR GRANT NUMBER: If appropriate, enter the applicable number of the contract or grant under which the report was written.

8b, 8c, & 8d. PROJECT NUMBER: Enter the appropriate military department identification, such as project number, subproject number, system numbers, task number, etc.

9a. ORIGINATOR'S REPORT NUMBER(S): Enter the official report number by which the document will be identified and controlled by the originating activity. This number must be unique to this report.

9b. OTHER REPORT NUMBER(S): If the report has been assigned any other report numbers *(either by the originator or by the sponsor)*, also enter this number(s).

10. AVAILABILITY/LIMITATION NOTICES: Enter any limitations on further dissemination of the report, other than those imposed by security classification, using standard statements such as:

(1) "Qualified requesters may obtain copies of this report from DDC."

(2) "Foreign announcement and dissemination of this report by DDC is not authorized."

(3) "U. S. Government agencies may obtain copies of this report directly from DDC. Other qualified DDC users shall request through _____."

(4) "U. S. military agencies may obtain copies of this report directly from DDC. Other qualified users shall request through _____."

(5) "All distribution of this report is controlled. Qualified DDC users shall request through _____."

If the report has been furnished to the Office of Technical Services, Department of Commerce, for sale to the public, indicate this fact and enter the price, if known.

11. SUPPLEMENTARY NOTES: Use for additional explanatory notes.

12. SPONSORING MILITARY ACTIVITY: Enter the name of the departmental project office or laboratory sponsoring *(paying for)* the research and development. Include address.

13. ABSTRACT: Enter an abstract giving a brief and factual summary of the document indicative of the report, even though it may also appear elsewhere in the body of the technical report. If additional space is required, a continuation sheet shall be attached.

It is highly desirable that the abstract of classified reports be unclassified. Each paragraph of the abstract shall end with an indication of the military security classification of the information in the paragraph, represented as *(TS), (S), (C), or (U)*.

There is no limitation on the length of the abstract. However, the suggested length is from 150 to 225 words.

14. KEY WORDS: Key words are technically meaningful terms or short phrases that characterize a report and may be used as index entries for cataloging the report. Key words must be selected so that no security classification is required. Identifiers, such as equipment model designation, trade name, military project code name, geographic location, may be used as key words but will be followed by an indication of technical context. The assignment of links, rules, and weights is optional.

GDCA-DDB 71-001

GENERAL DYNAMICS
Convair Aerospace Division

April 1971

FILM BOILING HEAT TRANSFER

AND

DRAG REDUCTION

Contract No. N00014-70-C-0095 and Mod. No. P.001

Prepared by: A. Gay
A. Gay

Approved by: S. A. Campbell
S. A. Campbell

TABLE OF CONTENTS

LIST OF FIGURES

LIST OF FIGURES (Continued)

LIST OF SYMBOLS

C_f local friction coefficient

C_{f_o} local friction coefficient with unheated plate

C_p specific heat at constant pressure; without subscript refers to vapor layer

h local heat transfer coefficient $q_w/(T_w-T_i)$

k thermal conductivity; without subscript refers to vapor

Nu Nusselt number, hx/k

Pr Prandtl number, $C_p\mu/k$

q local heat flux

Re_x Reynolds number based on stream properties

T static temperature

T_ℓ^* liquid layer reference temperature $T_\ell^* = \dfrac{T_i + T_s}{2}$

T_v^* vapor layer reference temperature $T_v^* = \dfrac{T_w + T_i}{2}$

u velocity in x-direction

u_e exhaust velocity of jet

x distance along plate from leading edge

y coordinate measuring distance normal to plate

Greek

β_o superheat parameter, $C_p(T_w-T_i)/\lambda$

$\beta_{o\ell}$ subcooling parameter, $C_{p_L}(T_i-T_s)/\lambda$

δ overall velocity boundary layer thickness

δ_L	liquid velocity boundary layer thickness
δ_v	vapor velocity boundary layer thickness
λ	latent heat of vaporization
μ	viscosity; without subscript refers to vapor
ρ	density; without subscript refers to vapor
τ	shear stress

Subscripts

i	conditions at interface
L	liquid properties, for u_L see Figure 3.1
ℓ	liquid properties, for u_ℓ see Figure 3.1
s	conditions outside boundary layer ("stream" conditions)
v	vapor layer
w	conditions at heated wall

1. INTRODUCTION

Skin friction is the predominant drag force with which bodies moving through dense fluids must contend. A promising technique for significantly reducing drag is the use of polymer additives to the fluid. Minute quantities of these additives have domonstrated large reductions of fluid friction. [1, 2] Polymeric addition is apparently only effective in the turbulent regime where drag may be reduced by as much as 50 to 70%. [2] An alternative method of drag reduction which is considered here, using film boiling, may be effective in both the laminar and turbulent flow regimes.

Forced-convection film boiling is established when the temperature of the heating surface is sufficiently high relative to the liquid temperature that a stable vapor layer exists between the heating surface and the moving liquid. Stable films have been observed experimentally in the laminar flow regime for hydrodynamically shaped bodies [3] and spheres [4] at surface temperatures above about 1000°F. It would appear that in such a situation, the vapor would serve as a lubricating sheet, reducing drag, as well as an insulating blanket.

Forced-convection film boiling has been studied in regard to heat transfer problems at low velocities, e.g. Bromley et al [5] considered flow in a horizontal cylinder. Bradfield et al [3, 6, 7], in analytical and experimental boundary layer studies indicated that very large skin friction coefficient reductions were possible (greater than 90%) through surface film boiling in laminar water flows. Results of theoretical analysis of the two-phase forced-convection laminar boundary layer flow problem by Cess and Sparrow [8, 9] also indicated large skin friction drag reductions.

The present study was initiated to extend the knowledge of film boiling flows into a higher speed regime by obtaining experimental skin friction and heat transfer data into the turbulent flow regime, using a flat plate type of model. Experiments were planned to be conducted in the

California Institute of Technology (CIT) high speed water tunnel. The experimental program has not yet been started. Major problems were encountered in developing a suitable model assembly, with a high surface heat flux capability, sound electrical insulation properties and the desirable power output control in the chordwise (flow) direction.

This report describes the model, instrumentation, and CIT water tunnel support equipment designed and fabricated at this time. In addition, the approximate laminar boundary layer theory of Reference 7 has been modified and extended to now apply to general liquid-vapor flow and gives good agreement to the flat plate Blasius-type analysis of Reference 9. Further, an analysis was performed on a turbulent boundary layer system assuming a modified form of the empirical Blasius equation. Although no experimental data are available to confirm the assumption the analysis is believed to give reasonable estimates under certain flow conditions and indicates an approach which can be adjusted when experimental data are available.

The analyses indicate that very large drag reductions may be obtained in both the laminar and turbulent flow regimes. In order to examine the utility of application of this potential drag reduction a coefficient of performance is examined for the water-steam case which accounts for the heat energy input required to maintain the film layer.

2. MODEL DESIGN AND INSTALLATION

The basic concept proposed for an experimental model is shown in Figures 2.1 and 2.2. The model upper and lower surfaces are flat plates and the model sides are enclosed by a hydrofoil. The model is connected via a shielded strut to a force balance. The surrounding hydrofoil is not connected to the force balance, but to the tunnel walls directly and it extends across the tunnel diameter. Heating of the model to the high temperatures required for film boiling was proposed by electrical heating with Kanthal heater strips or ribbon as illustrated schematically in Detail A-A of Figure 2.2. The approximate dimensions desirable for the model was estimated at 24 inch length, 4 inch span and minimum practical depth.

The present model design is fairly similar in principle to that proposed, except that the Kanthal heating strip concept had to be replaced with a system of cartridge heaters, and the dimensions were changed to suit the cartridge heater design.

2.1 Heaters

A total power input of 150 Kw was considered desirable for the film boiling experiments, with the power controllable in six zones, chordwise, to maintain control of the surface temperature under anticipated operating conditions. This allowed a nominal maximum total surface heat flux (for both upper and lower surfaces) of 780 watts/in.^{2} This value is close to the heat flux at the burn-out point for nucleate boiling in water at one atmosphere (e.g. see Reference 11). Figure 2.3 shows the estimated power requirements versus flow velocity with film boiling in water at one atmosphere and a wall temperature of 1000°F, for various distances from the leading edge of a flat plate. The results from the analysis of Cess and Sparrow, Reference 9, were used to obtain Figure 2.3. This applies, of course, only to laminar flow, but no similar analysis was available for turbulent flow. The power requirements vary also with ambient pressure, decreasing with decreasing

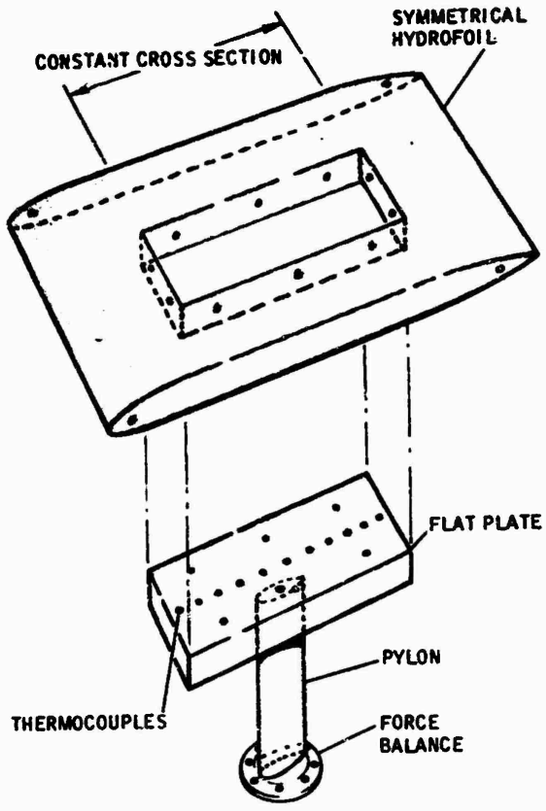

Figure 2.1. Flat-Plate Model

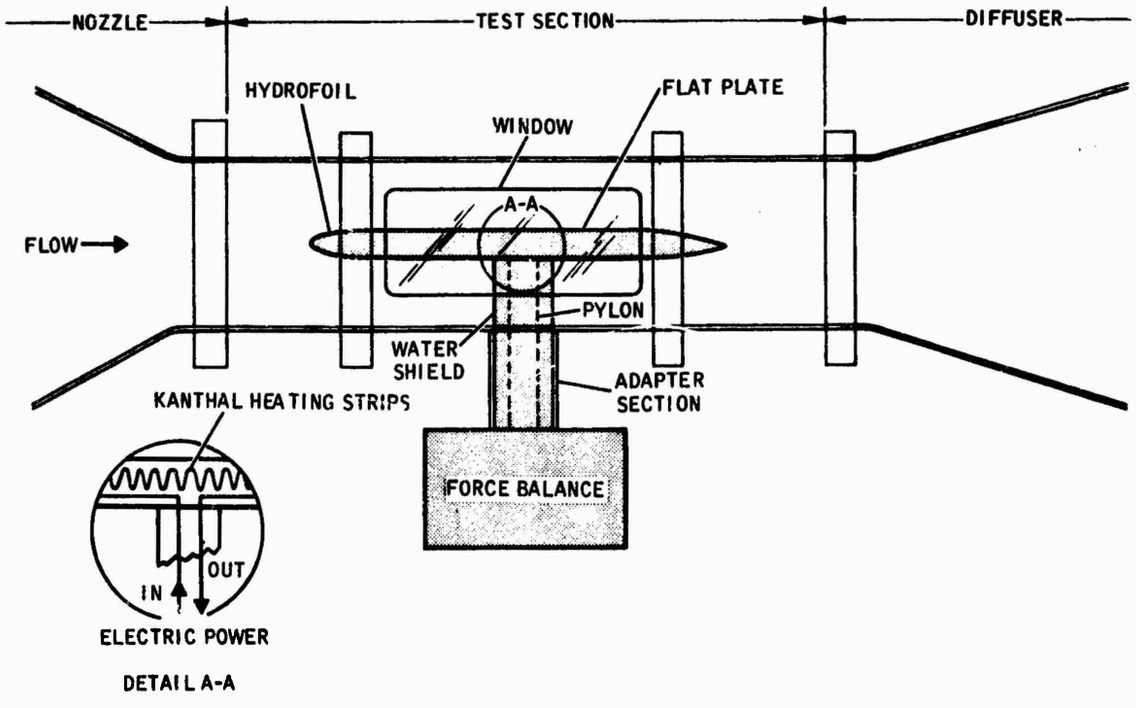

Figure 2.2. Experimental Arrangement

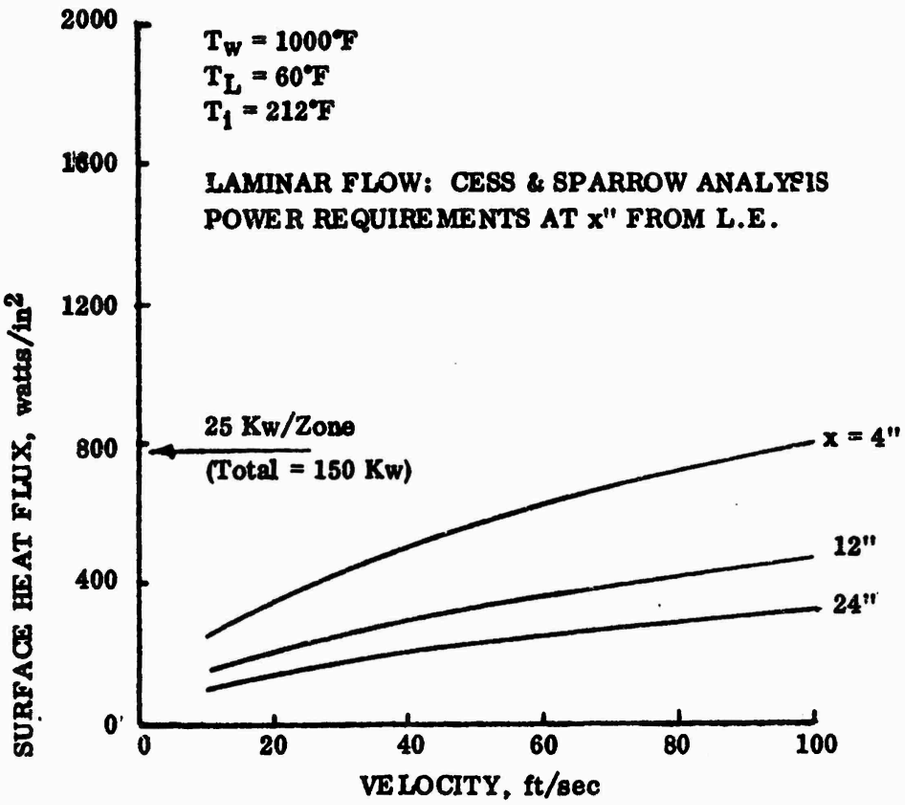

Figure 2.3. Surface Heat Flux Versus Velocity: Laminar Flow Film Boiling

pressure. The CIT water tunnel can be operated over a range from vapor pressure to three atmospheres.

2.1.1 Strip Heater Design

Design parameters were generated for the strip heater concept. This concept was abandoned, as stated previously, but some typical data are shown to illustrate the considerations for this type of heating. Figures 2.4 and 2.5 show the geometric parameters calculated for one strip heater coil (for one of six controllable chordwise zones) under the following conditions:

Chordwise length: 4 inches

Width of Coil: 4 inches

Resistivity of Kanthal Al = 0.0006777 ohm x in^2 x $ft.^{-1}$

E = 230 V.

Consideration was also given to temperature gradients within the model. The copper between heater coils was relatively thin with respect to the length of the conduction path to the cooled surface and hence an approximate analysis was performed. One dimensional heat flux as shown in Figure 2.4 was analyzed as for a thin fin. Constant heat flux from the strip heater surface was assumed. Referring to Figure 2.4, heat through fin section

$$\text{at } y = -kA \frac{\partial T}{\partial y}$$

$$\text{at } y + dy = \left(-k \frac{\delta T}{\delta y} - k \frac{\delta^2 T}{\delta y^2} dy - \ldots\ldots\right)A$$

$$\text{net gain from } y \text{ to } y + dy = kA \frac{\partial^2 T}{\partial y^2} dy$$

$$\text{from heater surface, } \Delta Q = \text{const. } dy = C_1 dy$$

Taking the assumptions stated and no heat flow across the centerline (due to symmetry) the solution is

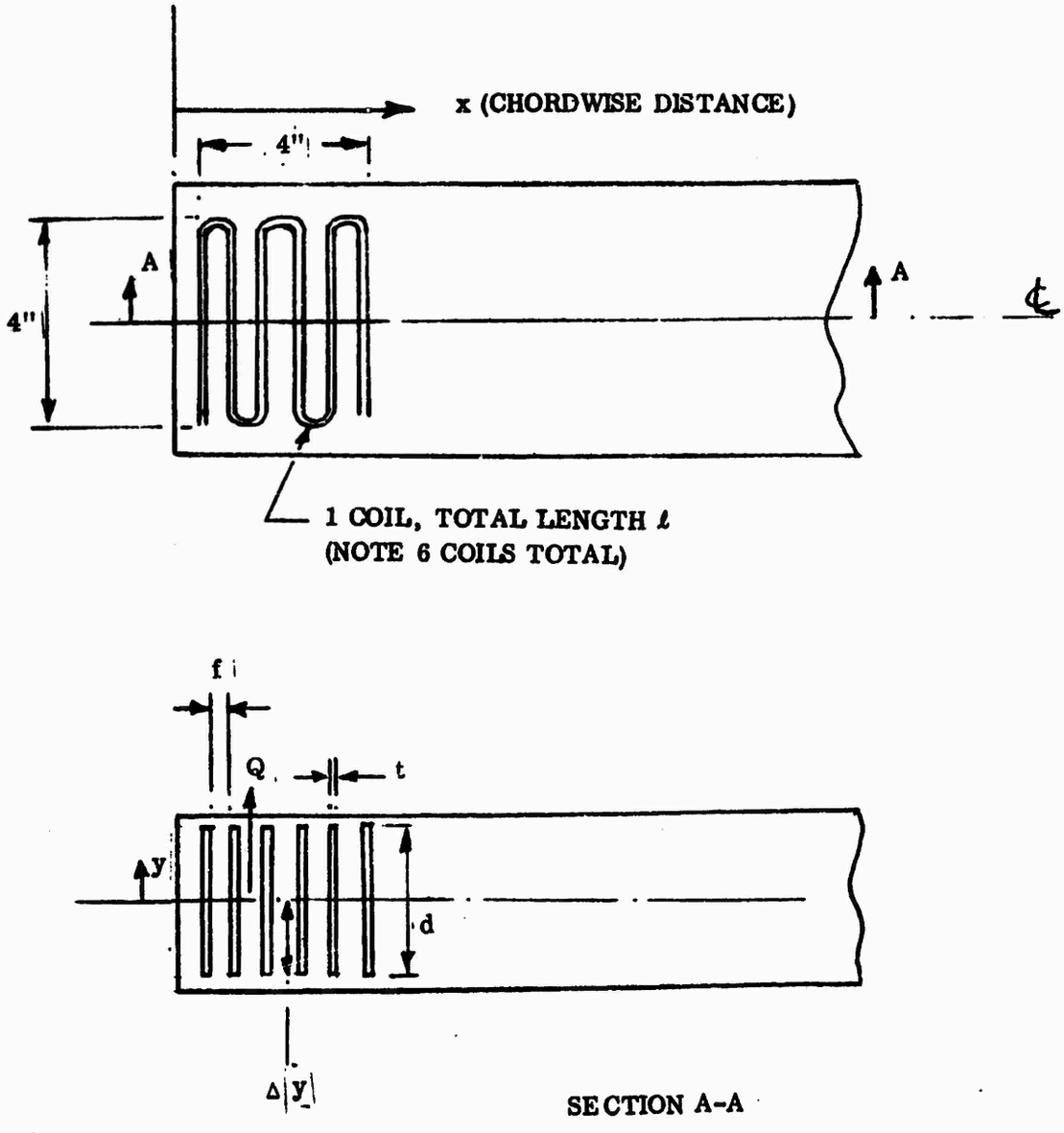

Figure 2.4. Strip Heater Geometry

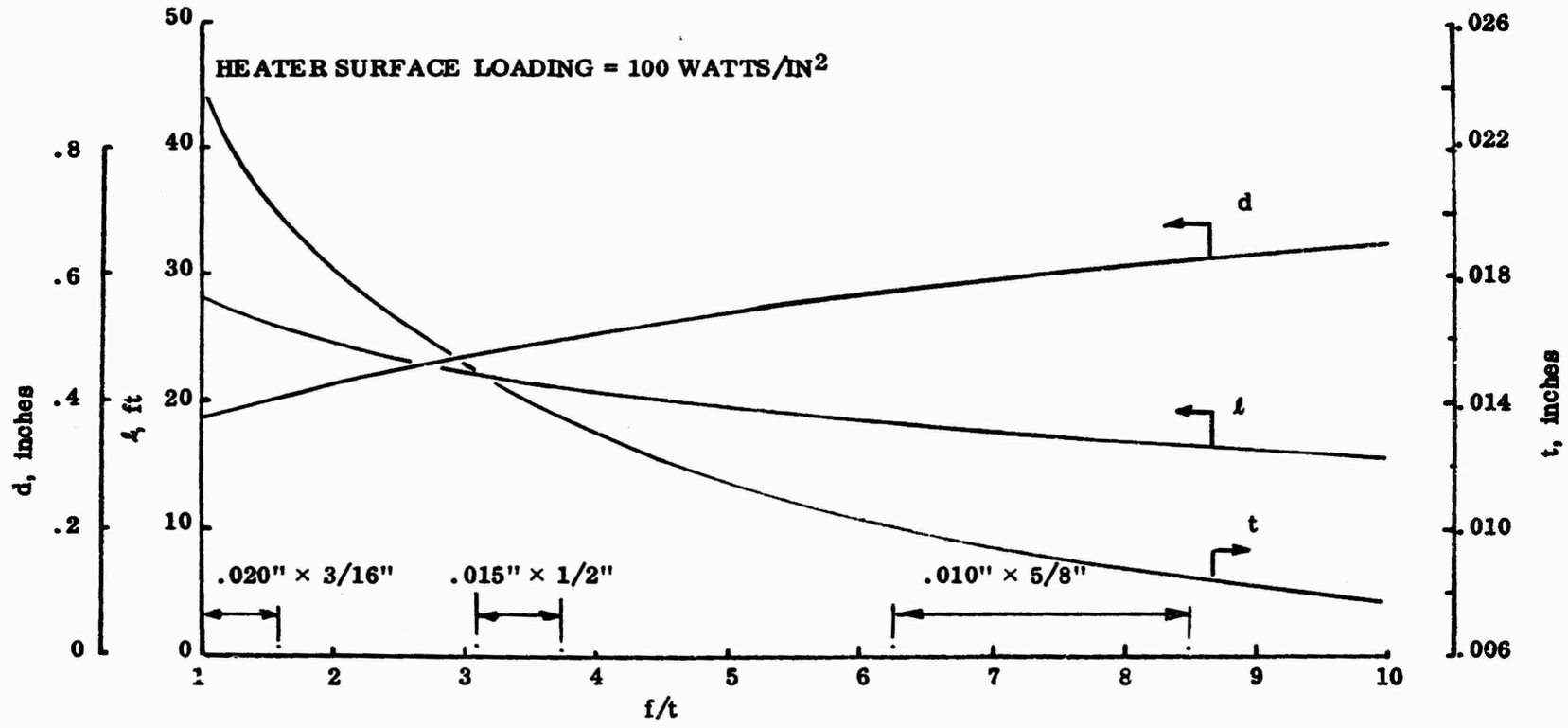

Figure 2.5. Strip Heater Design Curves

NOTE: TEMPERATURE DROP ACROSS
Δy in Figure 2.4

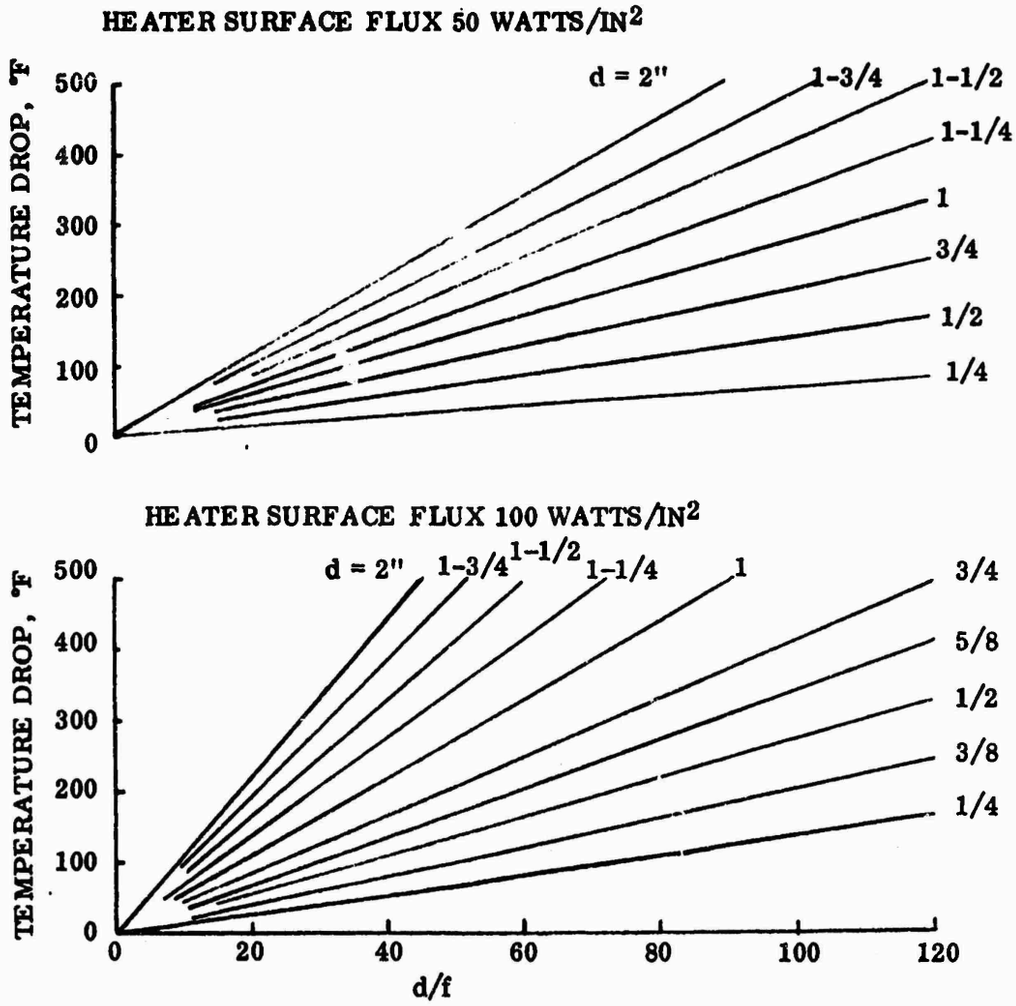

Figure 2.6. Temperature Drop for Various Strip Heater Designs

$$kA \quad \Delta T = \frac{C_1}{2} \Delta y^2$$

The results are shown in Figure 2.6 for the temperature drop along the fin restriction for various geometric parameters and surface power loadings of the heater strip.

From the various design considerations a selection was made of standard 5/8" x .010" Kanthal Al strip, coiled in grooves cut in the copper model, at spacings of 0.06". This heater material was considered initially, due to its high resistivity and capability of operation up to 2500F. It is a ferrous alloy (Al-Cr-Co) and if pre-oxidized in air a very stable coating of aluminum oxide is formed of high electrical resistance. Two problems resulted at this stage, however. Firstly material of this size (or similar) was not available from stock. Secondly, the manufacturers found that the oxide coating could be adversely affected by the presence of copper. Other strip material of nickel-chrome alloys were examined with the possibilities of refractory coatings for insulation, but this was found to be impractical. A cartridge type of heater was finally adopted as an alternative.

2.1.2 Cartridge Heater Design

Discussions with Western Controls who are suppliers of Vulcan Electric high flux cartridge heaters, were held on the cartridge heater concept. This type of heater is generally rated at about 100 watts/in^2 of surface area. However, these heaters have been used in previous nucleate boiling work for fluxes of the same magnitude required for the present work (approximately 500 watts/in^2). Special heaters were designed for the present application. The cartridge heater design incorporates a ceramic core around which is wound resistance wire (Kanthal wire for this case). Surrounding the wire windings is highly compacted magnesium oxide powder (approximately 0.050" thick) encased in an Inconel sheath.

Thermal analysis indicated that two rows of cartridge heaters were necessary as illustrated in Figure 2.7 and 2.8. The temperature gradient were estimated in a similar way to the previous analysis, with the one-dimensional equivelent fin path for conduction past the heaters indicated on the figures, to obtain an estimate of the maximum temperature of the heater wire at the core for a given model surface temperature. The temperature difference, ΔT shown on Figures 2.7 and 2.8 consists of the internal temperature drop of the heater from the wire surface to the surrounding copper surface of the model and the temperature drop from the centerline points of the model to the edge of the circumscribing rectangle containing the heaters. Figure 2.7 applies to 3/8 inch diameter heaters and Figure 2.8 applies to 1/2 inch diameter heaters. The heater diameter chosen was 1/2" which was the minimum diameter recommended by the manufacturer for high quality control of the heater assembly.

From the thermal analysis a design with 70 heaters consisting of two rows of 35 each was recommended for a 24 inch model length of a width as near to the model span as practical. However this was modified to a total of 61 heaters in the final design, mainly due to the removal of heaters from the central area where the strut connects, to allow space for power lead routing. The final heater specifications were as follows:

Electrical Supply	230 V, 3 phase, 60 cycle A.C.
Max. power rating	3 kw
Diameter	0.500 inches
Overall length	3.00 inches
Leads	2 feet long - .062" dia. (nickel)

Each heater was tested in air at 1800°F surface temperature for 30 minutes before final machining of the outside diameter to tolerance size.

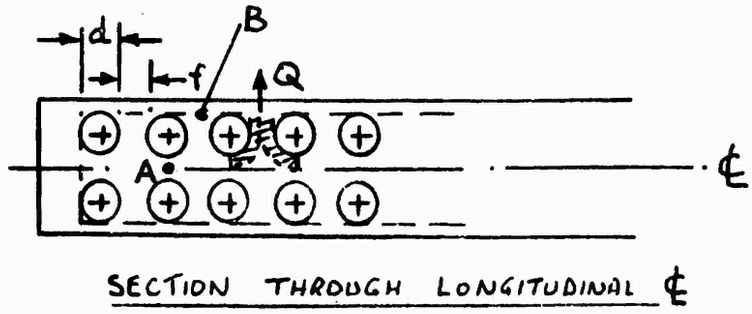

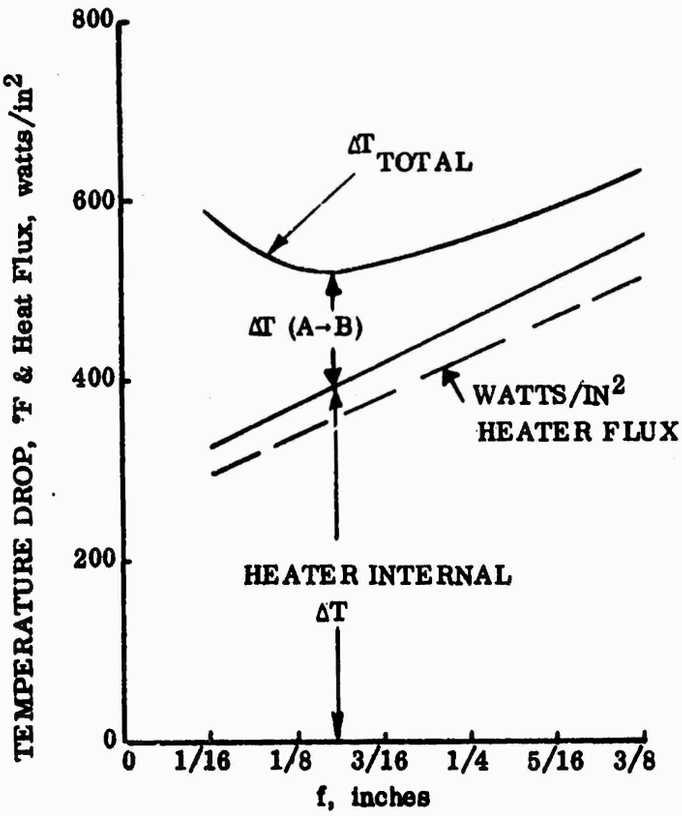

Figure 2.7. Temperature Drop 3/8" Dia. Cartridge Heaters

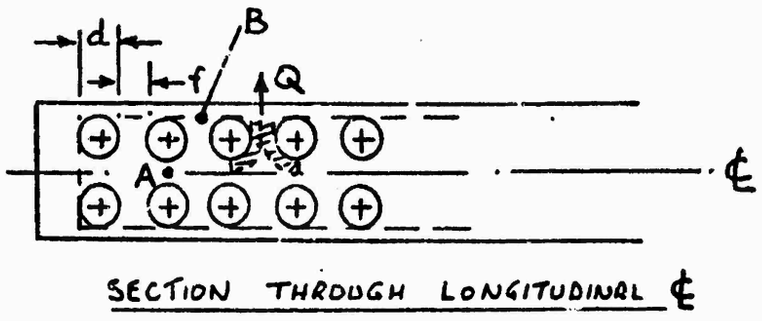

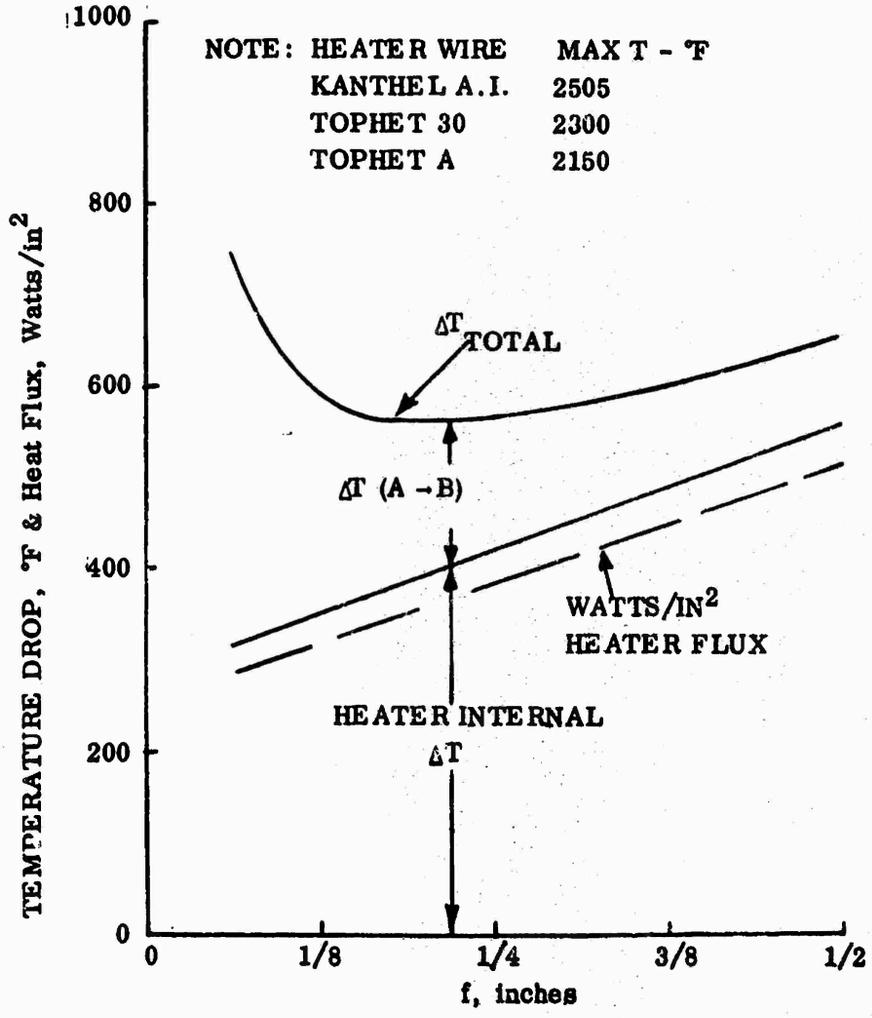

Figure 2.8. Temperature Drop 1/2" Dia. Cartridge Heaters

2.2 PRESENT MODEL AND STRUT ASSEMBLY

Full details of the model and strut assembly are shown in Drawing No. WT-70-104704 included in the detail design drawings at the end of this report. A brief description is given below to indicate the main features and dimensions.

A sketch of the model is shown in Figure 2.9 showing the major dimension, and location and numbering of the thermocouples and heaters. The model is made of O.F.H.C. copper and the connecting strut adapter of stainless steel welded to the model. The model is chrome-plated after assembly to prevent oxidation of the copper. It is anticipated also that the model may have to be re-plated during the course of the tests. It is particularly important that great care be taken during the plating process to shield the open end of the strut. The model was previously assembled and damaged during the plating process by electrolyte seepage in the absorbent ceramic potting compound. This necessitated considerable re-work of the model to replace all of the heaters damaged. The power leads to the heaters are insulated with (fiberglass) No. 16 VARGLASS 1600 sleeving. The thermocouples are Chromel Alumel with ungrounded ends, enclosed in .040 inch diameter Inconel sheathing with magnesium oxide insulation. Figure 2.10 shows photographs of the model taken during installation of the heaters and routing of the power leads. After all heaters are installed, the internal channels containing heater leads and thermocouples are potted in ceramic and copper side plates are welded on. The strut assembly parts are also shown in the photographs. It should be noted that the photographs were taken of a 62 heater system. One heater location (lower central) was later machined out to allow more room for routing the leads in the closely packed bend where the strut meets the model.

The fiberglass insulation for the power leads replaced the original Refrasil sleeving which was difficult to install without damage due to its poor mechanical properties. The fiberglass sleeving was tested to

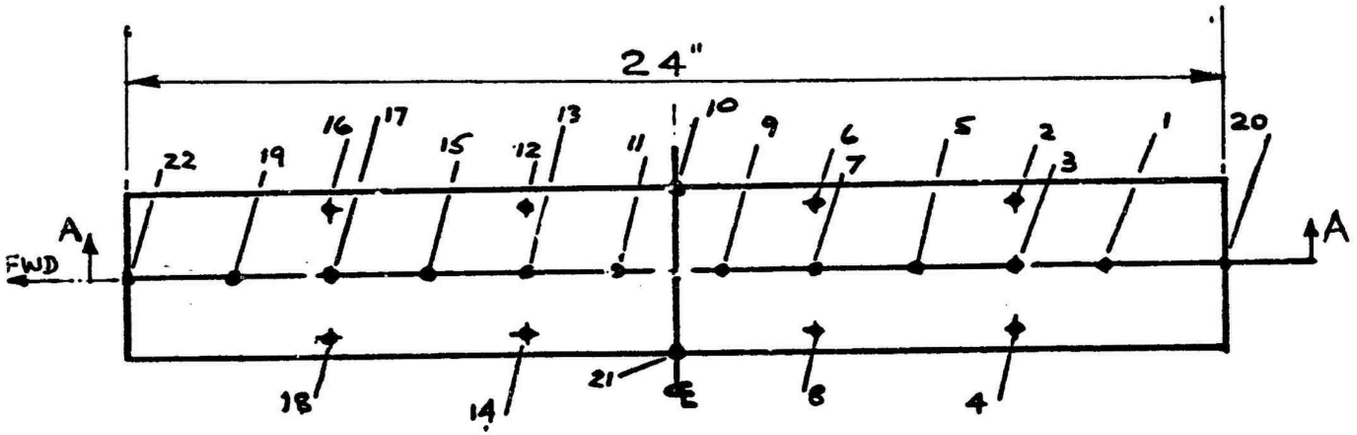

PLAN VIEW SHOWING THERMO COUPLE NUMBERING ON TOP SURFACE

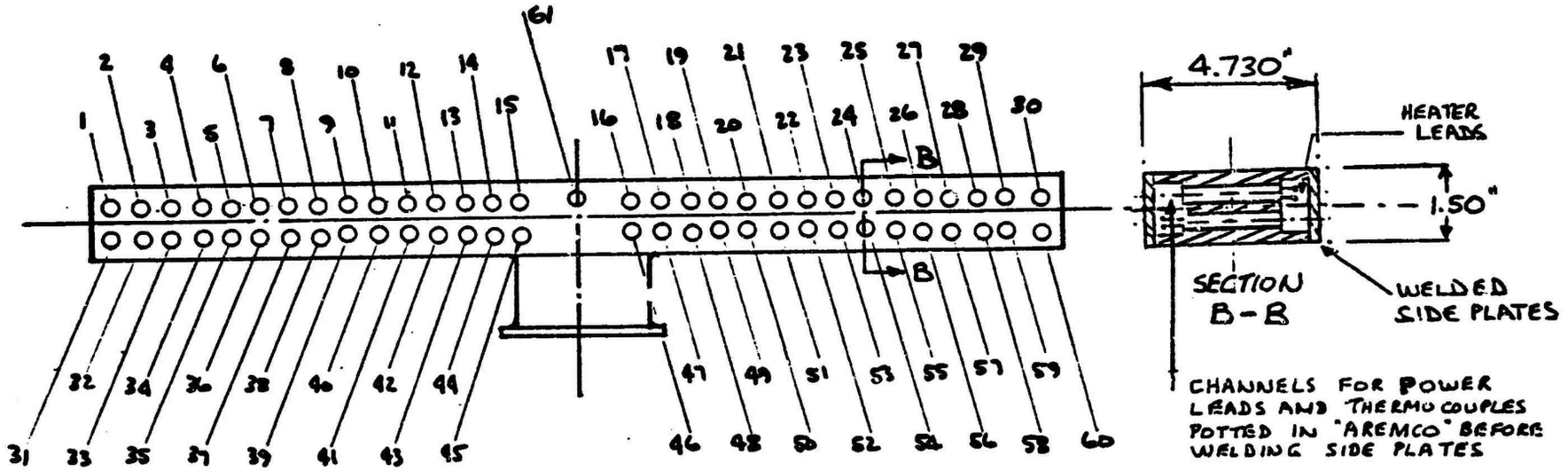

SECTION A-A SHOWING HEATER NUMBERING

Figure 2.9. Schematic of Model for Film Boiling Tests

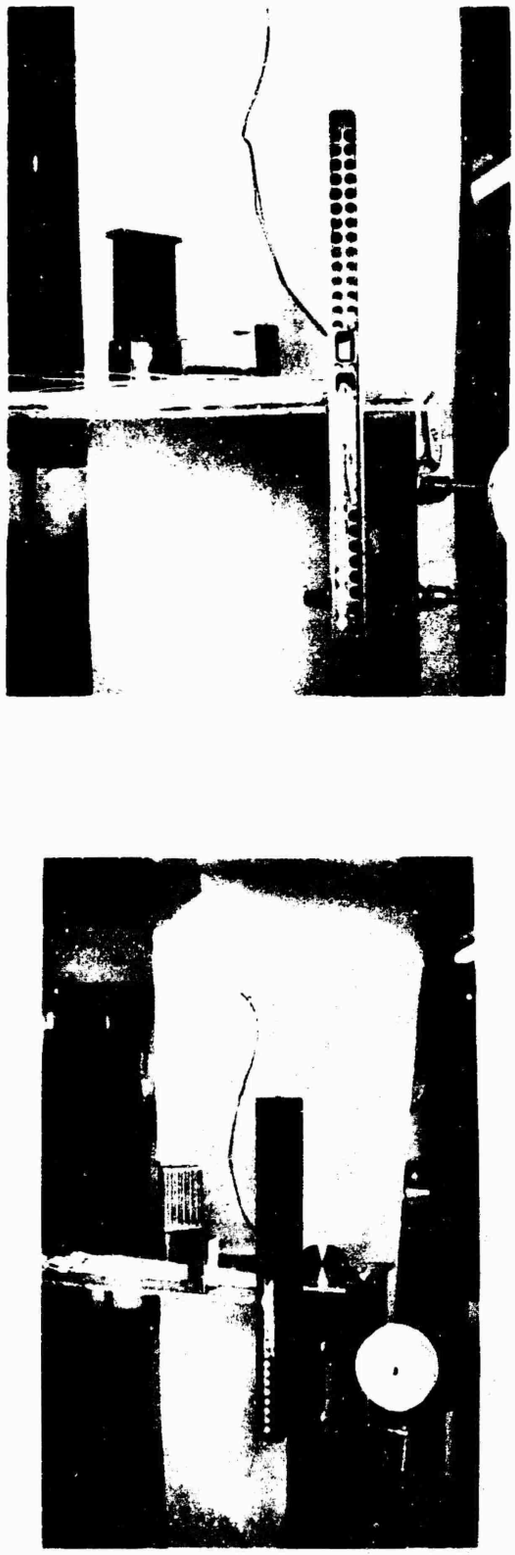

Figure 2.10. Model During Heater Installation

180°F and retained its flexibility and soundness. Figure 2.11 illustrates the proposed installation of the model in the CIT High Speed Water Tunnel. The drag forces on the model are transmitted to the force balance via a strut assembly and balance adapter. The strut is protected from the water flow velocity by a non-metric windshield as indicated. The power leads and thermocouples pass through two elbows at the lower end of the strut assembly to the connections on the side of the balance adapter leading to the power supply source and data readout system. The power leads at the (cold) strut exit are 20 gage copper wire with flexible Teflon insulation. The two lead bundles between the strut assembly elbows and the adapter wall connections must be protected by water-proof vinyl sleeving, since the balance adapter area contains water.

2.3 WATER TUNNEL PREPARATION

The experiments were planned to be run at the Hydrodynamics Laboratory of the California Institute of Technology in Pasadena, California, using the High Speed Water Tunnel. The Hydrodynamics Laboratory is under the direction of Mr. T. M. Ward.

Figure 2.12 is a sketch of the entire tunnel with the 3D test section in place. Water is pumped around the loop by a 475 kva electric motor which drives a single-stage turbine pump submerged in the water resevoir. This pump provides sufficient energy to attain a water speed of approximately 100 ft./sec. in the 14-inch diameter 3D test section. The water leaves the resevoir (58-feet under-ground) and enters a stilling chamber. The exit of this chamber has a honeycomb exit section for final flow straightening for entrance into the nozzle. The entrance nozzle is designed to accelerate the flow into the test section with minimum flow distortion and turbulence.

Water leaves the test section through an exit diffuser up to the return line size. On return the water may pass through water chillers to

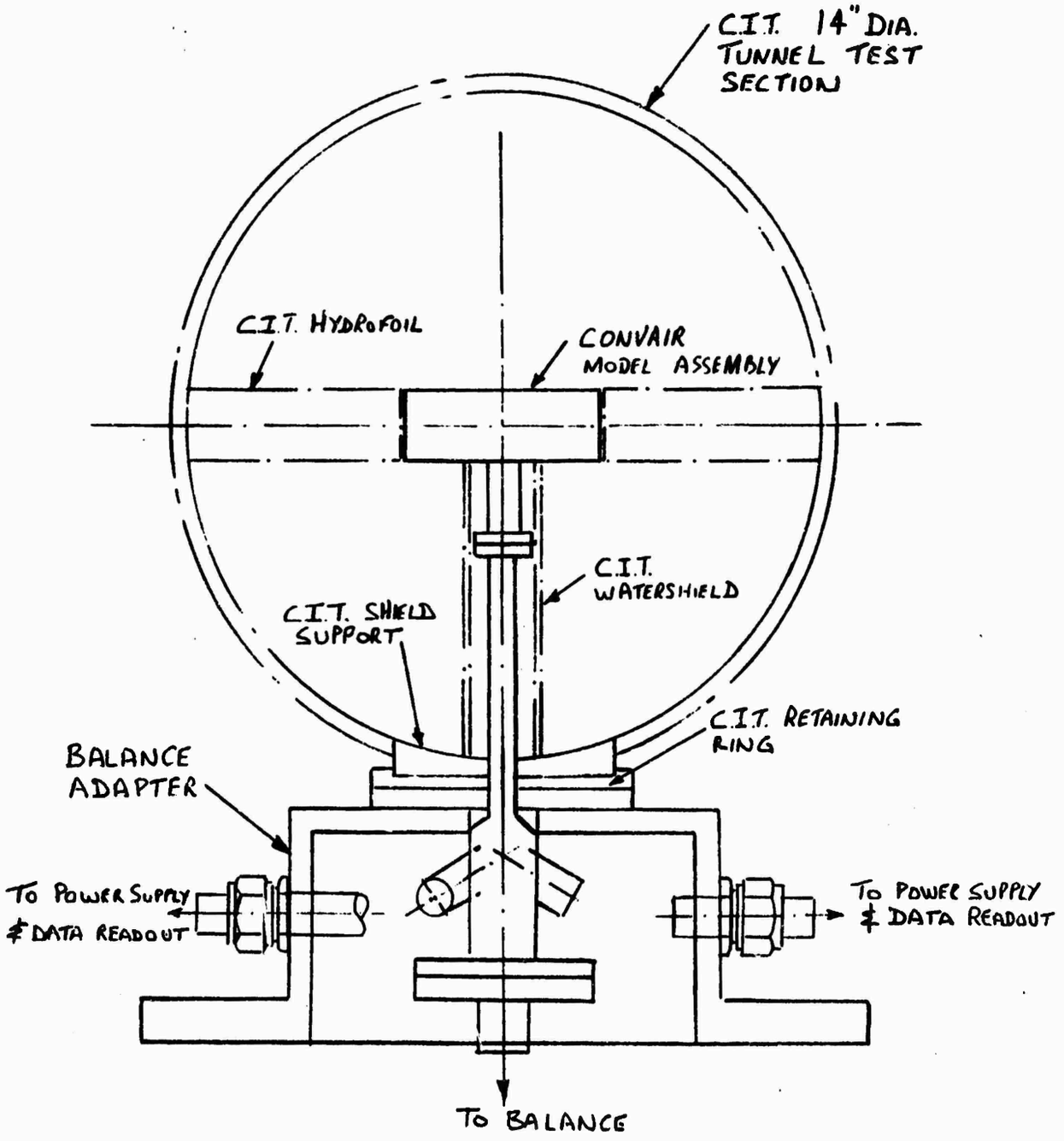

Figure 2.11. Schematic of Model Installation in C.I.T. Water Tunnel

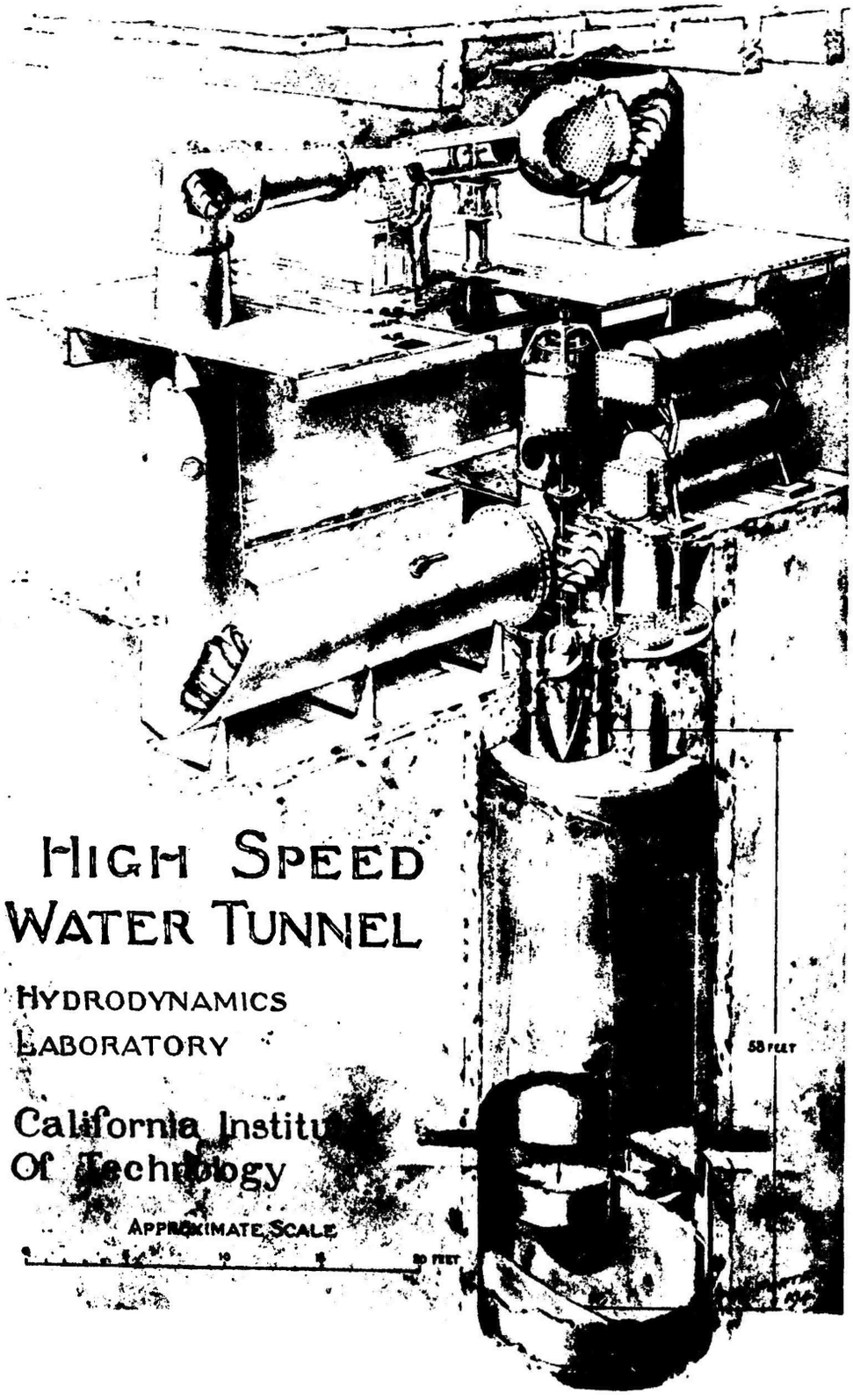

Figure 2.12. Water Tunnel

remove the heat added by the pump. However, size of the system resevoir and heat loss to the ground and surroundings is such that the chillers are not required and are generally bypassed. The water then returns to the resevoir where the hydrostatic head developed by having this tank 58-feet underground enhances reabsorption of any air bubbles released in the test section.

In preparation for the film boiling experiments design and fabrication of some components associated with the tunnel installation was completed. Figure 2.11 showed a schematic of the model installed in the test section, with the CIT components indicated. These are

i) the horizontal hydrofoil surrounding the Convair model

ii) the windshield (vertical hydrofoil) to shield the model strut from the free stream flow.

iii) the balance adapter with the windshield support and retaining ring to attach to the existing force balance

In addition, a further requirement for the film boiling experiments was operation of the 3D test section in the reverse direction from the standard installation. This necessitated,

iv) the fabrication of special connecting flanges for the 3D test section.

The following paragraphs describe the status of these items in more detail. The design drawings referenced are included at the end of this report.

2.3.1 Horizontal Hydrofoil

Design and fabrication of this item is completed per CIT drawing N-3454-ODD "Skin Friction Model - Horizontal Fairing". A photograph is shown in Figure 2.13. The fairing has been designed to provide adjustments of approximately 0.25 inch in the longitudinal and vertical directions. It was originally proposed that the fairing be fixed to the working section. As the program developed, and detailed consideration was given to the problem of

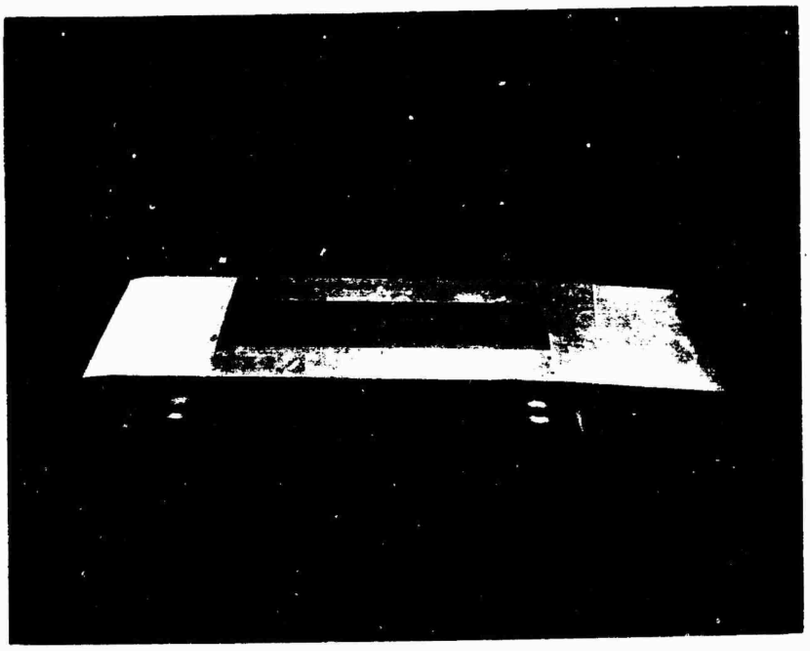

Figure 2.13. Horizontal Hydrofoil

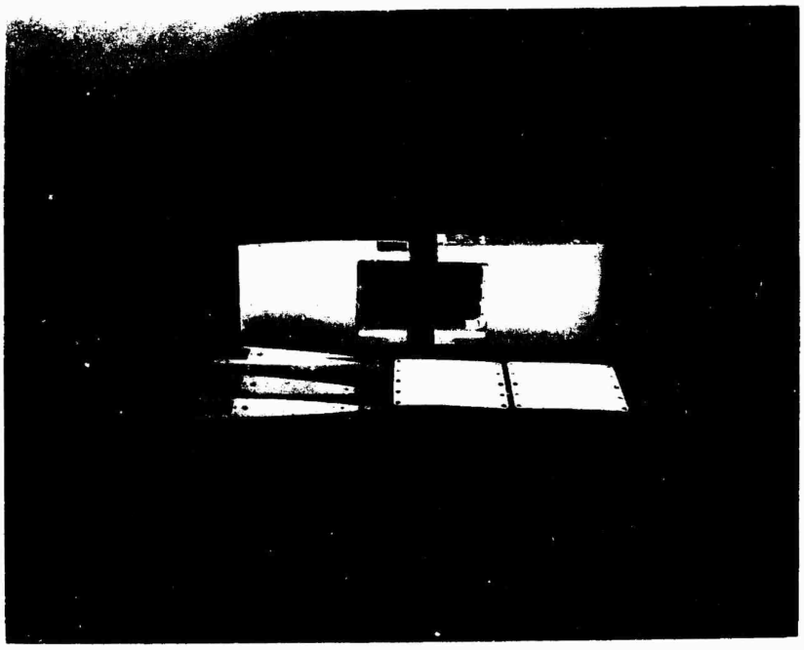

Figure 2.14. Vertical Windshield

aligning the model and fixed hydrofoil, it became apparent that a movable non-metric hydrofoil would be required due to the complexity of mounting the model and balance assembly.

2.3.2 Vertical Windshield

Fabrication of the windshield is complete. A photograph is shown in Figure 2.14. The original design is shown in Convair Drawing WT 70-104705. Changes as required by CIT are included in CIT Drawing "Details - Windshield, Film Boiling", dated 1 June 1970. Not shown on the drawings is the addition of a 1/8 inch stainless steel cap plate for thermal insulation to the aluminum windshield body. This plate has been fabricated and installed.

2.3.3 Balance Adapter

Design of the adapter is shown in Drawing WT-70-104701. Fabrication is completed except for the mounting of the two brass 7/8 inch tube fittings. A photograph is shown in Figure 2.15. The drawing calls for an O-ring groove to be located outside the bolt holes. This groove had to be relocated to the inside of the bolt circle. It was then necessary to bore and face each screw to provide sealing around the individual bolts. Also completed are the windshield support and retaining ring shown on Drawing WT-70-10472.

2.3.4 Model Installation

The 3D working section was removed from the high speed tunnel during another experimental program. This provided an opportunity to fit check the equipment. A mock-up of the model as shown in the photograph of Figure 2-16 was made and the equipment assembled for a dry-run fit check. The model mock-up measured 1.500 x 24.00 x 4.730 inches. It was determined that if the model span increased to 4.739 inches, the model will stick in the window opening (through which it enters the tunnel assembly). A model of 4.740 inches will not fit the opening. Final machining of the model was thus

Figure 2.15. Balance Adapter

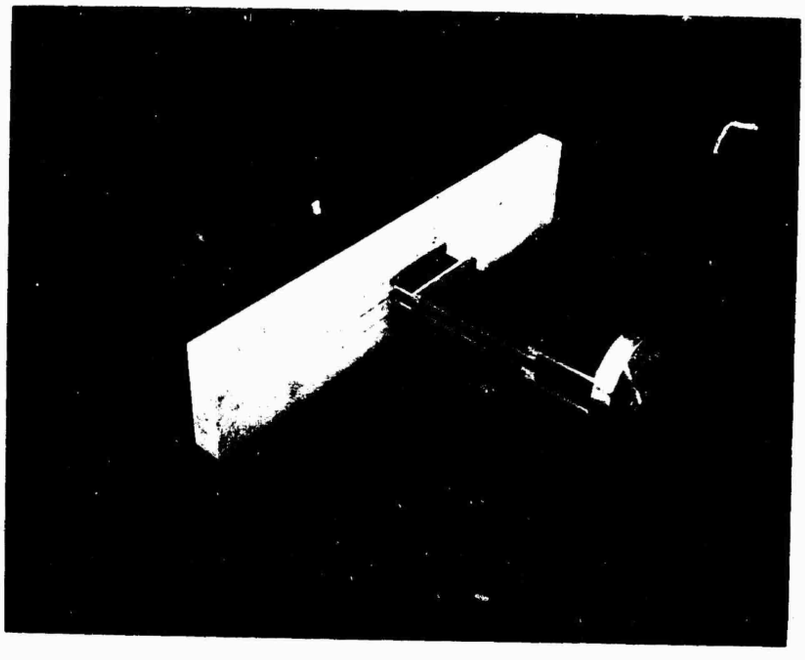

Figure 2.16. Mock-up of Film Boiling Model

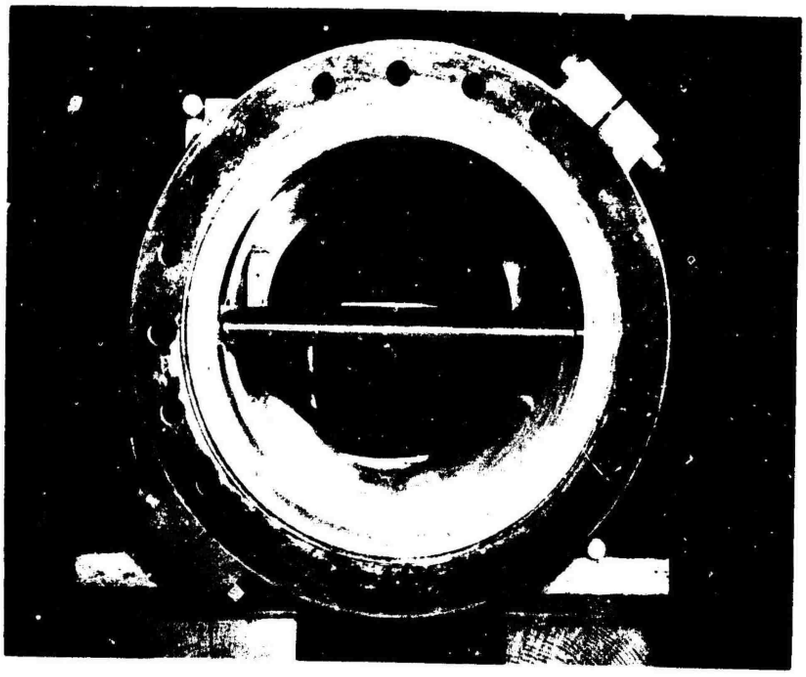

Figure 2.17. Test Section With Horizontal Hydrofoil in Position

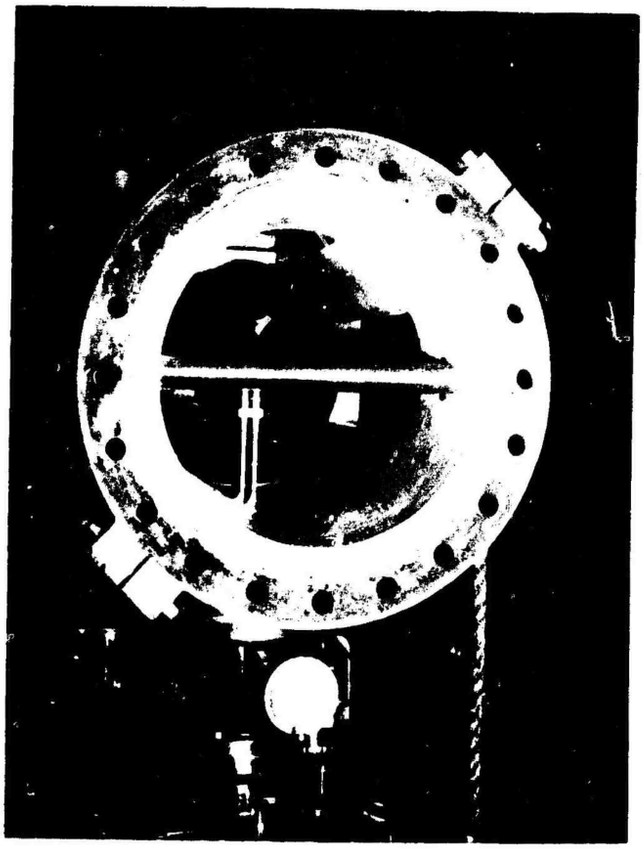

Figure 2.18. Fit-Check Sequence With Assembly Mounted to Balance and Prior to Vertical Windshield Installation

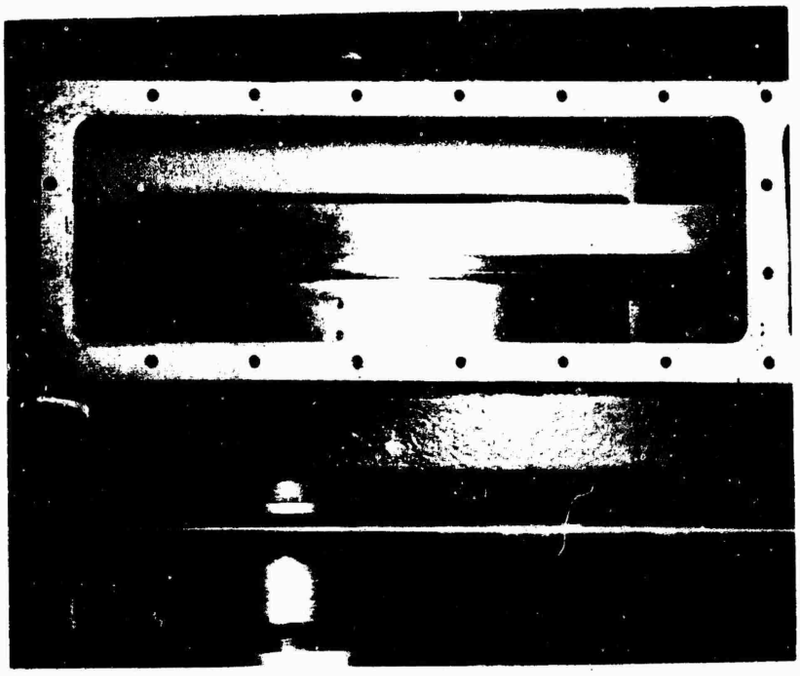

Figure 2.19. Fit-Check Assembly, Side View

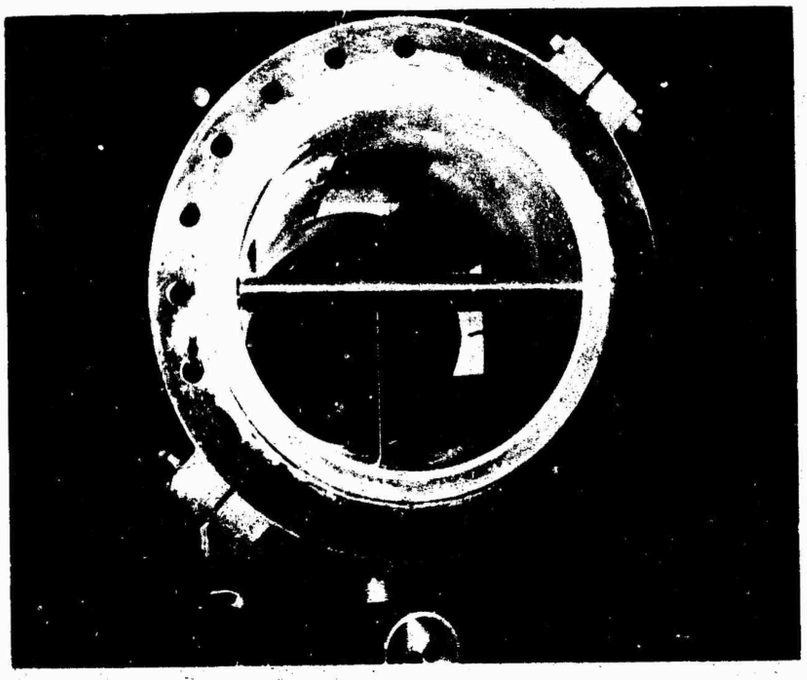

Figure 2.20. Fit-Check Assembly, Front View

specified at 4.730 inches. The assembly procedure was successful and is illustrated in Figures 2.17 through 2.20. Figure 2.17 shows the test section with the horizontal hydrofoil installed. Figure 2.18 shows the assembly after mounting on the balance installation and with the model in position. Figures 2.19 and 2.20 show a front and side view of the installation with the vertical windshield in position.

2.4 MODEL INSTRUMENTATION

The heater power control system was designed and built for operation on a 230 volt a.c., 3 phase, 60 Hz supply. The system consists of six power control units of the Triac thyristor type with a total power capability of 0-150 Kw. These are designed to provide precise heater power control and heater power monitoring. In addition to a fused input, each power control unit has a resetable overcurrent protection circuit. A switch-selectable kilowatt meter capable of monitoring the output of any of the six power control units is included.

Six temperature meters are mounted in a panel assembly with a read-out range 0-2000°F. These are intended for connection to one critical thermocouple from each of the six model chordwise zones, to guide manual control of the power settings.

It was planned to use the Convair Portable Read-out System with an IBM 026 Serial Punch Card Recorder, to record the test data during an experiment. This would allow rapid automatic recording of temperatures over the model during a test. The balance readings and other tunnel data could be manually input to the recorder so that all data for a given run would be recorded on punched cards.

Figure 2.21 shows photographs of the instrumentation. Figure 2.21(a)

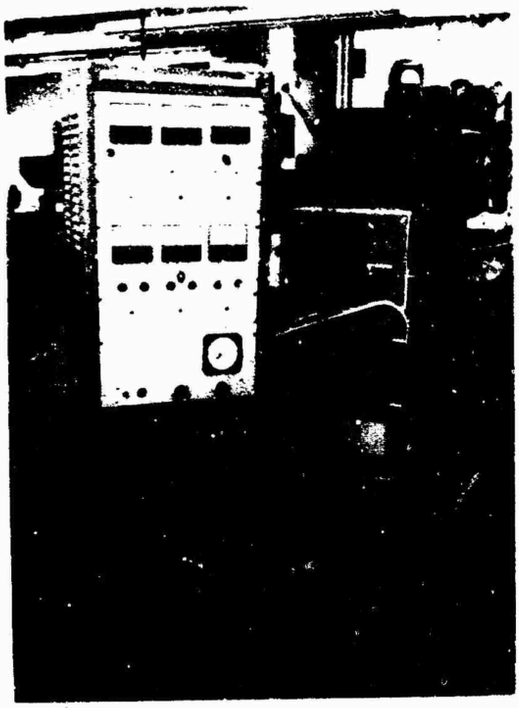

a) Six Temperature Panel Readouts
0 - 2000°F, Power Readout 0-30 Kw

b) Six Triac Power Control Units
0-25 Kw Each

c) Convair 30 Channel Automatic
Readout System

Figure 2.21. Model Instrumentation

shows the six temperature meters and the wattmeter, Figure 2.21(b) shows the Triac power control unit and Figure 2.21(c) shows the Convair Portable Data System.

Figure 2.22 shows a cable diagram for the major model instrumentation. Figures 2.23 through 2.26 are circuit diagrams for the power control units and temperature monitoring system. Figure 2.23 shows the power control unit Triac System and Figure 2.24 shows the overcurrent protection system circuit. Figure 2.25 is a diagram of the direct reading temperature monitor system, consisting of an operational amplifier and the meter. Figure 2.26 is a representative diagram of the overall temperature monitor system and recording system.

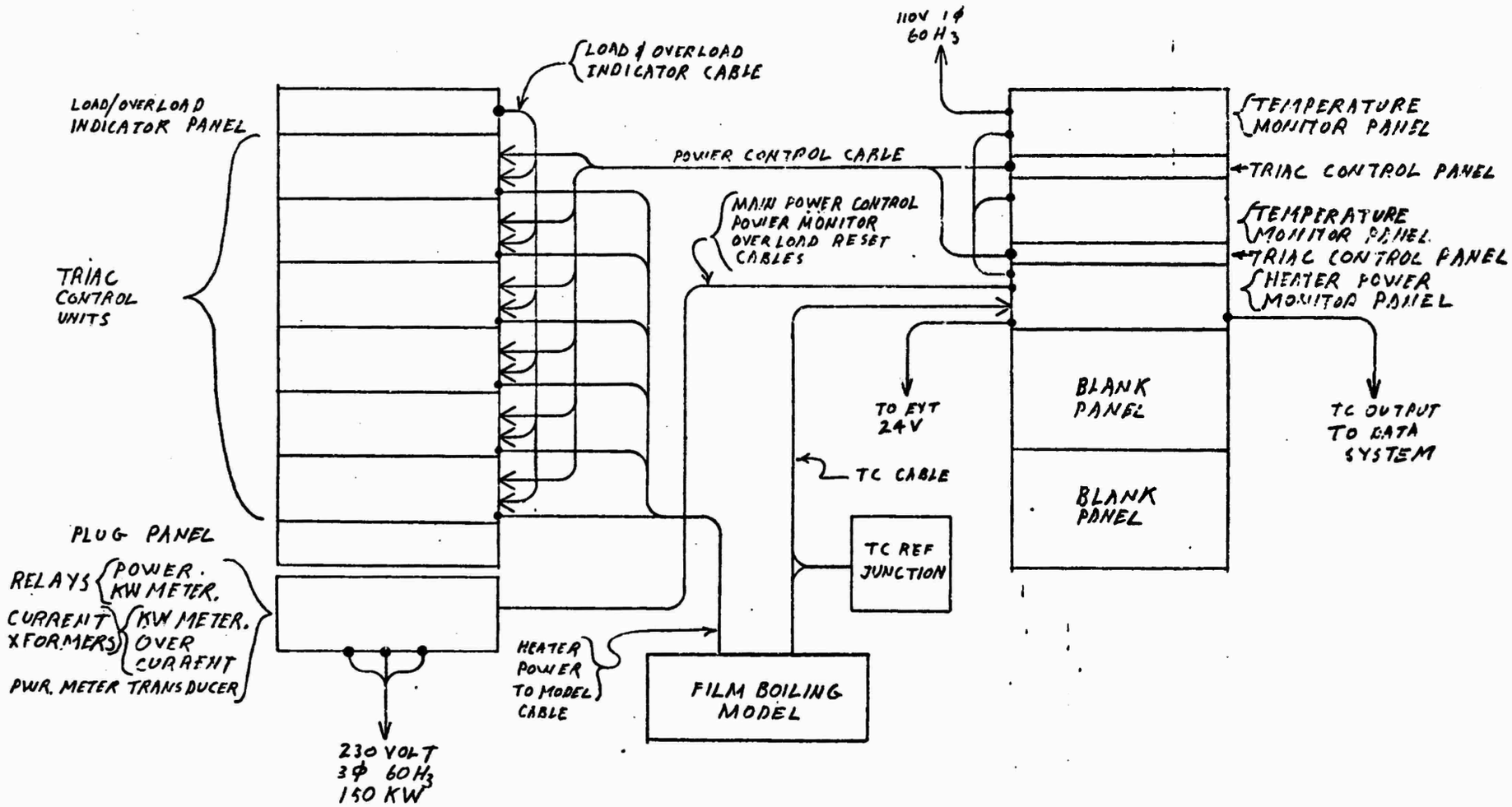

Figure 2.22. Cable Diagram

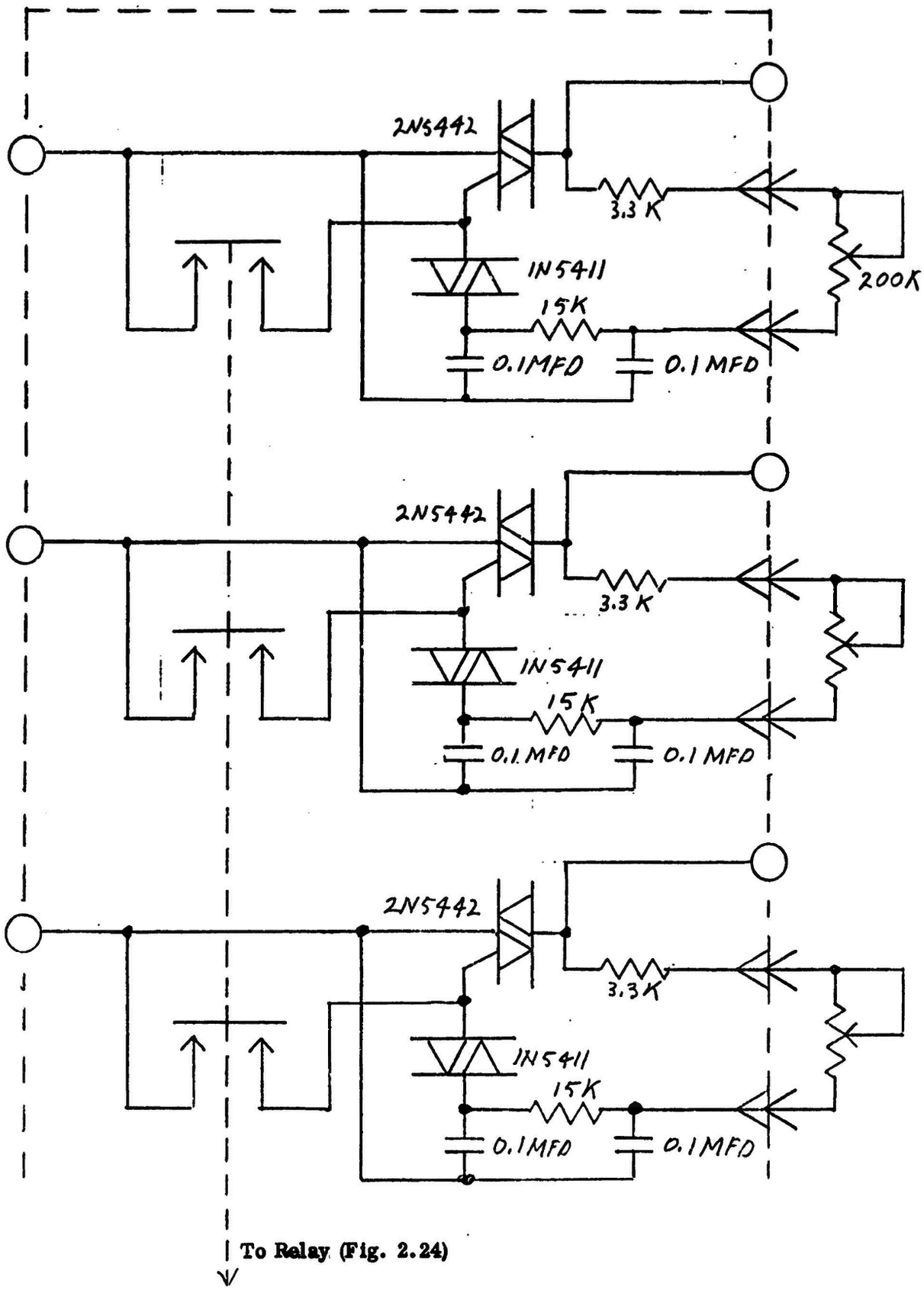

Figure 2.23. Power Control Unit Triac Section

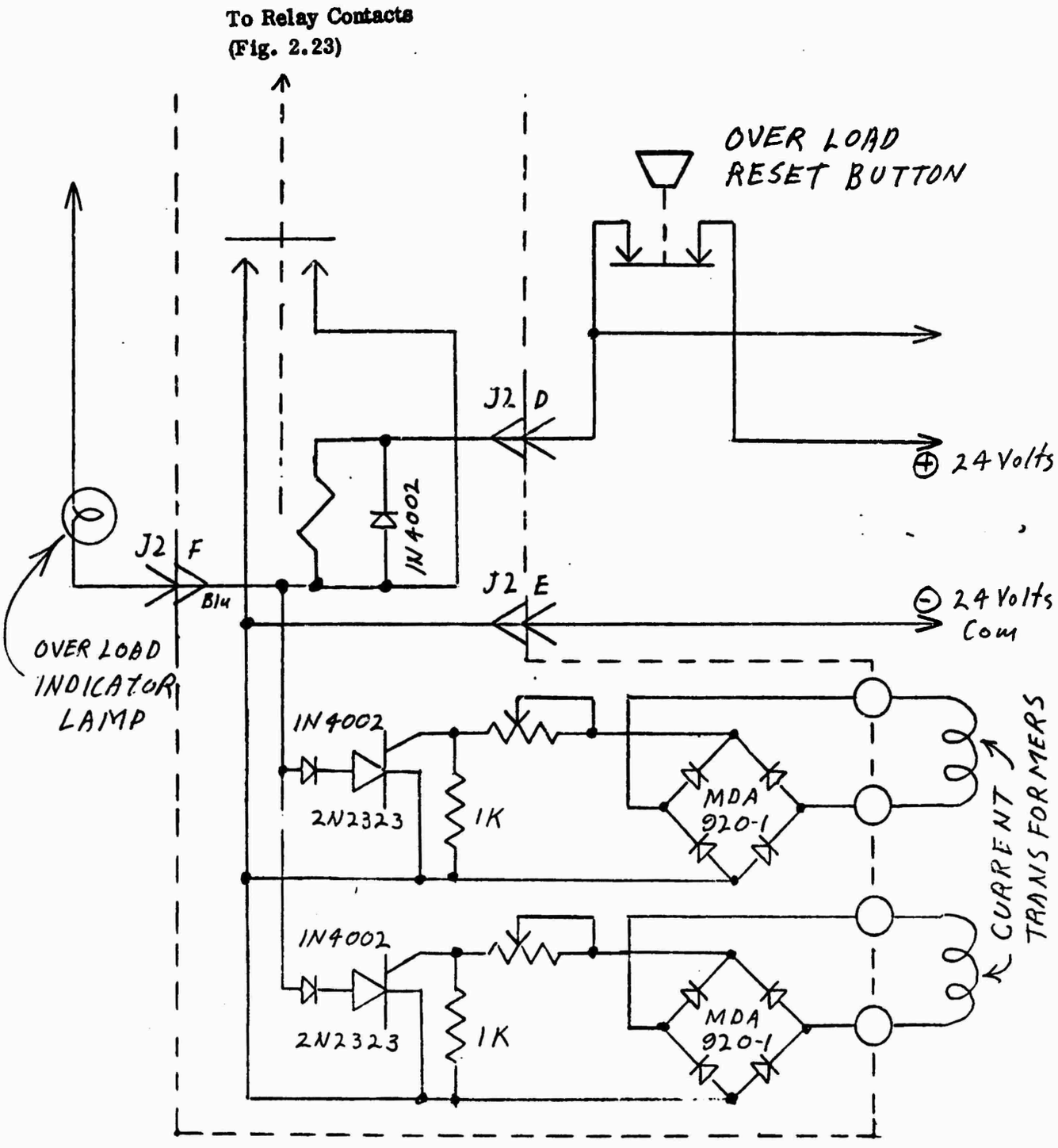

Figure 2.24. Power Control Unit Overcurrent Section

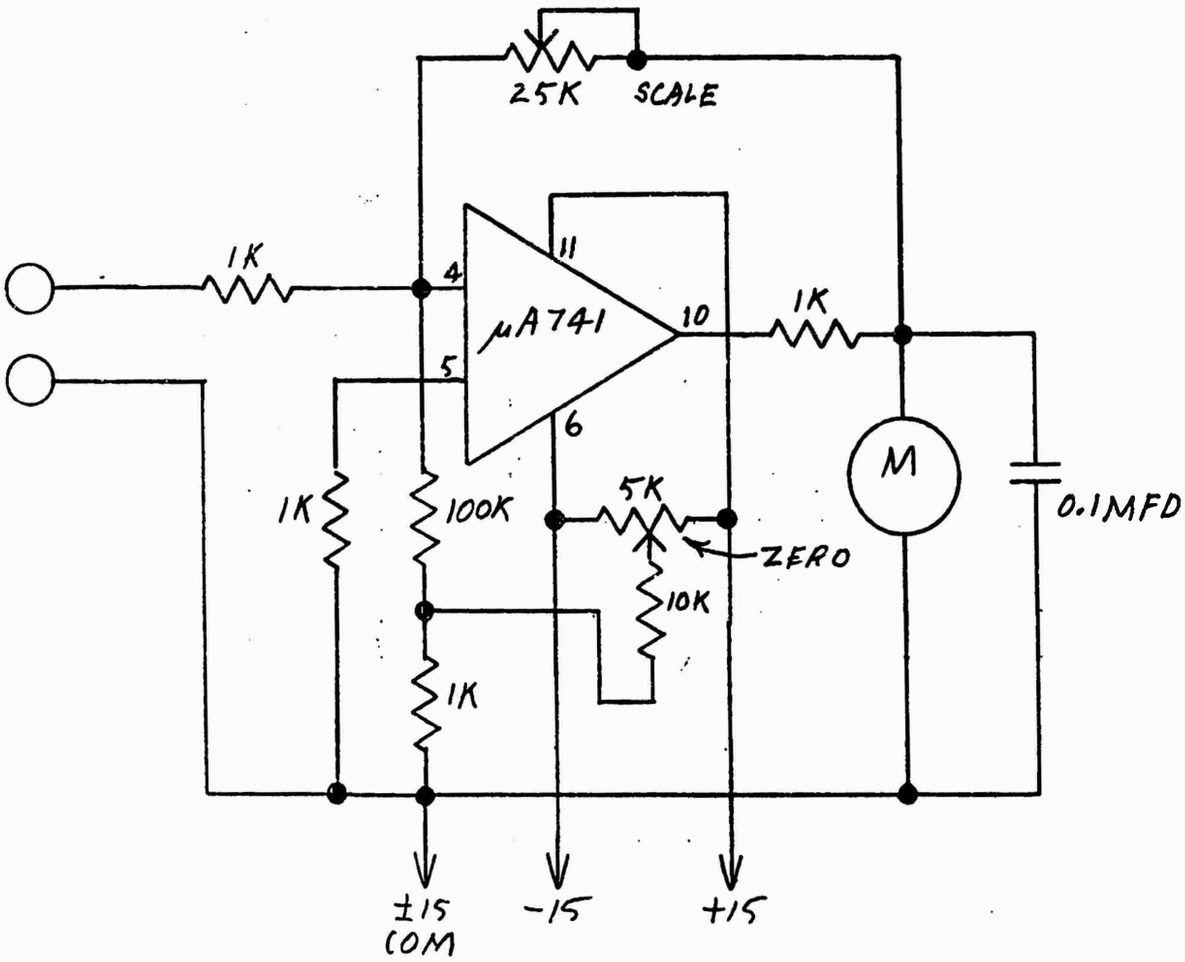

Figure 2.25. Temperature Monitor

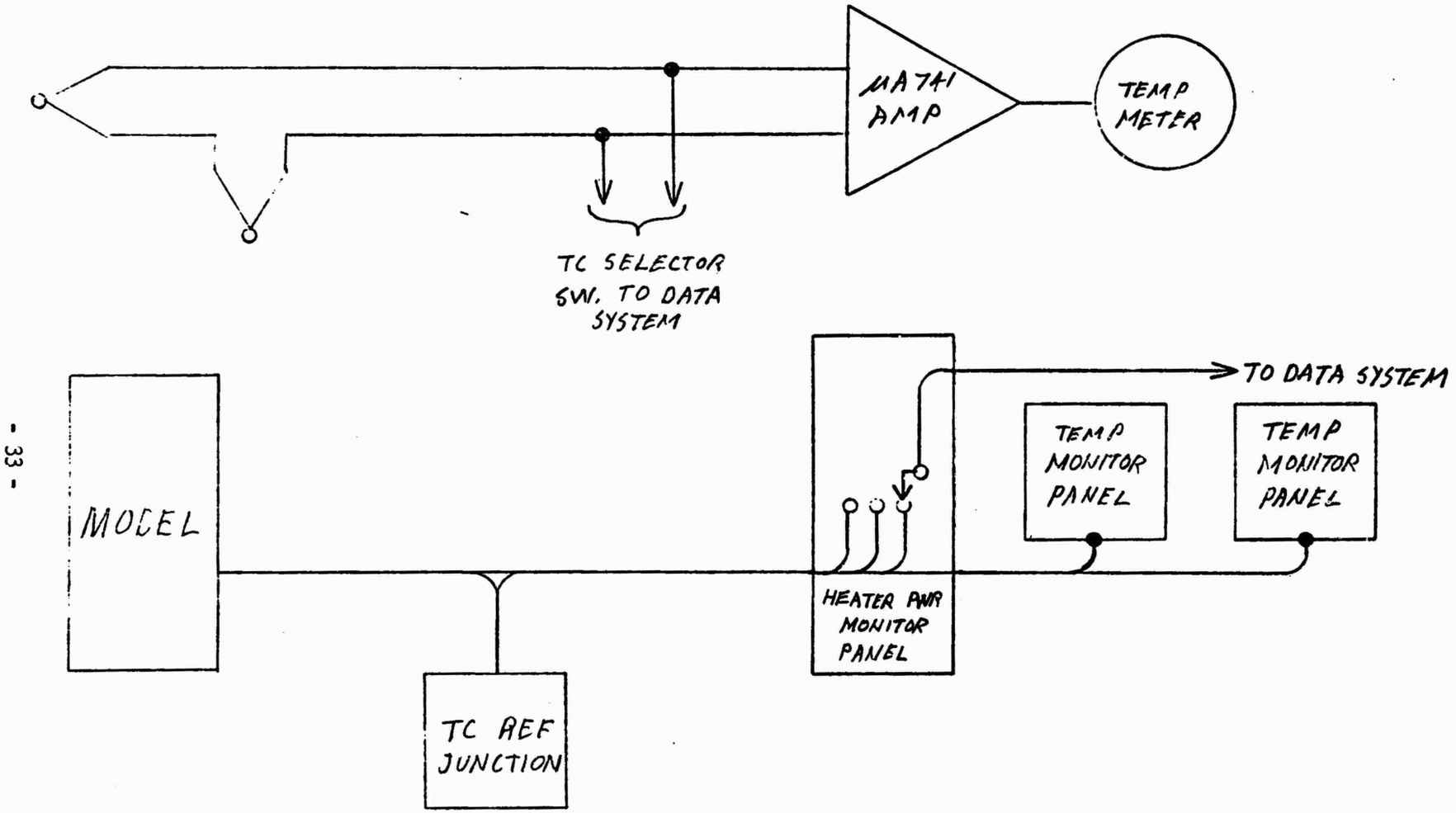

Figure 2.26. Film Boiling Temperature Monitor System

3. TWO-PHASE BOUNDARY LAYER ANALYSIS

3.1 Laminar Flow

A Blasius-type solution for flow on a flat plate has been obtained by Cess and Sparrow[9]. This is an exact formulation of the laminar boundary layer equations, although some approximation was involved in the solution of the equations. The equations were solved numerically and in more detail by Ito and Nishikawa[10], but their results were close to those of Cess and Sparrow over a fairly wide range of practical conditions.

The integral method of solution due to Pohlhausen is considered here (see e.g. Reference 11), to obtain an approximate solution to the problem. This is useful, of course, since approximate methods can be more easily applied to a greater range of flow conditions than the exact solutions. The analysis follows that of Reference 7, but the results are obtained for general fluids and also the momentum integral equation for the liquid layer is modified.

Assumptions:

(i) The flow is steady, two dimensional, and laminar in both vapor and liquid boundary layers,

(ii) The pressure is everywhere constant,

(iii) The heated surface temperature (T_w) is constant,

(iv) The liquid-vapor interface temperature (T_i) is equal to the saturated liquid temperature at ambient pressure,

(v) Thermodynamic and transport properties of the liquid and of the vapor are constant,

(vi) These properties are evaluated at a reference temperature defined by $T_v^* = (T_w + T_i)/2$ for the vapor and

$T_\ell^* = (T_i + T_s)/2$ for the liquid,

(vii) Thermal radiation effects on the liquid and vapor layers are neglected,

(viii) Buoyancy effects on the forced-convection boundary layers are neglected.

The velocity and temperatures profiles are assumed linear in the vapor layer and parabolic in the liquid layer. Figure 3.1 shows the physical model of the flow and the notation used for velocities.

The velocity in the vapor layer is given by

$$u = u_i \frac{Y}{\delta_V} \tag{1}$$

The velocity in the liquid layer is given by

$$\frac{u_\ell}{u_L} = \frac{3}{2} \frac{Y_1}{\delta_L} - \frac{1}{2} \left[\frac{Y_1}{\delta_L} \right]^3 \tag{2}$$

where $$Y_1 = Y - \delta_V \tag{3}$$

Continuity of velocity at the interface gives,

$$u_s = u_i + u_L \tag{4}$$

The momentum integral equation is applied to the liquid layer,

$$I = \rho_L \int_0^{\delta_L} (u_s - u)\, u \, dy_1 \tag{5}$$

$$= \rho_L \int_0^{\delta_L} (u_L - u_\ell)\, (u_i + u_\ell)\, dy_1$$

which on expanding and integrating leads to

$$I = \rho_L \, u_L^2 \, \delta_L \left[\frac{39}{280} + \frac{3}{8} \frac{u_i}{u_L} \right] \tag{6}$$

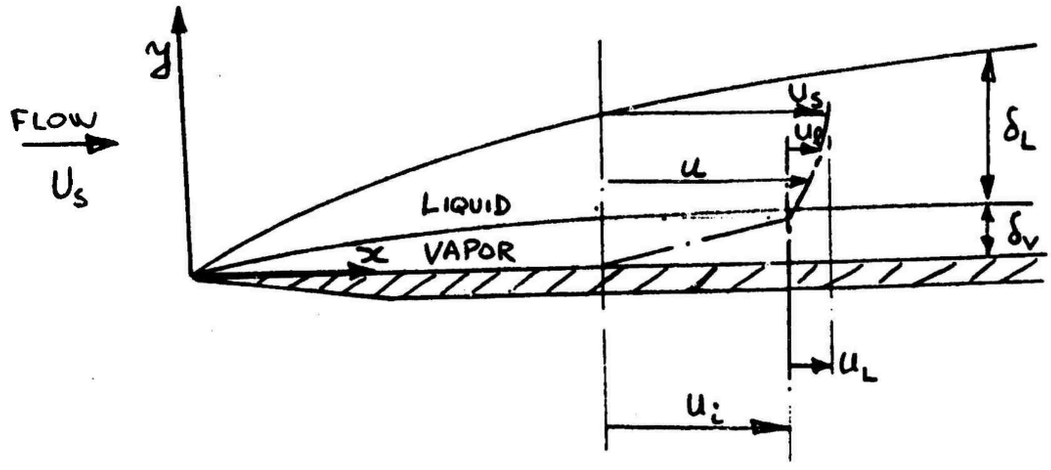

Figure 3.1. Physical Model and Coordinate System for Two Phase Boundary Layer

thus,

$$\tau_i = \frac{d}{dx}(I) = \mu_L \left|\frac{du}{dy_1}\right|_{y_1=0} = \frac{3}{2}\frac{u_L}{\delta_L}\mu_L \tag{7}$$

which gives

$$\delta_L d\delta_L = \frac{3/2\ \mu_L}{\left[\frac{39}{280} + \frac{3}{8}\frac{u_i}{u_L}\right]} \frac{dx}{\rho_L u_L} \tag{8}$$

leading to the relation between δ_L and x

$$\left[\frac{\delta_L}{x}\right]^2 = \frac{3}{\frac{\rho_L u_L x}{\mu_L}\left[\frac{39}{280} + \frac{3}{8}\frac{u_i}{u_L}\right]} \tag{9}$$

this can be expressed in terms of the Reynolds number of the stream flow as,

$$\left[\frac{\delta_L}{x}\right]^2 = \frac{280}{13}\left[Re_x\left(1 + \frac{22}{13}\frac{u_i}{u_s}\right)\right]^{-1} \tag{10}$$

Continuity of shear at the interface gives,

$$\frac{\delta v}{\delta_L} = \frac{2}{3}\frac{\mu}{\mu_L}\frac{u_i}{u_L} \tag{11}$$

and the shear stress can be obtained as

$$\tau_w = \tau_i = 0.323 \frac{\rho_L u_s^2}{R_{ex}^{1/2}} \frac{u_L}{u_s}\left[1 + \frac{22}{13}\frac{u_i}{u_s}\right]^{1/2} \tag{12}$$

From (9)

$$\frac{d\,\delta_L}{dx} = \left[\frac{70/13}{\left(1 + \frac{22}{13}\,\frac{u_i}{u_s}\right) Re_x} \right]^{1/2} \tag{13}$$

which gives with (11)

$$\frac{d\,\delta_v}{dx} = \frac{\mu}{\mu_L}\,\frac{u_i}{u_L}\left[1 + \frac{22}{13}\,\frac{u_i}{u_s}\right]^{-1/2}\left[\frac{280/117}{Re_x}\right]^{1/2} \tag{14}$$

Mass conservation in the vapor layer gives

$$\frac{d\,m_v}{dx} = \rho\,\frac{u_i}{2}\,\frac{d\delta_v}{dx} \tag{15}$$

Single Phase Liquid Layer: for this case equation (10) and (12) reduce to the Von Karman solutions

$$\frac{\delta}{x} = \frac{4.64}{Re_x^{1/2}} \tag{10A}$$

$$\tau_w = \frac{.323\,\rho_L\,u_s^2}{Re_x^{1/2}} \tag{12A}$$

Heat Transfer Relations:

Taking Reynolds analogy for the liquid and steam layers separately gives

$$\frac{q_L}{\rho_L\,u_L\,C_{pL}\,(T_i - T_s)} = \frac{\tau_i\,Pr^{-2/3}}{\rho_L\,u_L^2} \tag{16}$$

and

$$\frac{q_w}{\rho u_i C_p (T_w - T_i)} = \frac{\tau_w}{Pr\, \rho u_i^2} \tag{17}$$

For the vapor layer growth,

$$q_v = \rho \frac{d\delta_v}{dx} \frac{u_i}{2} \lambda \tag{18}$$

Energy balance

$$q_w = q_v + q_L \tag{19}$$

Putting

$$\beta_o = \frac{1}{2} C_p (T_w - T_i) / \lambda \tag{20}$$

and

$$\beta_{oL} = \frac{1}{2} C_{p_L} (T_i - T_s) / \lambda \tag{21}$$

equations (16) to (19) yield

$$\frac{Pr}{4\beta_o} \frac{\rho u_i^2}{\tau_w} \frac{d\delta_v}{dx} + \frac{\beta_{oL}}{\beta_o} \frac{Pr}{Pr_L^{2/3}} \frac{u_i}{u_L} - 1 = 0 \tag{22}$$

substituting for τ_w and $\frac{d\delta_v}{dx}$ from (12) and (14)

$$\frac{1.1961\, Pr}{\beta_o} \frac{\rho_\mu}{\rho_L \mu_L} \frac{u_L}{u_s} \left[\frac{u_i}{u_L}\right]^3 + \frac{\beta_{oL}}{\beta_o} \frac{Pr}{Pr_L^{2/3}} \frac{u_i}{u_L} \left[1 + \frac{22}{13} \frac{u_i}{u_s}\right]$$

$$- \left(1 + \frac{22}{13} \frac{u_i}{u_s}\right) = 0 \tag{23}$$

Putting

$$\frac{Pr}{\beta_o} \frac{\rho \mu}{\rho_L \mu_L} = K_1 \tag{24}$$

and

$$\frac{\beta_{o_L}}{\beta_o} \frac{Pr}{Pr_L^{2/3}} = K_2 \tag{25}$$

and $$\frac{u_i}{u_s} = \eta \tag{26}$$

and noting $\frac{u_L}{u_s} = 1 - \frac{u_i}{u_s}$ etc. from (4)

a solution can be obtained for the velocity ratio η, as

$$A\eta^3 + B\eta^2 + C\eta - 1 = 0 \tag{27}$$

where

$$A = 1.1961 K_1 - \frac{22}{13} K_2 - \frac{22}{13} \tag{28}$$

$$B = 31/13 + 9/13 K_2 \tag{29}$$

$$C = K_2 + 4/13 \tag{30}$$

Once equation (27) is solved for $\eta = u_i/u_s$ the other variables of interest can be readily obtained, i.e. from (12) and (12A) the friction coefficient ratio can be obtained as,

$$\frac{C_f}{C_{f_o}} = \left[1 - \frac{u_i}{u_s}\right]\left[1 + \frac{22}{13}\frac{u_i}{u_s}\right]^{1/2} \tag{31}$$

and a heat transfer parameter can be obtained as

$$\frac{Nu}{Re_x^{1/2}} \frac{\mu}{\mu_L} = .323\left[\frac{u_s}{u_i} - 1\right]\left[1 + \frac{22}{13}\frac{u_i}{u_s}\right]^{1/2} \tag{32}$$

Solutions for the velocity ratio u_i/u_s from equation (27) are shown for a wide range of the parameters in Figure 3.2. Figures 3.3 and 3.4 show the corresponding solutions for equation (31) and (32).

It is readily seen that for large values of the parameter

$$\frac{\beta_o}{Pr}\,\frac{\rho_L \mu_L}{\rho \mu}$$

the solution becomes insensitive to this parameter and then the solutions can be represented by single curves as shown on Figure 3.5. These curves become a good approximation to the solutions for say

$$\frac{\beta_o}{Pr}\,\frac{\rho_L \mu_L}{\rho \mu} > 10^4 \qquad \text{and} \qquad \frac{\beta_{oL}}{\beta_o}\,\frac{Pr}{Pr_L^{2/3}} > 0.05$$

It should be noted that for this case the velocity ratio can be obtained from equation (23) by neglecting the first term, as simply

$$\frac{u_i}{u_s} = \frac{1}{1 + K_2} \tag{33}$$

For a typical case of say water at 1 atmosphere with $T_s = 70^\circ F$, and $T_w = 1000^\circ F$, the magnitude of these parameters are

$$\frac{\beta_o}{Pr}\,\frac{\rho_L \mu_L}{\rho \mu} = 1.193 \times 10^4; \quad \frac{\beta_{oL}}{\beta_o}\,\frac{Pr}{Pr_L^{2/3}} = 0.178$$

Care should be used, however, in obtaining absolute values of the friction coefficient or heat transfer parameters from these approximate curves for very low values of $(\beta_{oL}/\beta_o)\,(Pr/Pr_L^{2/3})$.

Some results are given below for the case of laminar flow in a water-steam system.

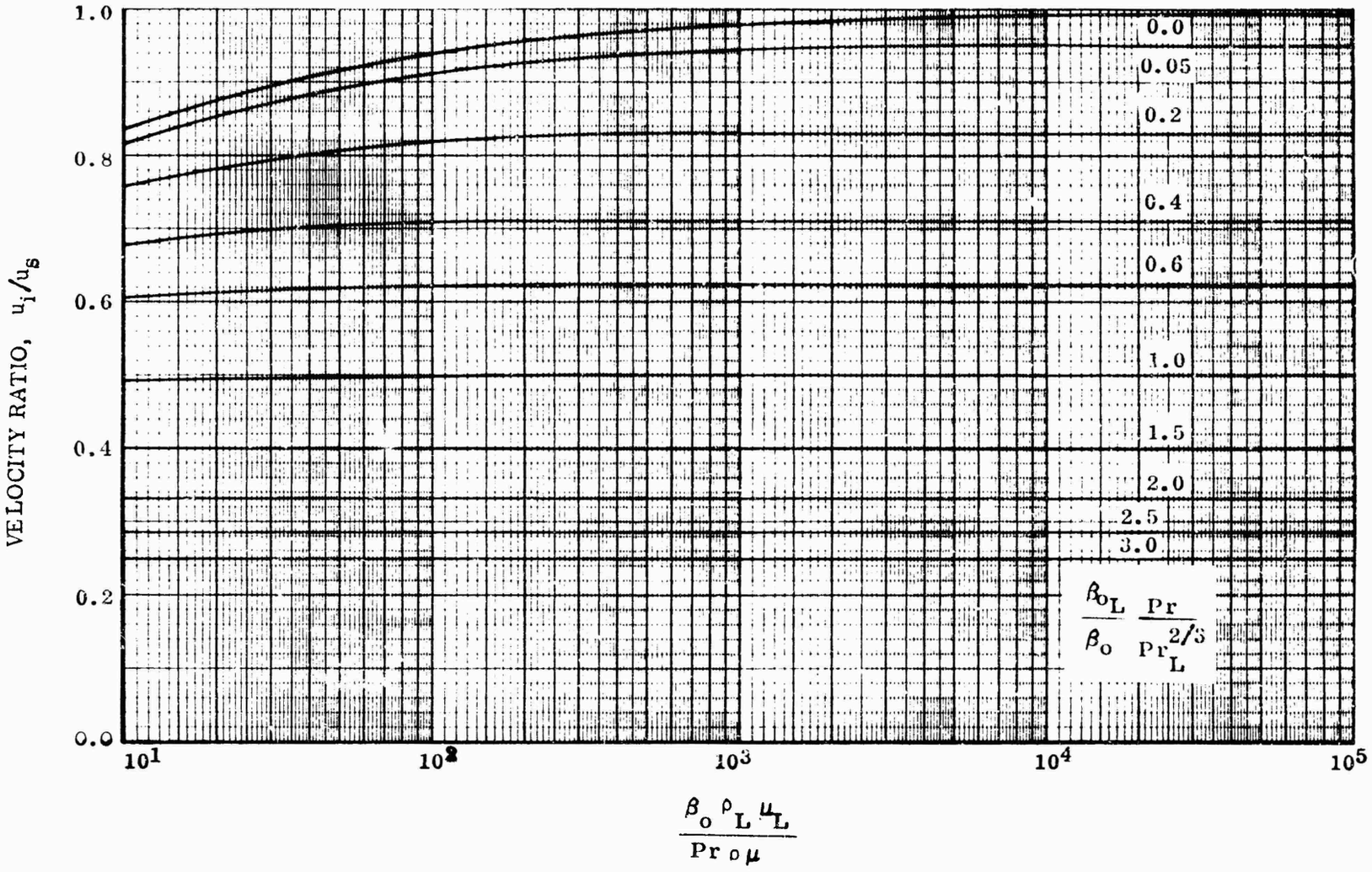

Figure 3.2. Laminar Flow Velocity Ratio

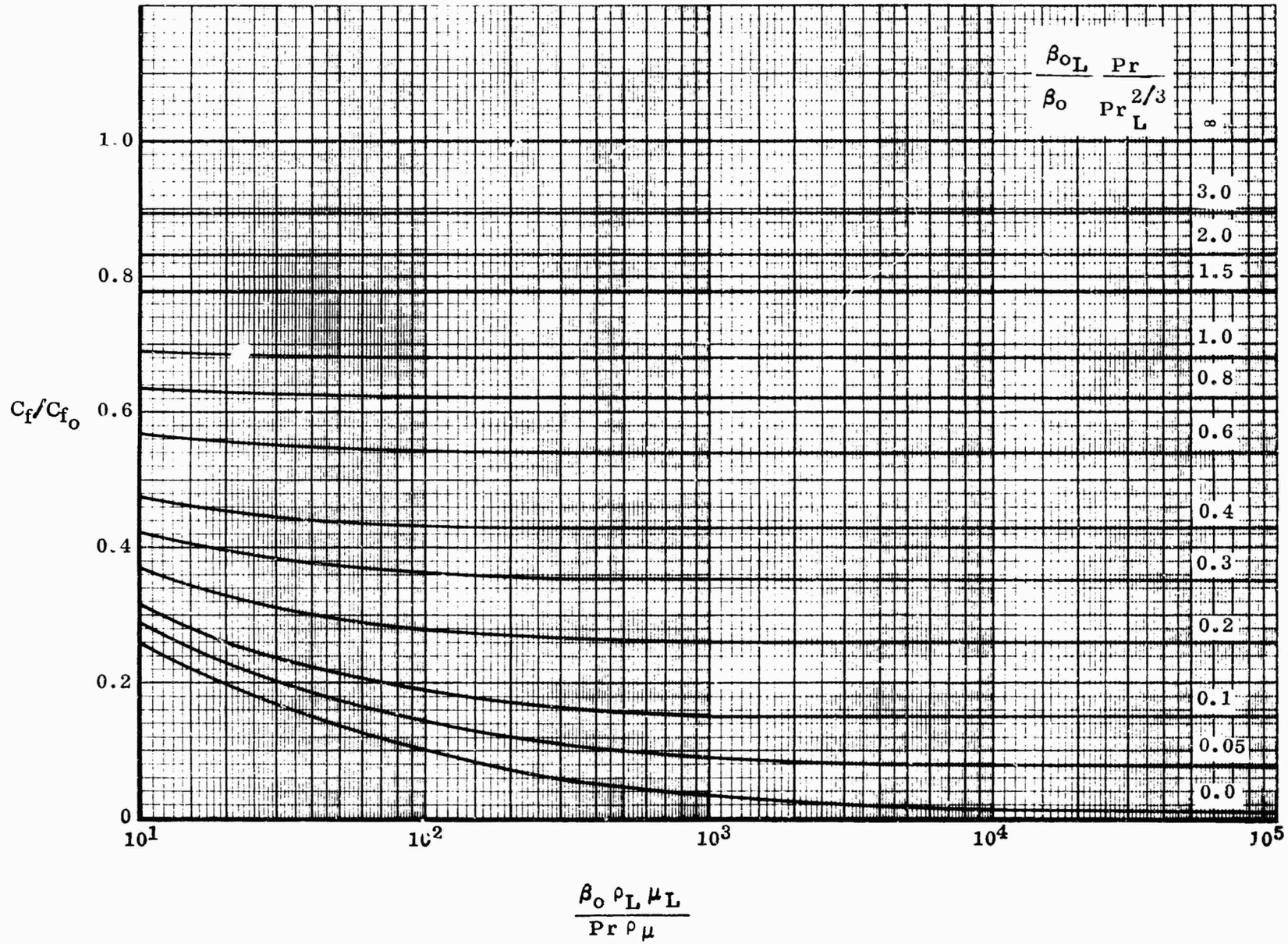

Figure 3.3 Laminar Flow Friction Coefficient

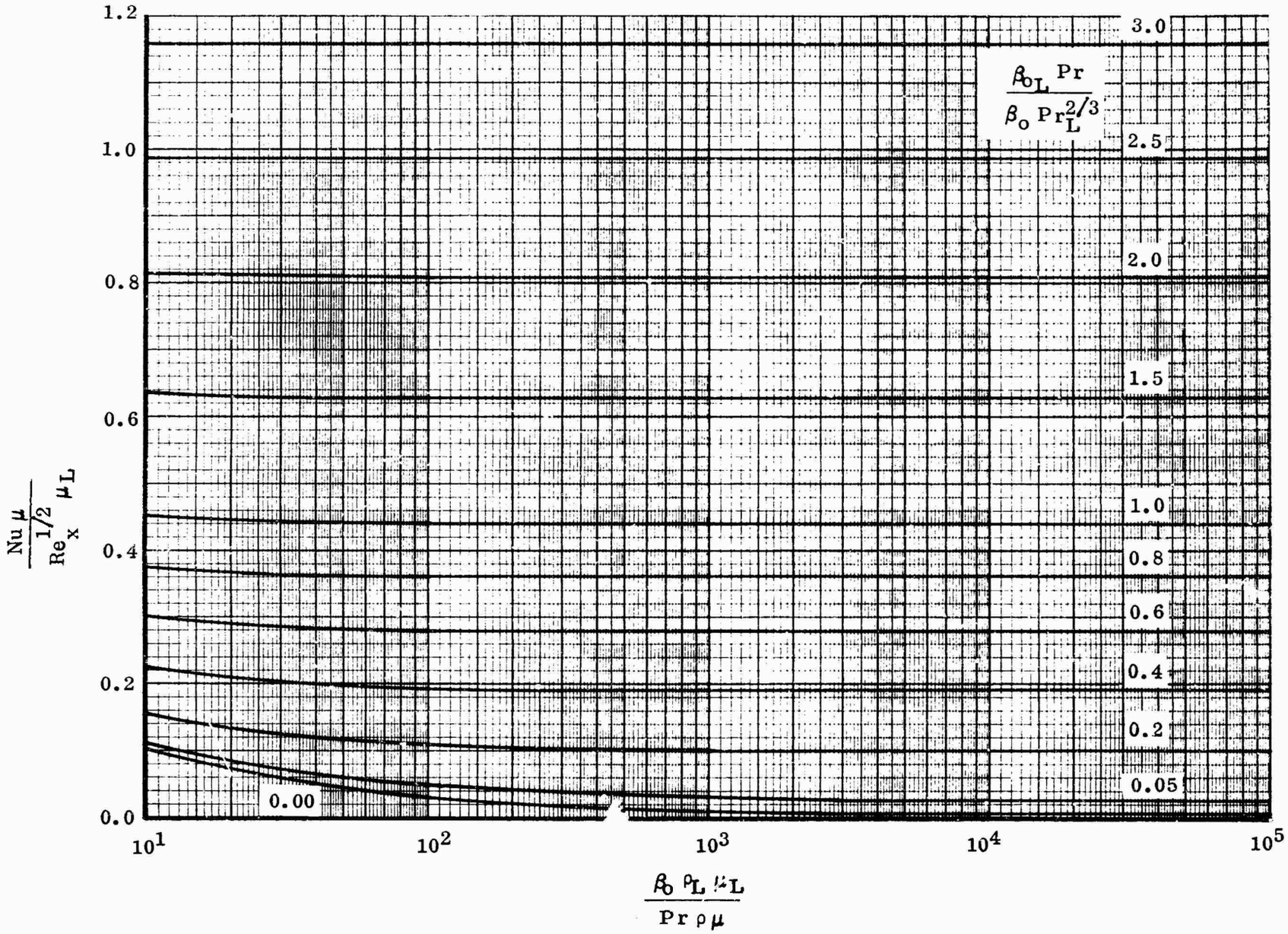

Figure 3.4. Laminar Flow Heat Transfer

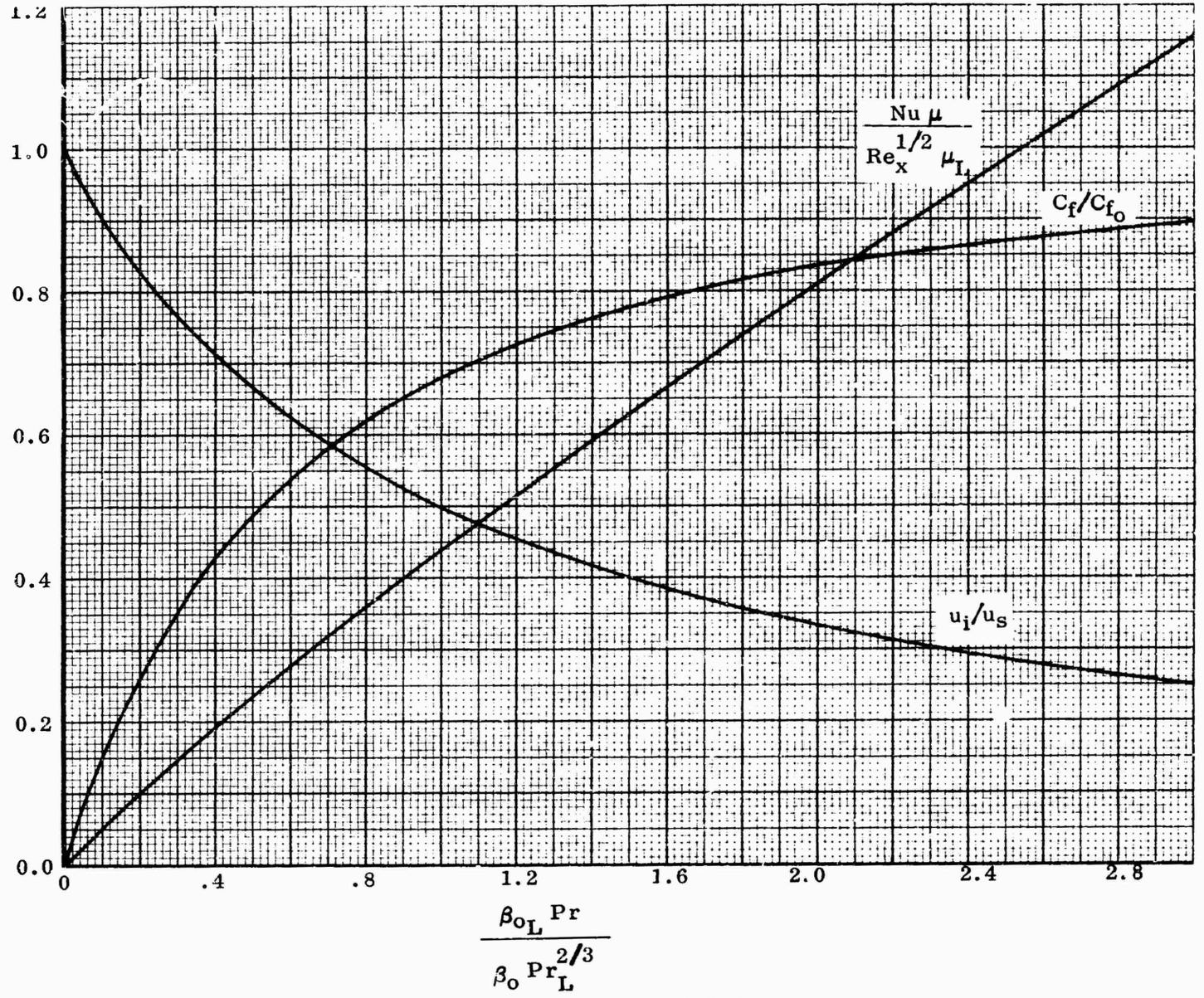

Figure 3.5. Laminar Flow Approximate Solutions

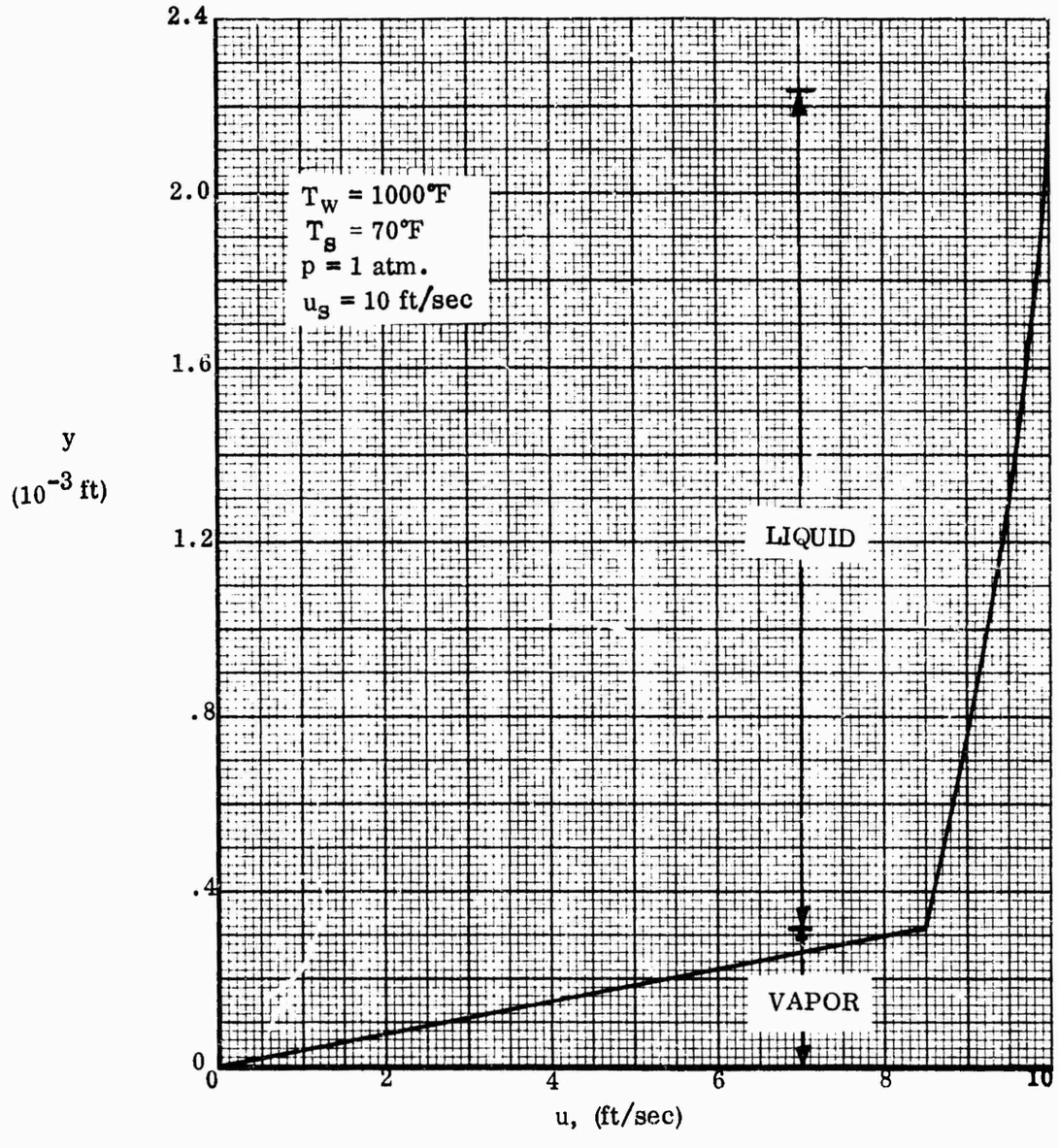

Figure 3.6. Laminar Flow Velocity Profile

$T_s = 70°F$ $p_s = 1$ Atm. $u_s = 10$ ft/sec $x = 1$ ft

T_w °F	1000	2000	3000
C_f/C_{f_o}	.236	.11	.08
q(BTU x HR^{-1} x Ft^{-2})	38,376	41,857	45,528

A computed velocity profile is shown in Figure 3.6.

3.2 Turbulent Flow

The assumptions for the laminar case are retained here, except that the liquid layer is turbulent. The case is considered when the vapor layer is extremely thin compared to the liquid layer, so that it can be considered as a laminar sublayer with a linear velocity profile as before. The thickness of the vapor layer will be computed for a typical case with water later.

The liquid layer is assumed to have a power-law profile. Referring to Figure 3.1 for notation

$$\frac{u_\ell}{u_L} = \left[\frac{y_1}{\delta_L}\right]^{1/7} \tag{34}$$

and as before the velocities are related by

$$u_s = u_i + u_L \tag{35}$$

A further assumption is that the empirical Blasius friction formula can be applied to the liquid layer in the following form

$$\tau_i = 0.0228\, \rho_L\, u_L^2 \left[\frac{\mu_L}{\rho_L\, u_L\, \delta_L}\right]^{1/4} \tag{36}$$

Applying the momentum integral equation to the liquid layer

$$I = \rho_L \int_0^{\delta_L} u\,(u_s - u)\,dy_1$$

giving on using (34) and (35)

$$I = \rho_L u_L^2 \left[\frac{7}{72} + \frac{1}{8}\frac{u_i}{u_L}\right]\delta_L \tag{37}$$

thus

$$\left[\frac{7}{72} + \frac{1}{8}\frac{u_i}{u_L}\right]\rho_L u_L^2 \frac{d\delta_L}{dx} = \tau_i = 0.0228\,\rho_L u_L^2 \left[\frac{\mu_L}{\rho_L u_L \delta_L}\right]^{1/4} \tag{38}$$

which gives on integrating,

$$\delta_L = \left[\frac{0.0285}{\frac{7}{72} + \frac{1}{8}\frac{u_i}{u_L}}\right]^{4/5} \left[\frac{\mu_L}{\rho_L u_L}\right]^{1/5} x^{4/5} + \text{constant} \tag{39}$$

The assumption is made that the constant in (39) is zero, similar to the approximation usually made for single-phase flow. This leads to the following result

$$\frac{\delta_L}{x} = \left[\frac{0.0285 \times 72/7}{1 + \frac{2}{7}\frac{u_i}{u_s}}\right]^{4/5} \left[\frac{u_L}{u_s}\right]^{3/5} Re_x^{-1/5} \tag{40}$$

when $u_L = u_s$ and $u_i = 0$, the single phase result is obtained as

$$\frac{\delta}{x} = \frac{0.376}{Re_x^{1/5}} \tag{40A}$$

Also,

$$\frac{d\delta_L}{dx} = \frac{4}{5}\left[\frac{2.052/7}{1 + 2/7\,u_i/u_s}\right]^{4/5} \left[\frac{u_L}{u_s}\right]^{3/5} \frac{1}{Re_x^{1/5}} \tag{41}$$

Continuity of shear stress at the interface gives

$$\tau_w = \tau_i = \mu \frac{u_i}{\delta_v} \tag{42}$$

so,

$$\frac{d\delta_v}{dx} = \mu\,\mu_i \frac{d}{dx}\left(\frac{1}{\tau_i}\right) \tag{43}$$

τ_w can be written from (36) and (40) as

$$\tau_w = \tau_i = \frac{0.0296\,\rho_L\,u_s^2}{Re_x^{1/5}}\left[1+\frac{2}{7}\,\frac{u_i}{u_s}\right]^{1/5}\left[\frac{u_L}{u_s}\right]^{8/5} \tag{44}$$

and (43) becomes

$$\frac{d\,\delta_v}{dx} = \frac{\mu u_i}{5\,x\,\tau_w} \tag{45}$$

Heat Transfer Relations

Taking Reynolds analogy for the steam and liquid layers as before,

$$\frac{q_L}{\rho_L\,u_L\,C_{p_L}\,(T_i - T_s)} = \frac{Pr_L^{-2/3}\,\tau_i}{\rho_L\,u_L^2} \tag{46}$$

and

$$\frac{q_w}{\rho\,u_i\,C_p\,(T_w - T_i)} = \frac{\tau_w}{Pr\,\rho\,u_i^2} \tag{47}$$

For the vapor layer growth,

$$q_v = \rho\,\frac{d\,\delta_v}{dx}\,\frac{u_i}{2}\,\lambda \tag{48}$$

Energy Balance

$$q_w = q_v + q_L \tag{49}$$

(46), (48) and (49) yield

$$h = \frac{C_p}{4\,\beta_o}\,\rho\,u_i\,\frac{d\,\delta_v}{dx} + C_p\,\frac{\beta_{o_L}}{\beta_o}\,\frac{\tau_w}{u_L\,Pr_L^{2/3}} \tag{50}$$

substituting (50) in (47) and using (43) and (44), the following can

be obtained

$$\frac{Pr}{20\beta_o}\,\frac{\rho\mu}{\rho_L\mu_L}\,\frac{\left[1+22/13\;u_i/u_s\right]^{-2/5}}{0.0296^2\,Re_x^{3/5}}\left[\frac{u_i}{u_s}\right]^3\left[\frac{u_s}{u_L}\right]^3\left[\frac{u_s}{u_L}\right]^{1/5}$$

$$+\frac{Pr}{Pr_L^{2/3}}\,\frac{\beta_{o_L}}{\beta_o}\,\frac{u_i}{u_L}-1=0 \tag{51}$$

Putting $\alpha = u_i/u_L$ (52)

$$K_3 = Re_x^{3/5}\,\frac{\beta_o}{Pr}\,\frac{\rho_L\mu_L}{\rho\mu} \tag{53}$$

and

$$K_4 = \frac{Pr}{Pr_L^{2/3}}\,\frac{\beta_{o_L}}{\beta_o} \tag{54}$$

Also, let

$$E = \left[K_3 \times 20 \times .0296^2\right]^{-1} \tag{55}$$

Then (51) can be written

$$E\,(1+\alpha)^{3/5}\,(1+9/7\,\alpha)^{-2/5}\,\alpha^3 + K_4\,\alpha - 1 = 0 \tag{56}$$

Equation (56) in α is the basic equation to be solved. Once α is known, the other results can be readily obtained.

One difficulty is that the equation in α contains a term with Re_x. It was implicitly assumed throughout that $\alpha = u_i/u_L$ was independent of x. Hence the solution is approximately correct only provided the dependence on x is very weak.

When equation (56) is solved for α the other major variables can be obtained, e.g., u_i/u_s can be obtained from (35).

The friction coefficient ratio is obtained from (44) as

$$\frac{C_f}{C_{f_o}} = \left[1 + \frac{22}{13}\frac{u_i}{u_s}\right]^{1/5}\left[\frac{u_L}{u_s}\right]^{8/5} \tag{57}$$

and the heat transfer coefficient parameter can be obtained as

$$\frac{Nu}{Re_x^{4/5}}\frac{\mu}{\mu_L} = 0.0296\left[1 + \frac{22}{13}\frac{u_i}{u_s}\right]^{1/5}\left[1 - \frac{u_i}{u_s}\right]^{8/5}\left[\frac{u_s}{u_i}\right] \tag{58}$$

Equation (56) has been solved for a wide range of conditions to specify u_i/u_s, C_f/C_{f_o} and the heat transfer parameter. The results are shown in Figure 3.7, 3.8 and 3.9. It is apparent that the results are insensitive to the parameter $Re_x^{3/5}\frac{\beta_o}{Pr}\frac{\rho_L}{\rho}\frac{\mu_L}{\mu}$ and hence Re_x; for the cases being considered here a minimum value of the parameter is about 10^6-10^7. Under these conditions the results can be represented by single curves as shown in Figure 3.10, provided the value of $\frac{\beta_{oL}}{\beta_o}\frac{Pr}{Pr_L^{2/3}}$ is not extremely low.

Under these conditions the first term of equation (56) has negligible influence and the solution for the velocity ratio becomes

$$\frac{u_i}{u_L} = \frac{1}{K_4} \tag{59}$$

and

$$\frac{u_i}{u_s} = \frac{1}{1 + K_4} \tag{60}$$

which is the same result as for laminar flow. The same result is obtained in both cases, since neglecting the influence of the parameters in equation (24) and (53) is equivalent to the assumption that the heat transferred to maintain growth of the vapor layer is negligible compared to the heat transferred to

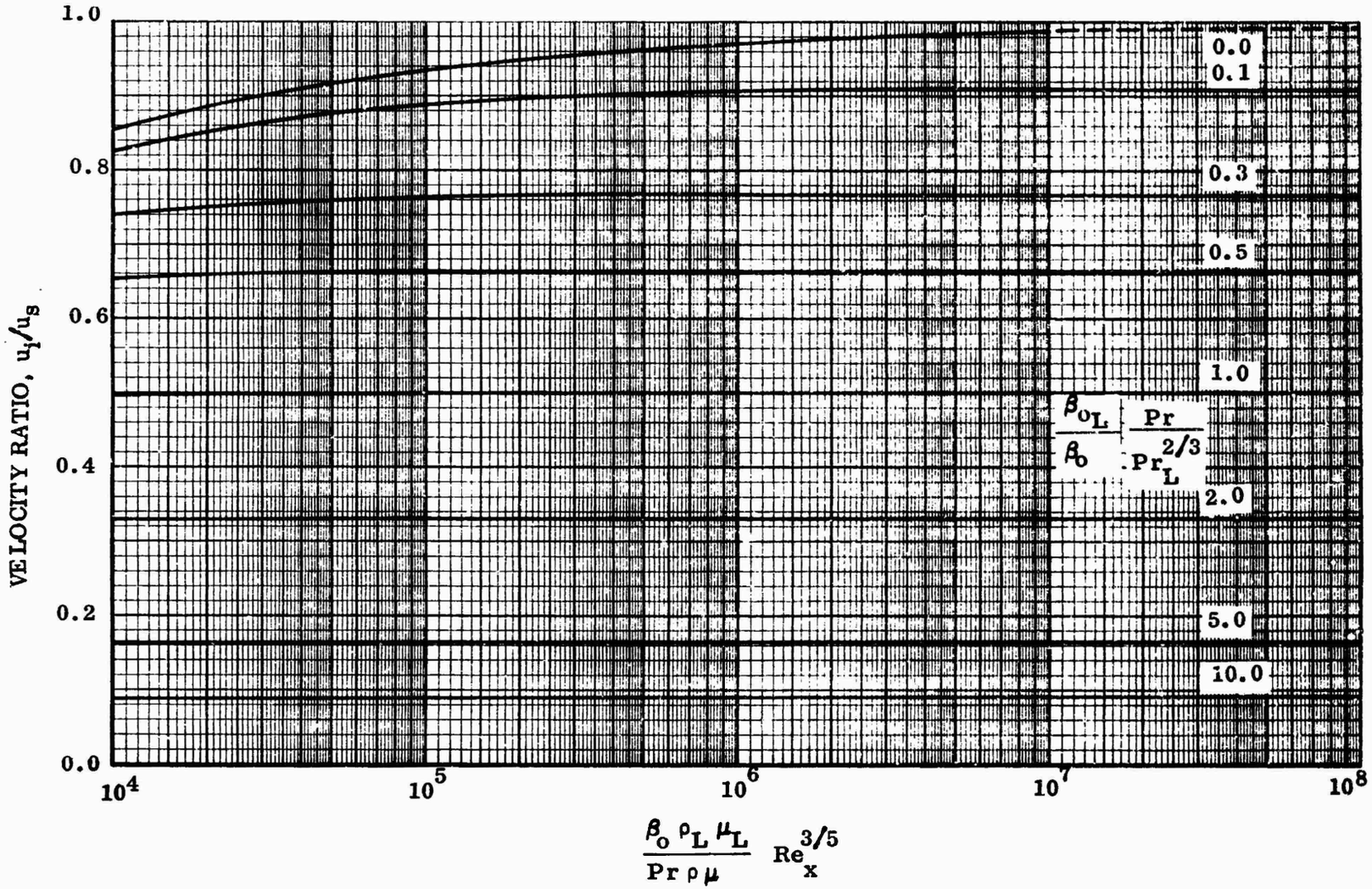

Figure 3.7. Turbulent Flow Velocity Ratio

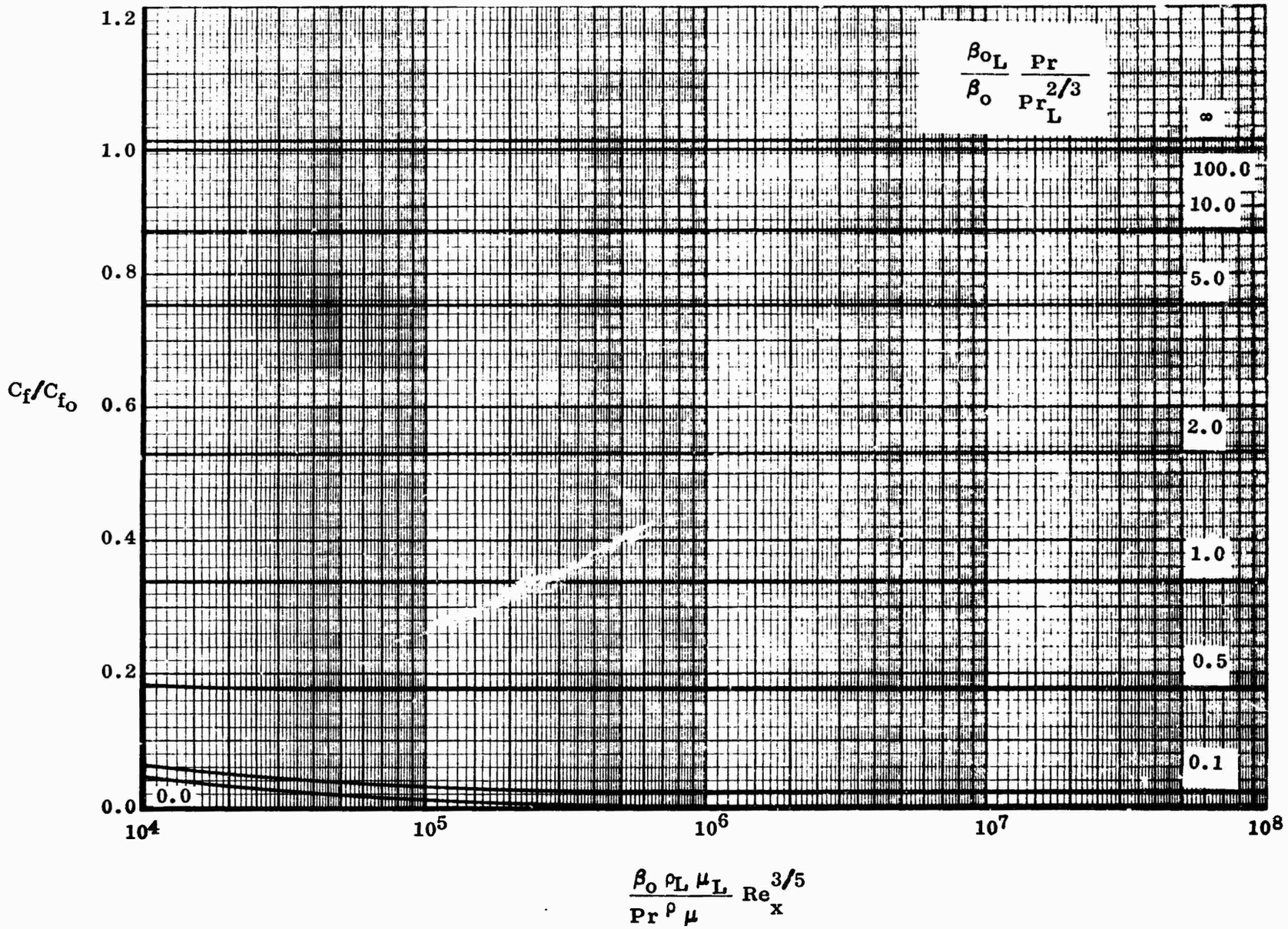

Figure 3.8. Turbulent Flow Friction Coefficient

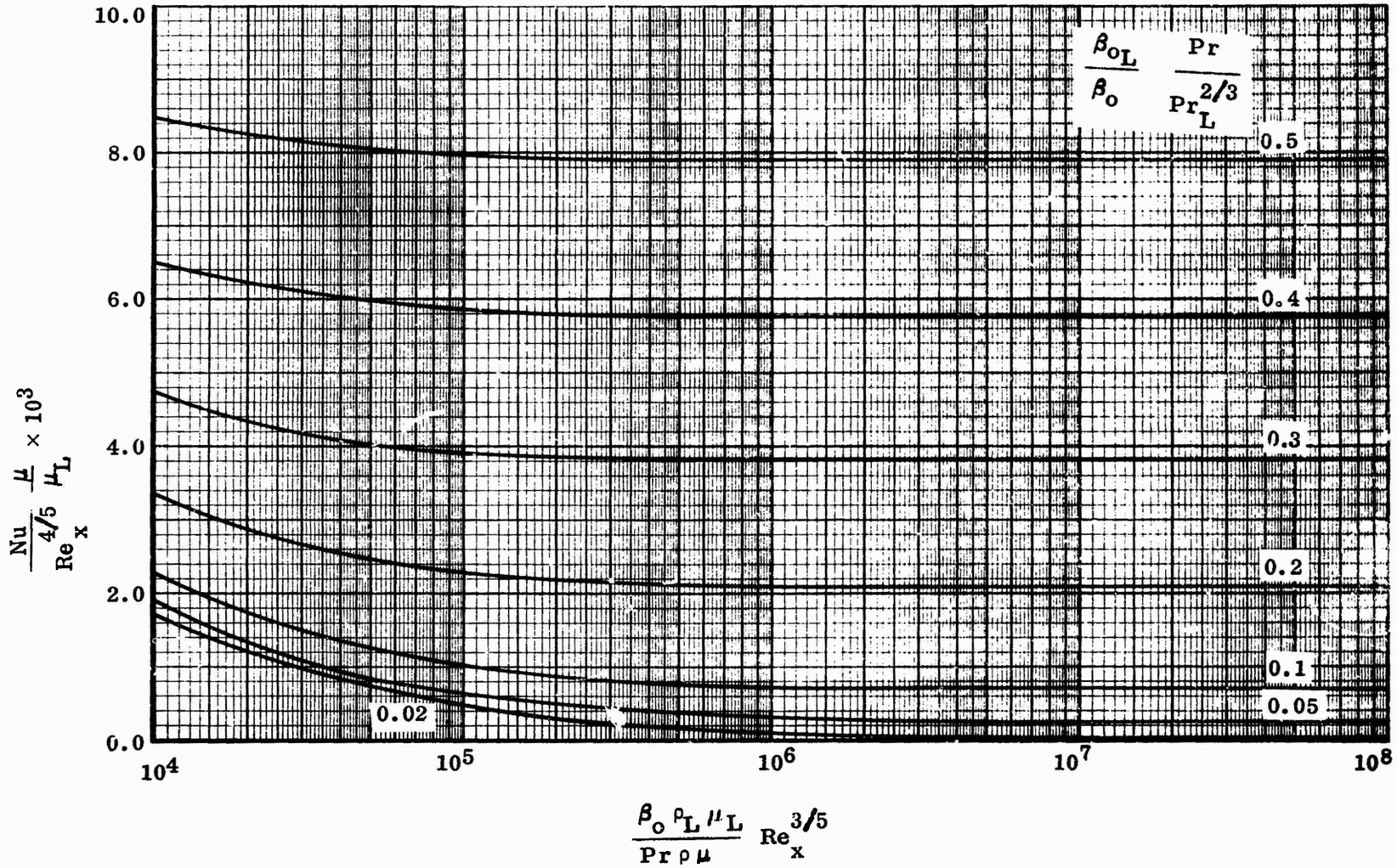

Figure 3.9. Turbulent Flow Heat Transfer

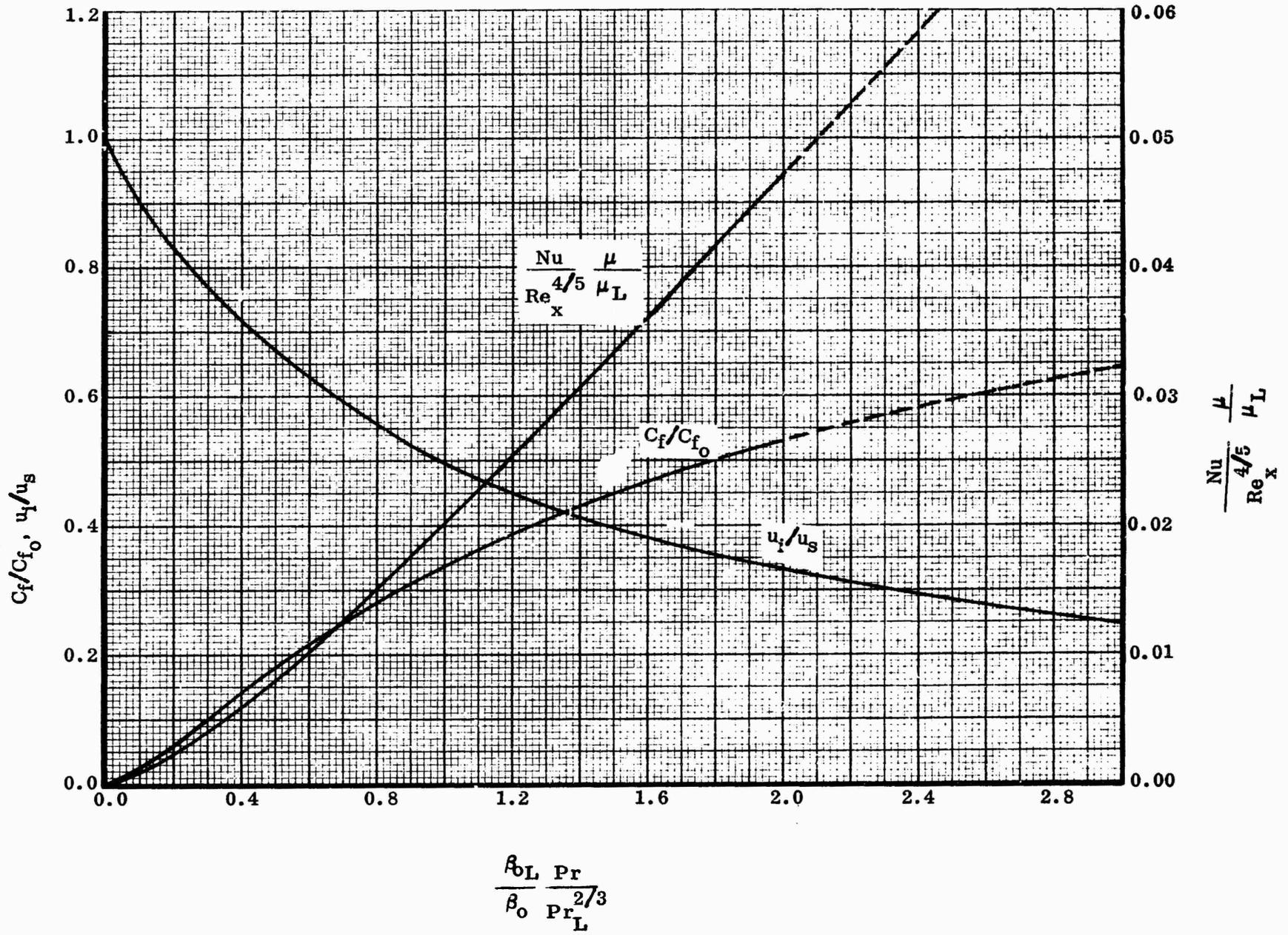

Figure 3.10. Turbulent Flow Approximate Solutions

the liquid. Reynolds analogy applies to the laminar and turbulent liquid layers in the same form.

The case of flow in water was examined for the following conditions

u_s = 50 ft/sec

x = 10 ft

T_w = 1000°F

T_s = 70°F

p = 1 Atm.

The results obtained were as follows

C_f/C_{f_o} = .051

q = 116,230 BTU x hr^{-1} x ft^{-2}

$\frac{\delta_v}{\delta_L} = 6.098 \times 10^{-3}$

δ_L = .0294 ft

For the pure liquid phase the boundary layer thickness was computed as 0.11 feet. These results indicate that the assumption of an extremely thin vapor layer compared to the liquid boundary layer thickness may be valid for many practical conditions.

Consider the case of flow in water over a constant temperature plate with an initial film boiling laminar boundary layer and then transition to fully turbulent flow occurring along the plate length. A description of the flow is provided by the above analyses. The vapor film will serve as a thin lubricating sheet which reduces friction drag and will also act as an insulation layer between the hot wall and the water. Calculations indicate that the steam layer is considerably thinner for fully developed turbulent flow than for the laminar case. Thus the transition region should be characterized

by a mixed-phase flow in the boundary layer until the excess vapor is absorbed by the fluid. Such a "froth" flow was reported by Bradfield, et al[7], at transition from laminar flow. It might also be expected that the onset of turbulent flow may be suppressed by film boiling and it was suggested by Bradfield et al[7] that transition may depend on a Reynolds number based on the relative velocity of the liquid. The results of the analyses here suggest that the relative velocity of the liquid is the same for either laminar or turbulent flow for the same stream condition and wall temperature. This may support to some extent the assumed value of the constant in equation (39).

3.3 Application of Film Boiling to Drag Reduction

A possible application is considered to be an underwater vehicle propelled by a solid rocket. This is considered because it offers a convenient means of supplying heat to the external wall of the vehicle besides providing propulsive power. Rockets are generally competitive with gas generator systems only for a restricted range of high speed missions[12] due to the low propulsive efficiency of rocket propulsion at low running speeds relative to the exhaust jet velocity.

The foregoing analyses have indicated that considerable skin friction drag reduction can be achieved in both the laminar and turbulent flow regimes. However heat energy is required to be expended to achieve this drag reduction. It is of interest therefore to compare the efficiency of this concept with the propulsive efficiency of the cold-wall rocket propelled system.

Defining a coefficient of performance as

$$C.O.P = \frac{\text{Drag energy overcome}}{\text{Heat energy expended}} \qquad (61)$$

Then,

$$C.O.P. = \frac{1/2\,\rho_L\, u_s^2\,(C_{f_o} - C_f)}{h\,(T_w - T_i)}$$

From the preceding equations, it can be shown that for laminar flow,

$$C.O.P. = \frac{.323\,[\,1 - C_f/C_{f_o}\,]}{C_p\,(T_w - T_i)\,\gamma_1}\; u_s^2 \qquad (62)$$

where γ_1 is the heat transfer parameter

$$\gamma_1 = \frac{Nu}{Re_x^{1/2}}\,\frac{\mu}{\mu_L} \qquad (63)$$

and for turbulent flow,

$$C.O.P. = \frac{0.0296\,[\,1 - C_f/C_{f_o}\,]}{C_p\,(T_w - T_i)\,\gamma_2}\; u_s^2 \qquad (64)$$

where γ_2 is the heat transfer parameter

$$\gamma_2 = \frac{Nu}{Re_x^{4/5}}\,\frac{\mu}{\mu_L} \qquad (65)$$

Values of C.O.P. were examined for the case of water at 1 atm. Figure 3.11 shows the results for turbulent flow which is of interest here. Also shown on Figure 3.11 is the propulsive efficiency for a solid propellant system without film boiling, with an assumed rocket I_{sp} = 215 sec. The propulsive efficiency can be obtained from

$$\eta_p = \frac{2\,u_e/u_s}{(u_e/u_s)^2 + 1}$$

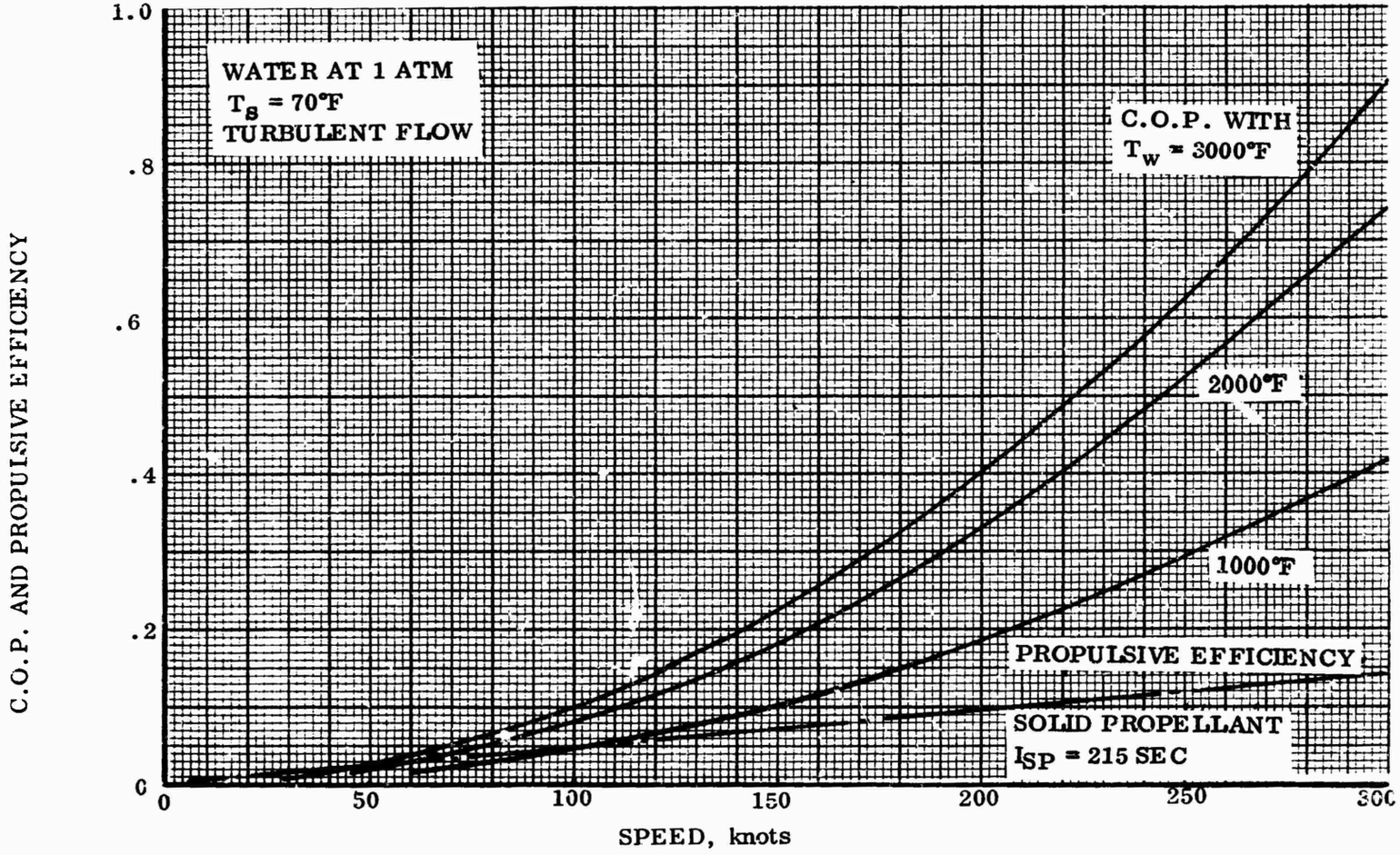

Figure 3.11. Coefficient of Performance Versus Velocity

or in terms of I_{sp} as

$$\eta_p = \frac{2g\, I_{sp}/u_s}{(g\, I_{sp}/u_s)^2 + 1} \tag{66}$$

Examination of Figure 3.11 reveals that under the conditions considered an advantage is indicated with film boiling at a velocity of 50 to 100 knots depending on the surface temperature. The indicated efficiency of film boiling drag reduction increases rapidly above these velocities.

3.4 Discussion of Analytical Results

It should be noted that the results of the turbulent flow analysis must be regarded as approximate only. This analysis was undertaken as a guide to the experimental investigations necessary to establish turbulent forced-convection film boiling data. The fundamental assumptions here were

i) a very thin, laminar, vapor layer exists at the wall, which can be assumed to have approximately linear velocity and temperature profiles

ii) the liquid layer can be assumed to have a power profile law and the empirical Blasius friction formula can be applied to the liquid layer in the form of equation (36).

The assumptions should be checked and modified where necessary from the results of an experimental program. Observations are required too, on the transition "froth" flow, in particular to observe if a stable two-phase layer re-occurs after fully turbulent flow is established in the liquid layer.

REFERENCES

1. Little, R. C., "A review of 6.1 Work Units in Drag Reduction with Emphasis on Current Problems, Progress and Landmarks," NRL Memorandum Report 1957 (Jan. 1969)

2. Lumley, J. L., "The Toms Phenomenum: Anamalous Effects in Turbulent Flow of Dilute Solutions of High Molecular Weight Linear Polymers," Appl. Mech. Rev. 20, 1139, (Dec. 1967)

3. Bradfield, W. S., "Film Boiling on Hydrodynamic Bodies," Convair Scientific Research Laboratory, Res. Note 37, (Dec. 1960), A 26526

4. Jacobson, R. N., Shair, F. H., "Film Boiling from a Sphere During Forced Convection of Subcooled Water." I.&.E.C. Fundamentals, 9, 183, Feb. 1970

5. Bromley, L. A., LeRoy, N. R., Robbers, J. A., "Heat Transfer in Forced Convection Film Boiling," Ind. Eng. Chem., 45, 2639 (1953)

6. Bradfield, W. S., "Plane Laminar Forced Convection Film Boiling with Subcooling," Convair Scientific Research Laboratory, Res. Note 35, (July 1960), A 24812

7. Bradfield, W. S., Barkdoll, R. O., Byrne, J. T., "Some Effects of Boiling on Hydrodynamic Drag," Int. J. Heat and Mass Transfer, 5, 615 (1962)

8. Cess, R. D., Sparrow, F. M., "Film Boiling in a Forced-Convection Boundary-Layer Flow," Trans. A.S.M.E., J. Heat Transfer, 83, 370 (1961)

9. Cess, R. D., Sparrow, E. M., "Subcooled Forced-Convection Film Boiling on a Flat Plate," Trans. A.S.E.M., J. Heat Transfer, 83, 377 (1961)

10. Ito, T., Nishikawa, K., "Two-Phase Boundary-Layer Treatment of Forced Convection Film Boiling," Int. J. Heat and Mass Transfer, 9, 117 (1966)

11. Eckert, E. R., Drake, R. M., Jr., Heat and Mass Transfer (2nd Ed.), McGraw Hill, New York (1959)

12. Tryk, D. E., "Applications of Extended Burning Rate Solid Propellants to High Speed Underwater Rockets," AIAA Paper 64-462 (1964)

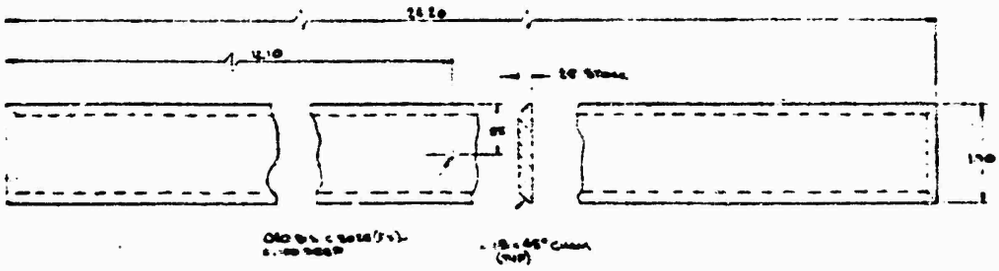

-15 END PLATE

MATL: CARBON - ALLOY STEEL

2 REQD

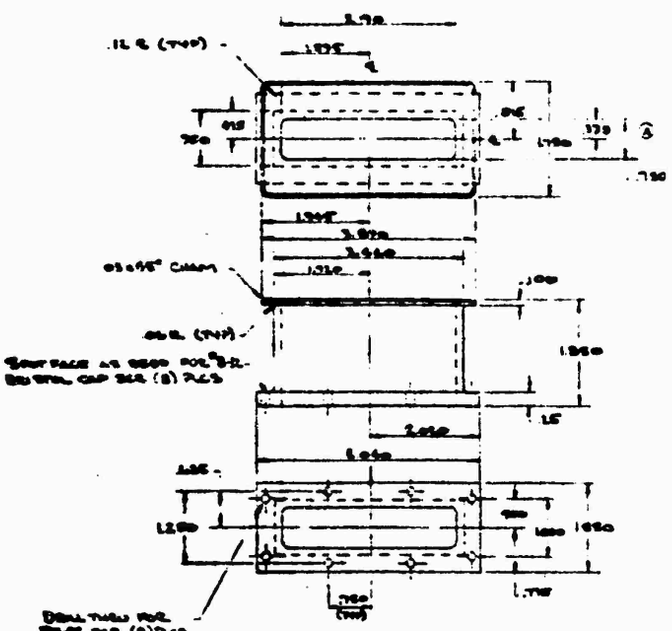

-13 ADAPTER

MATL: 316 SS

1 REQD

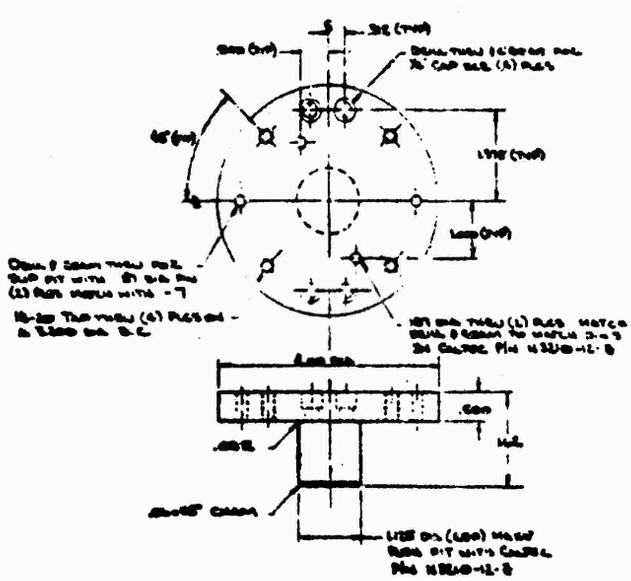

-21 ADAPTER

MATL: [illegible]

1 REQD

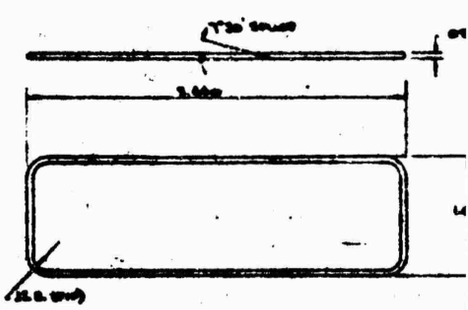

-23 O-RING

MATL: [illegible]

[illegible] REQD

A

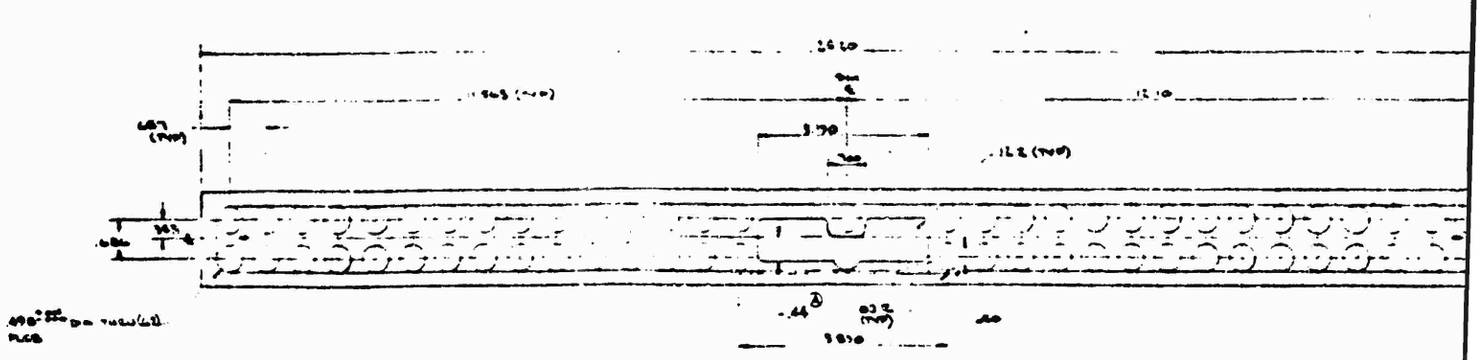

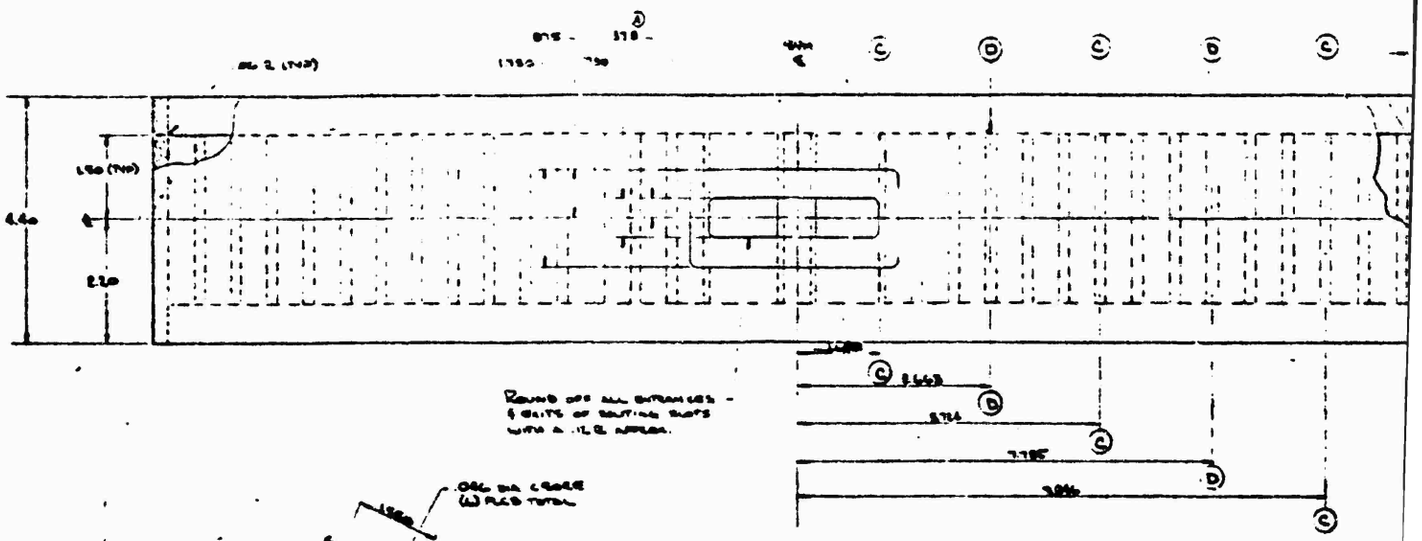

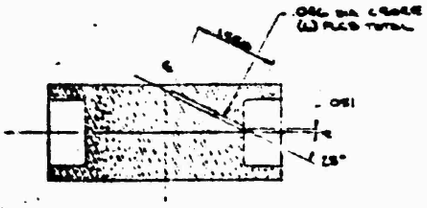

SECTION C-C

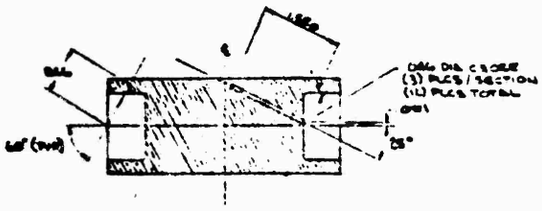

SECTION D-D

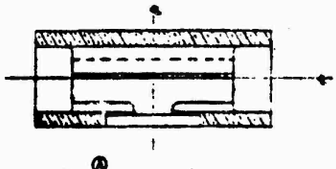

SECTION @ ℄ SLOT

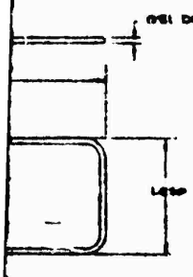

-11 MODEL

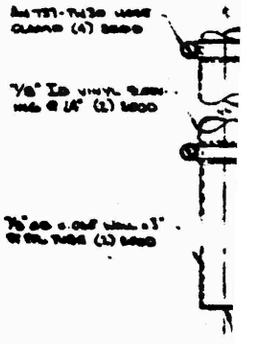

-RING

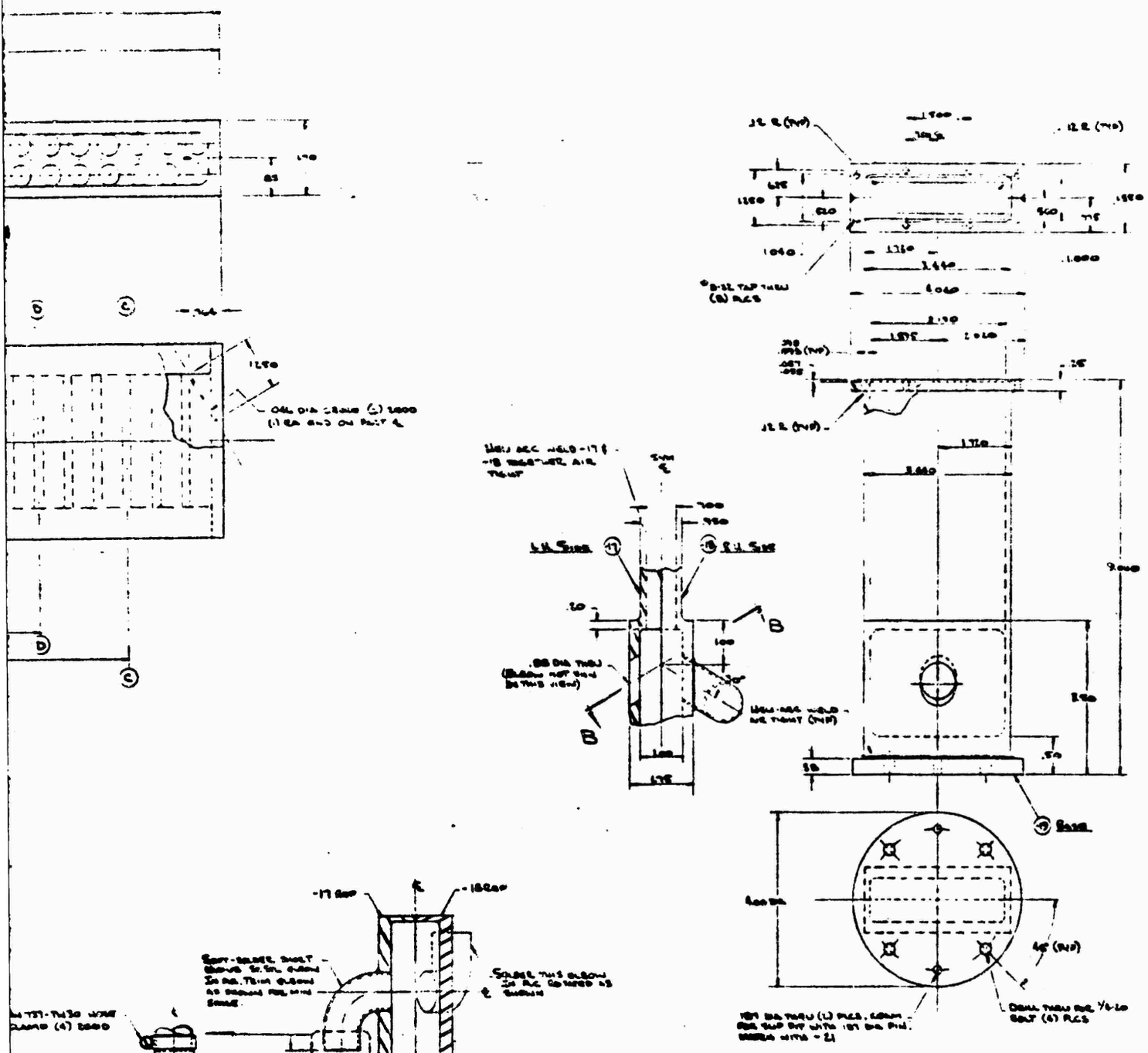

SECTION B-B

-9 STRUT ASSY

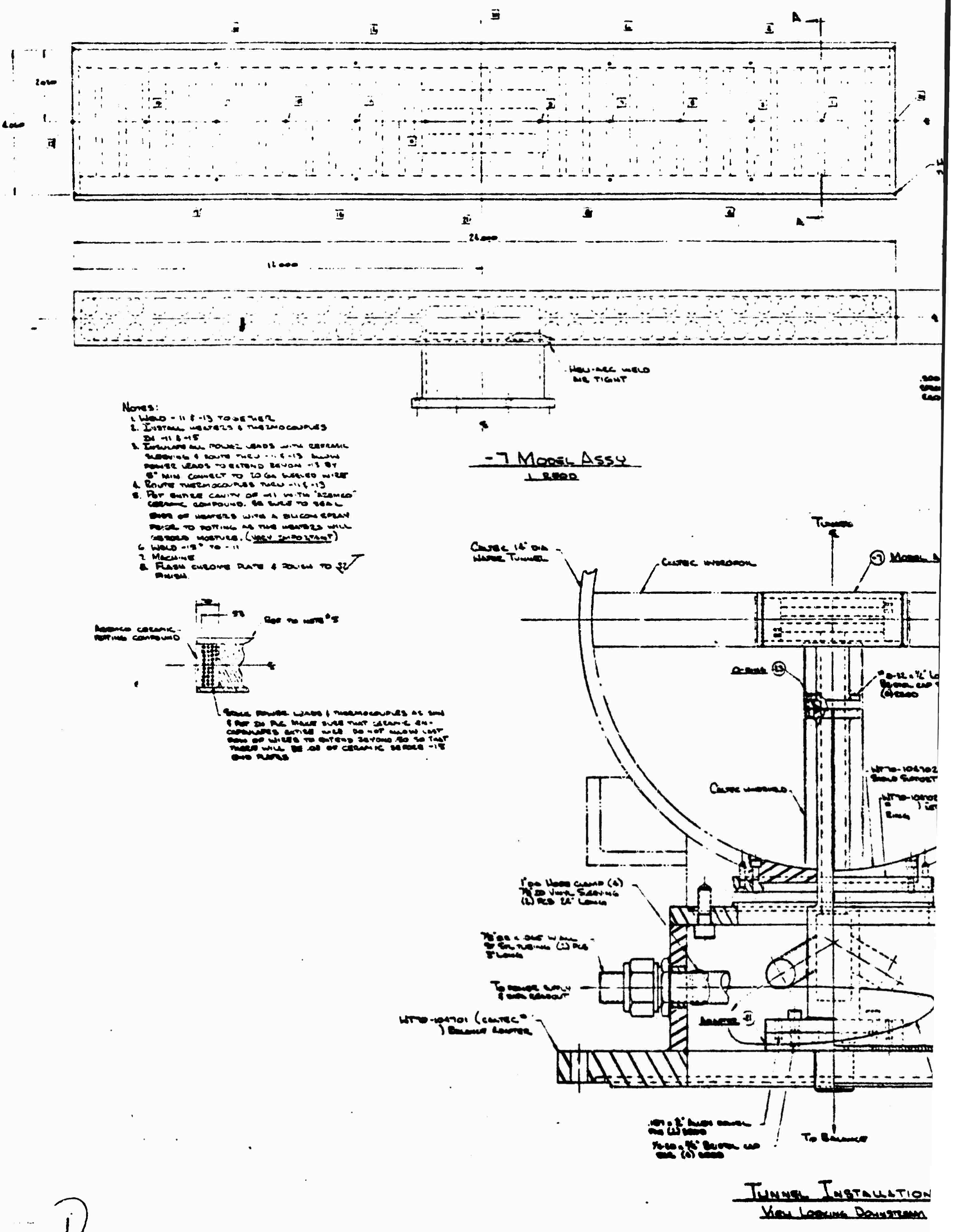
24.000
12.000
Heli-arc weld air tight
Notes:
1. Weld -11 & -13 together
2. Install heaters & thermocouples in -11 & -15
4. Route thermocouples thru -11 & -13
(Very important)
7. Machine
8. Flash chrome plate & polish to 32 finish
-7 Model Assy
Caltec 14" dia water tunnel
Caltec hydrofoil
O-ring
To balance
Tunnel Installation
View Looking Downstream

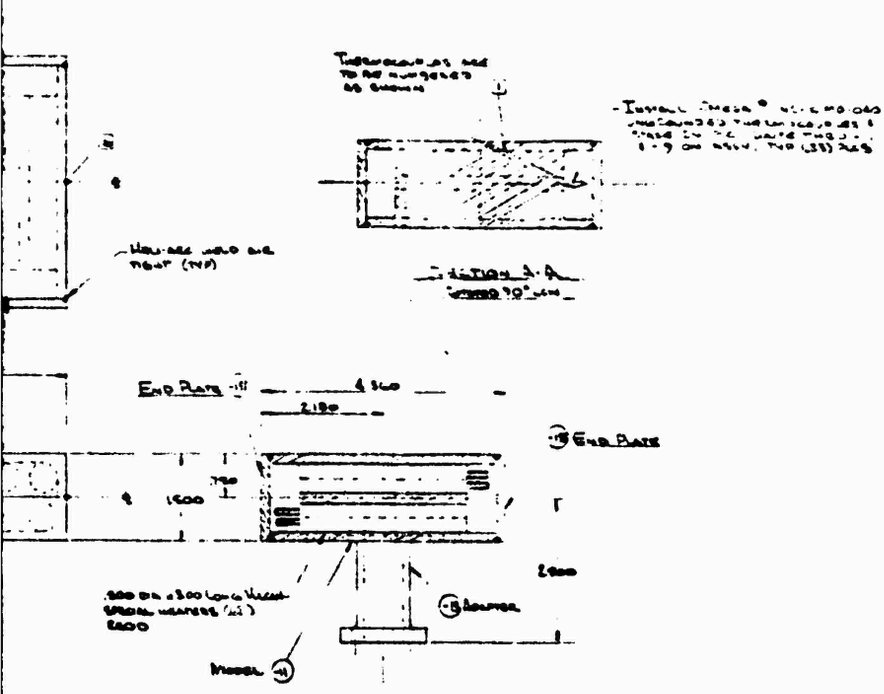

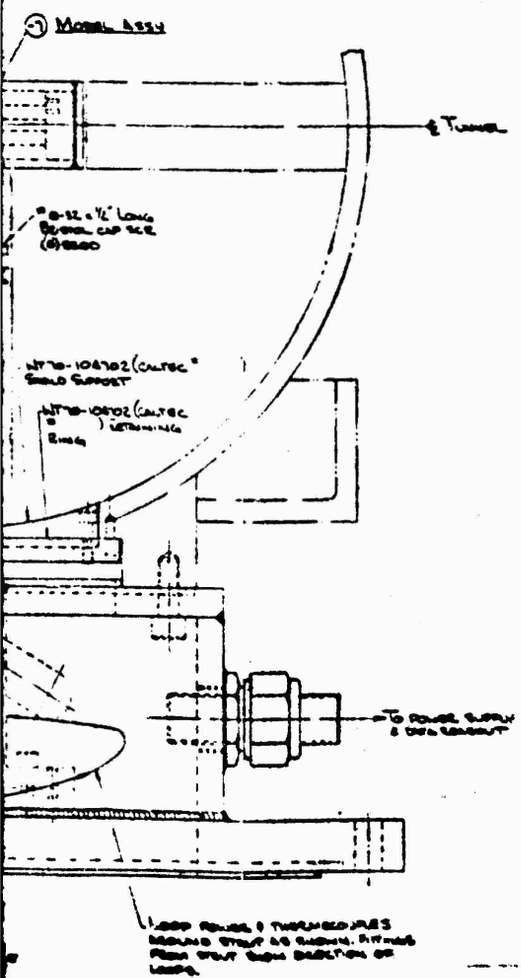

4				4
	13			13
	14			14
2'				2'
	4mm'			4mm'
	4mm'			4mm'
				2
				2
				8
				2

WT70-104706 A

		-13				A
		-14				
		-15				1
1/4		-16				1/4
	2	-18				2
	1	-19				1
	1	-21				1
—		-8				
	—	-7				
-9	-7					

DETAIL & ASSEMBLY

CSUMD Conver Wind Tunnel

WT-70-104703

SECTION A-A

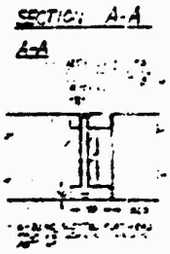

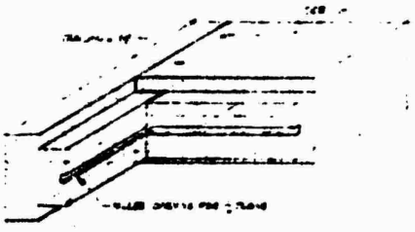

VIEW OF CULVERT

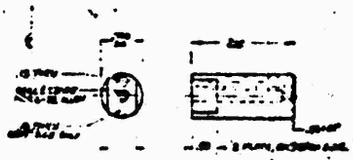

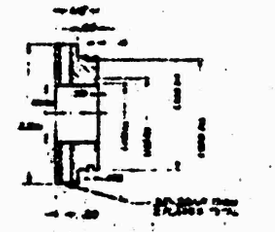

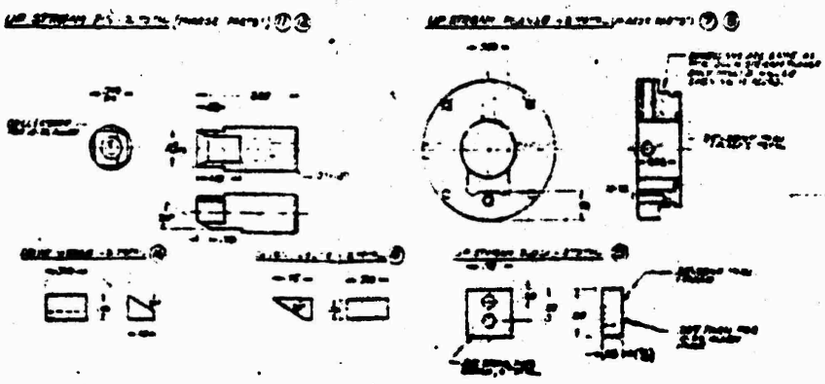

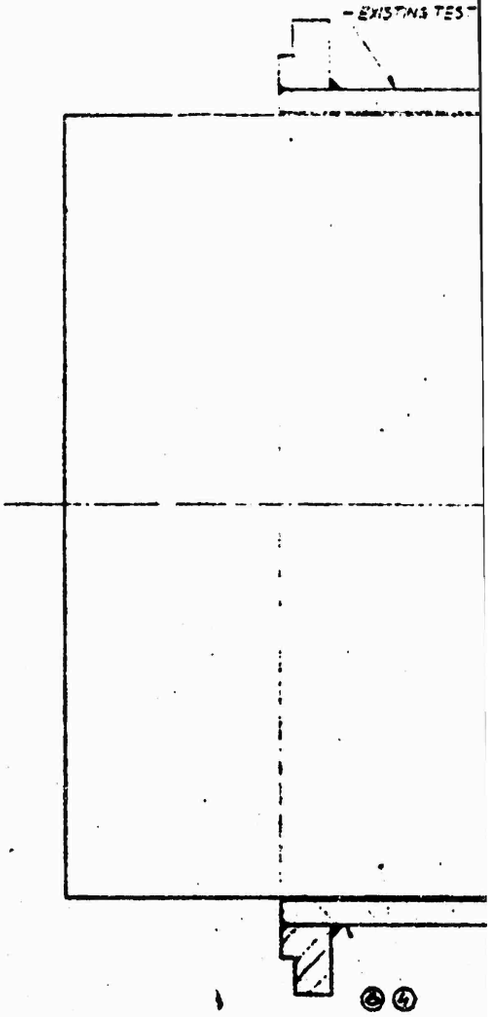

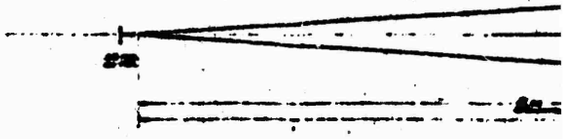

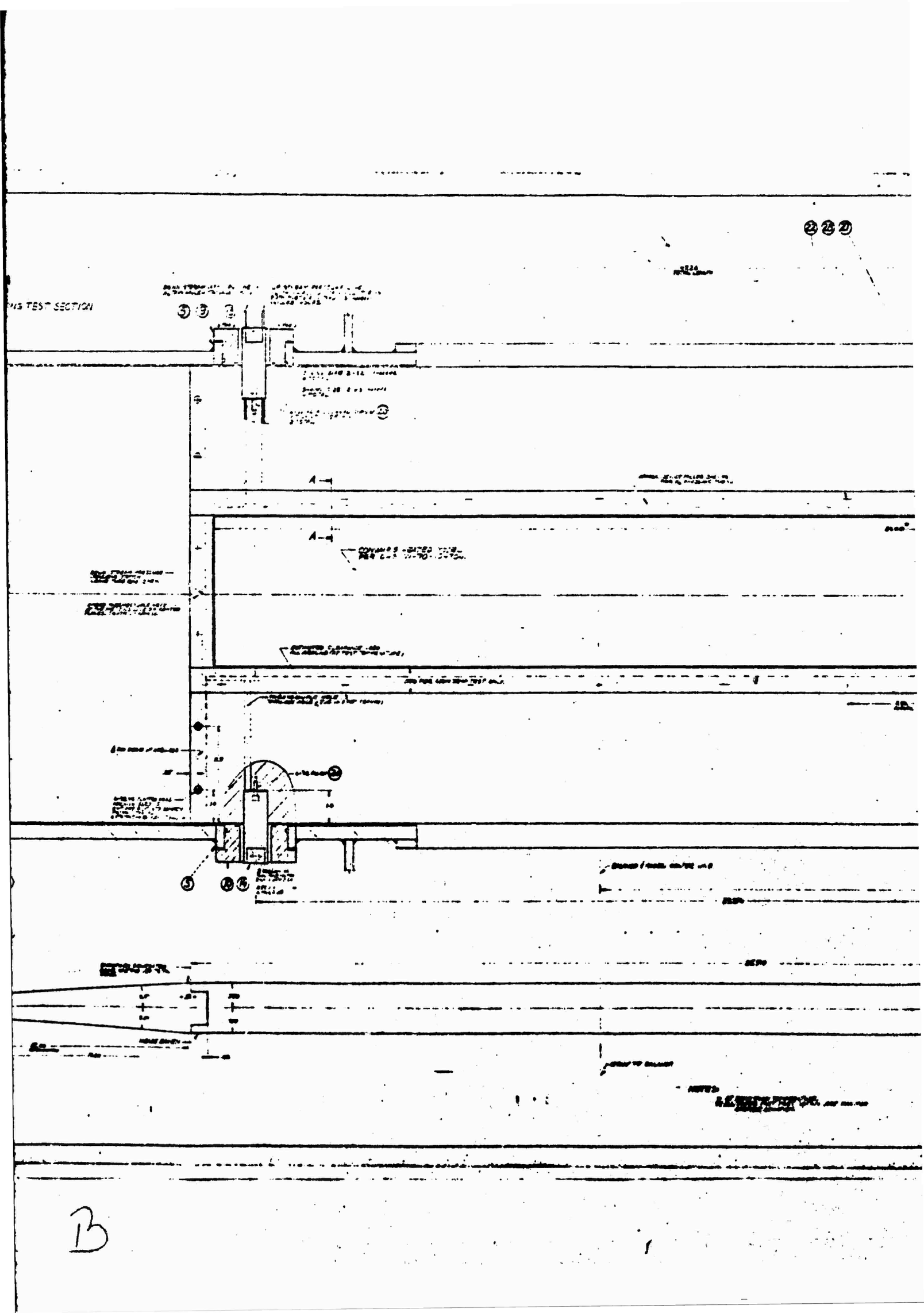

B

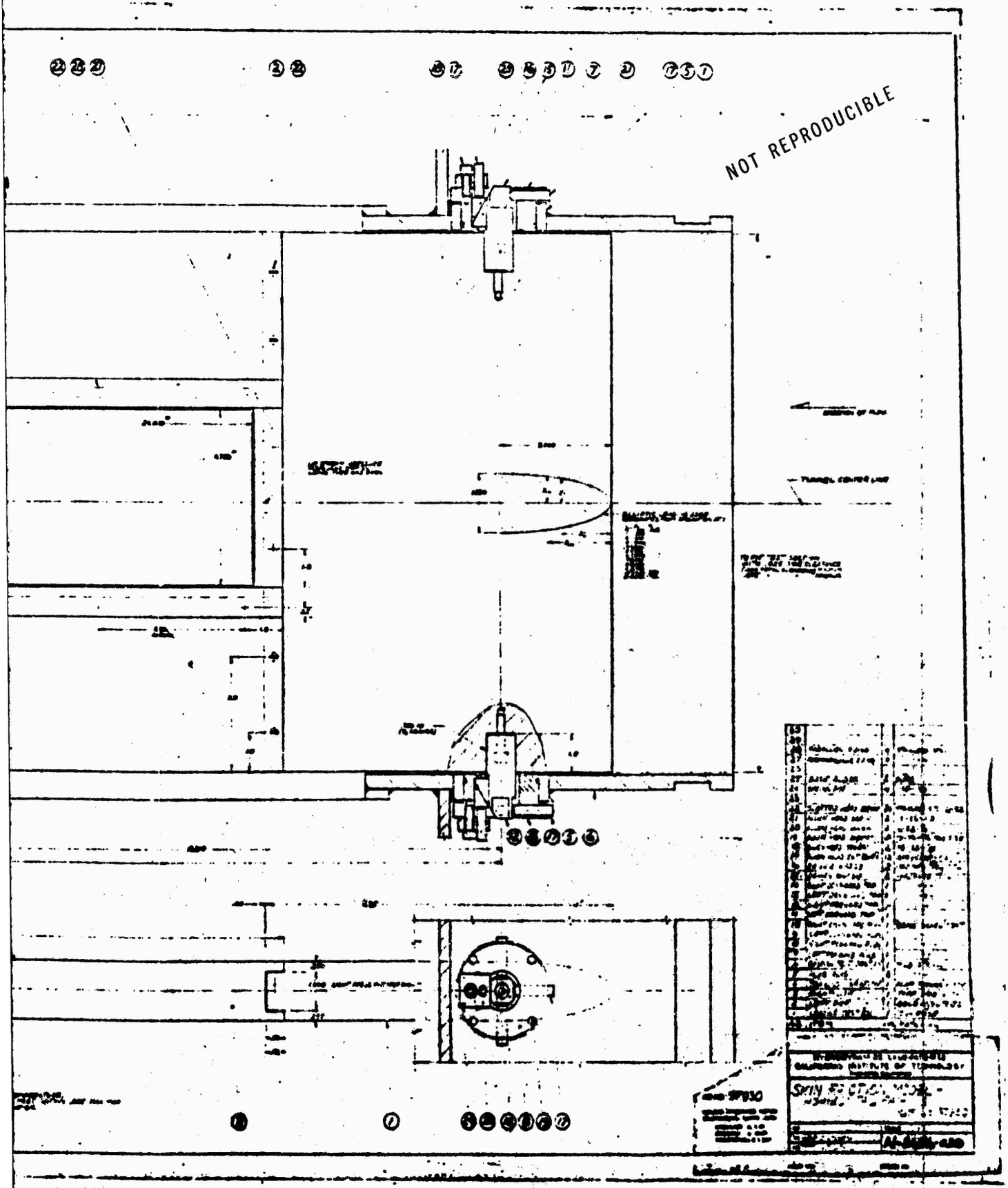
NOT REPRODUCIBLE

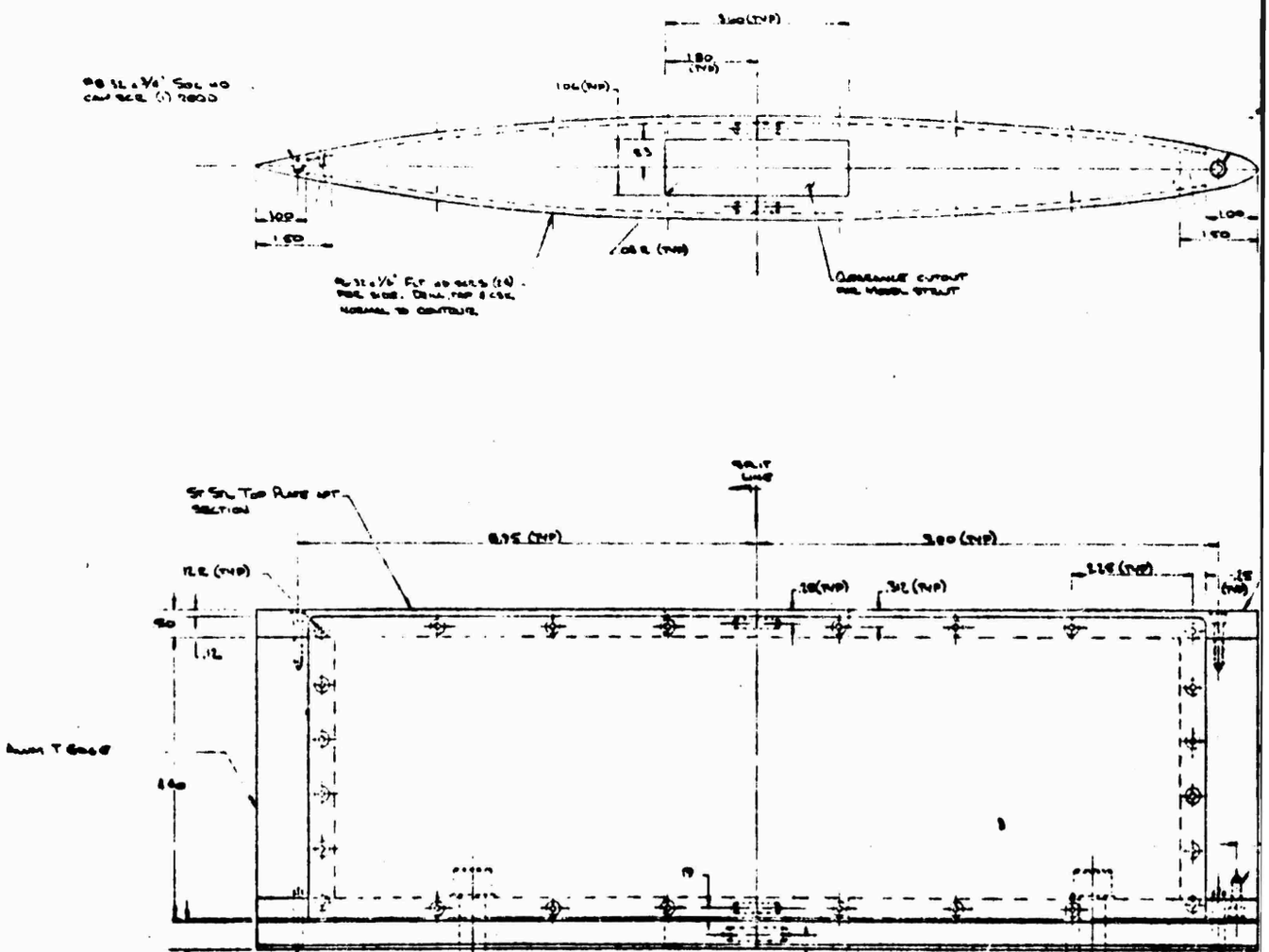

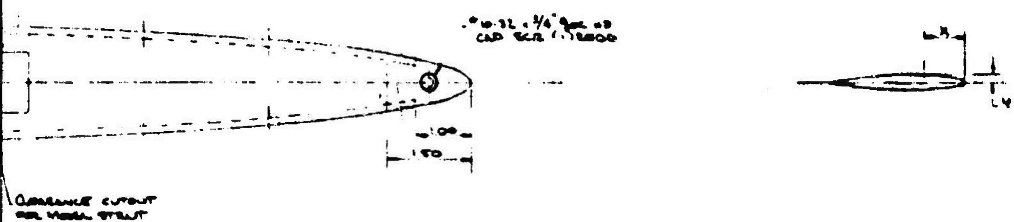

X	Y
[illegible]	[illegible]
0	0
.384	.210
.480	.293
.975	.407
1.463	[illegible]
1.950	.561
2.925	.671
3.900	.757
5.850	.879
7.800	.950
9.750	.976
11.700	[illegible]
13.650	[illegible]
[illegible]	[illegible]
[illegible]	[illegible]
[illegible]	[illegible]
[illegible]	[illegible]

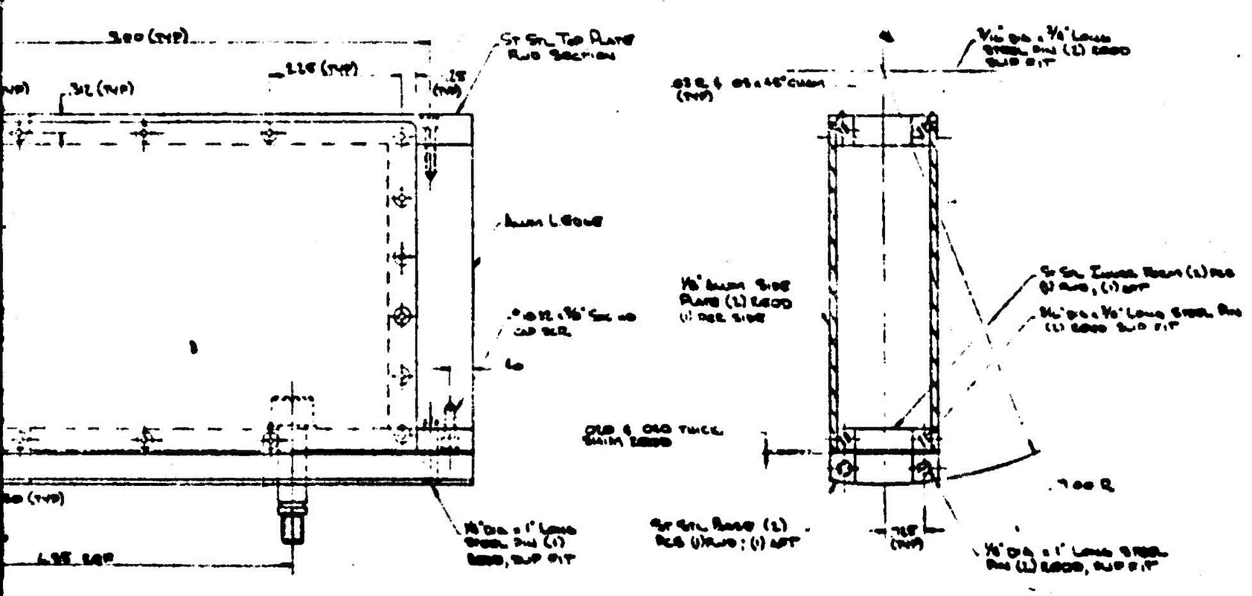

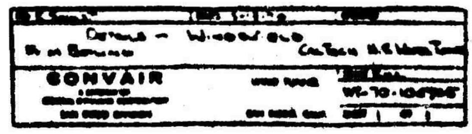

NOTE:

1. WHILE PH VI[illegible] MAX. GAP WITH [illegible] THICK MODEL.

2. USE WITH CONVAIR DWG. NO. WT-70-104705 DATED 3-19-70, NO CHANGES. DESIGNED TO MATE WITH CONVAIR DWG. NO. WT-70-104704 DATED 7-[illegible]-70, NO CHANGES.

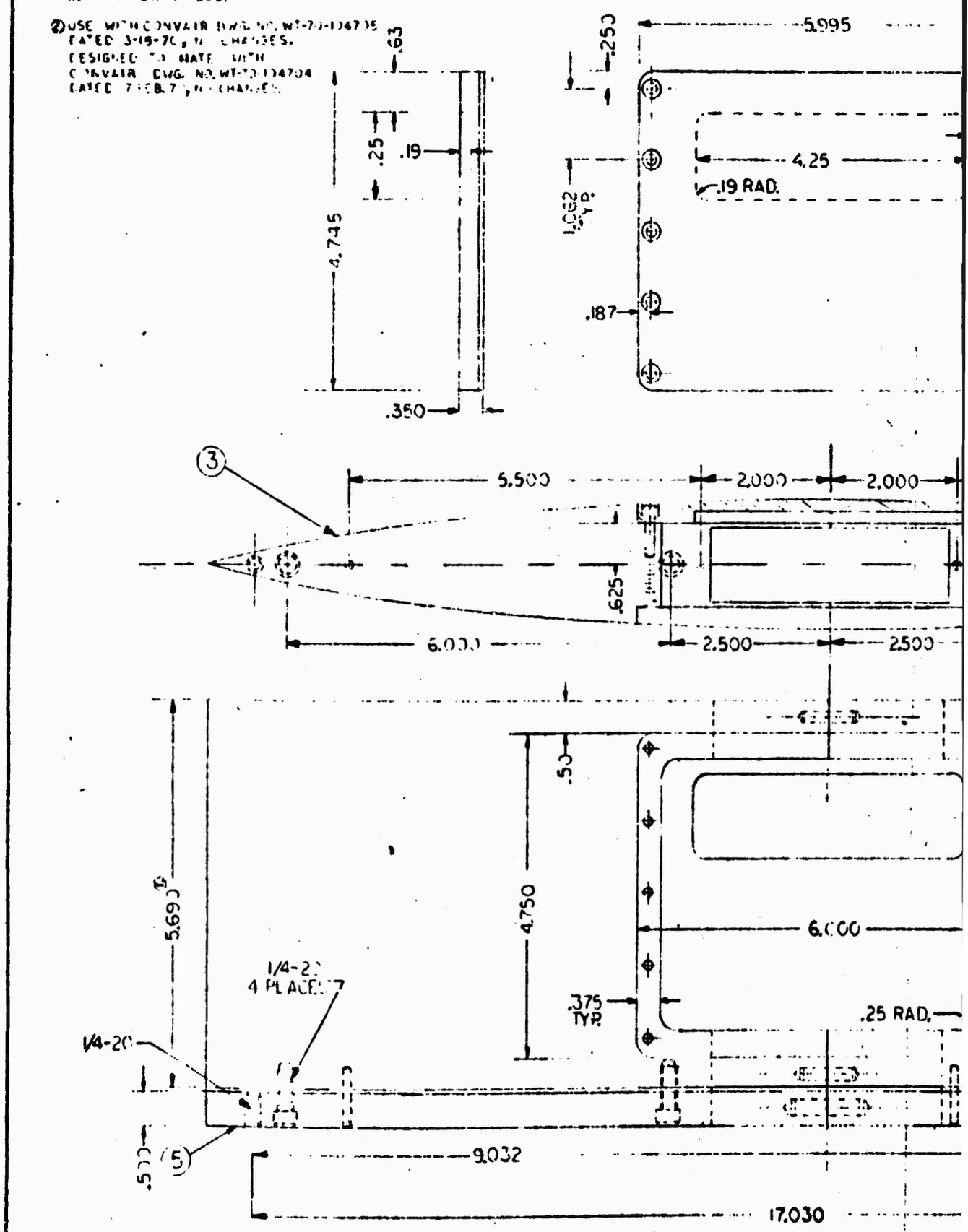

BILL OF MATERIAL

ITEM	NAME	REQ'D	MATERIAL	REMARKS
1	PLATE	2	ALUM.	
2	FWD. SECTION	1	ALUM.	
3	REAR SECTION	1	ALUM.	
4	FWD. BASE	1	ALUM.	
5	REAR BASE	1	ALUM.	
6	SHIM	2	ALUM.	.020 & .040
7	MTG. SCREW	2	STEEL	
8	BOLT	2	BRASS	

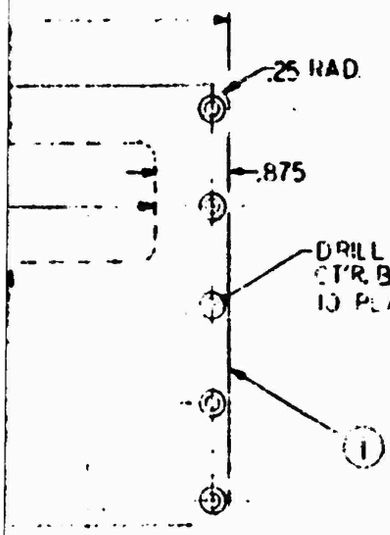

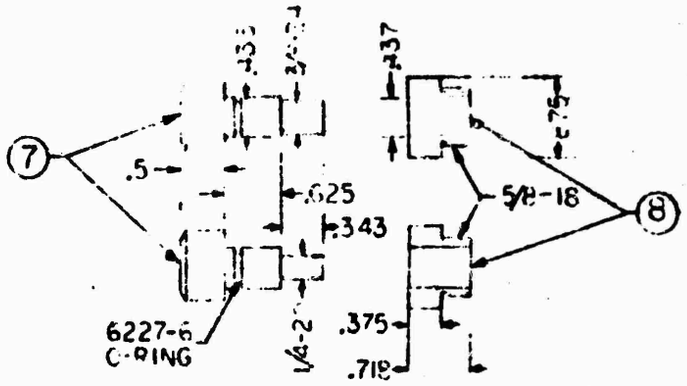

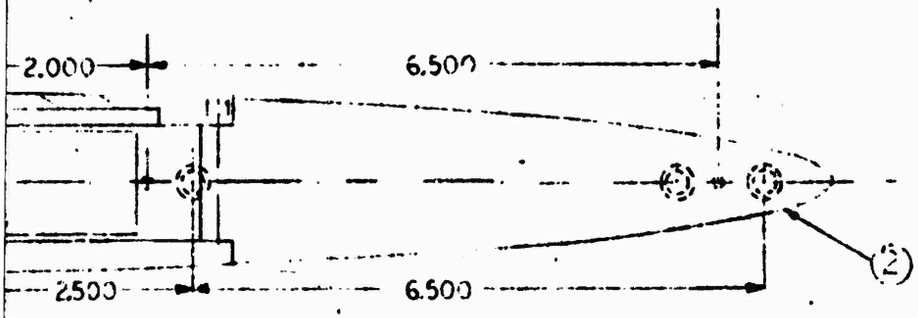

CHANGES

LTR	DESCRIPTION

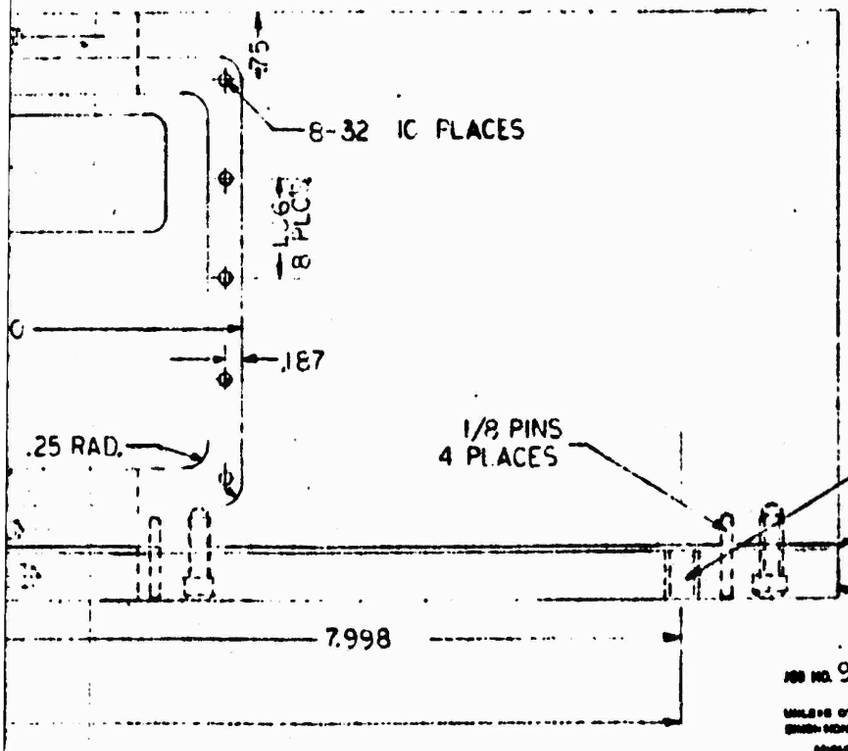

B

JOB NO. 97930

UNLESS OTHERWISE NOTED DIMENSIONAL LIMITS ARE:
ANGULAR ± 1/2°
DECIMAL ± .005"
FRACTIONAL ± 1/32"

HYDRODYNAMICS LABORATORIES
CALIFORNIA INSTITUTE OF TECHNOLOGY
PASADENA, CALIFORNIA

DETAILS-WINDSHIELD
FILM BOILING
1-JUNE-70

DR G.H.L.	SCALE FULL
CH T.W.	CONVAIR
AP T. WAHL	WT-70-104705 Y

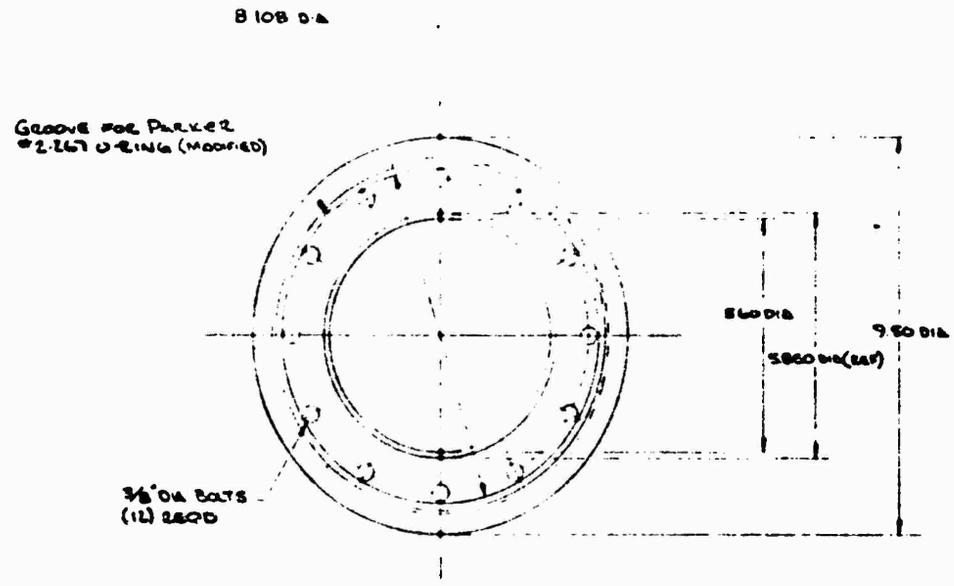

SECTION A-A

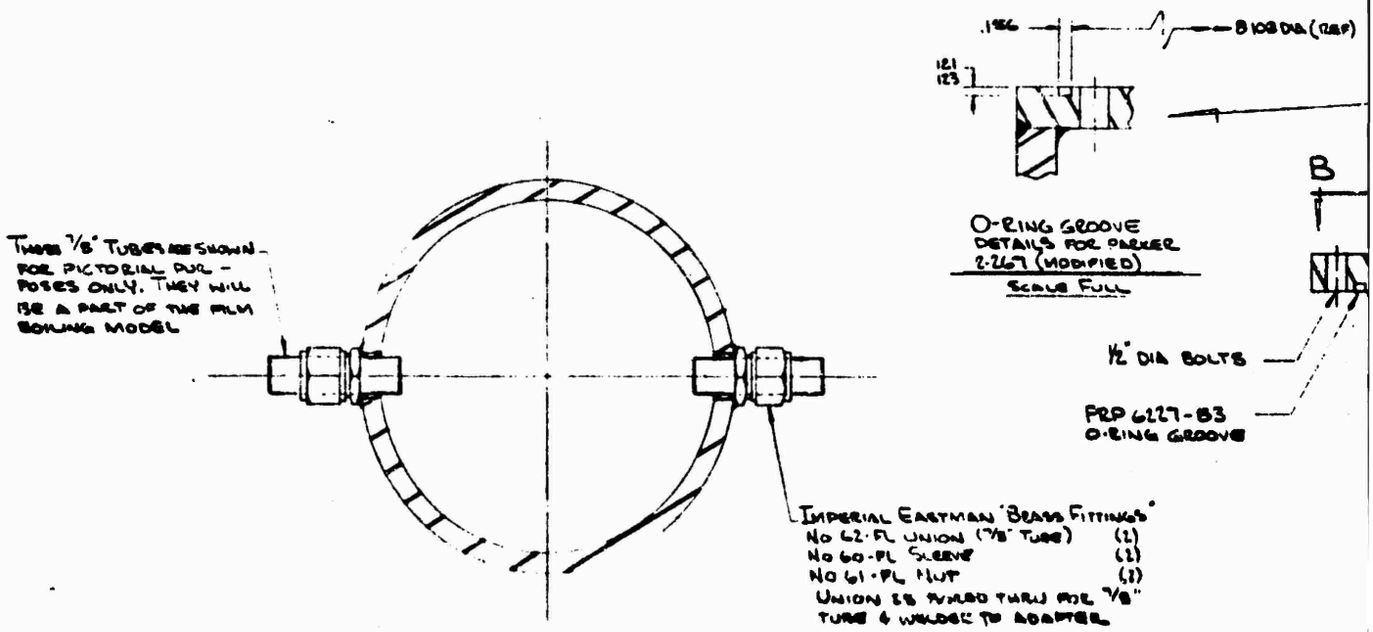

SECTION B-B

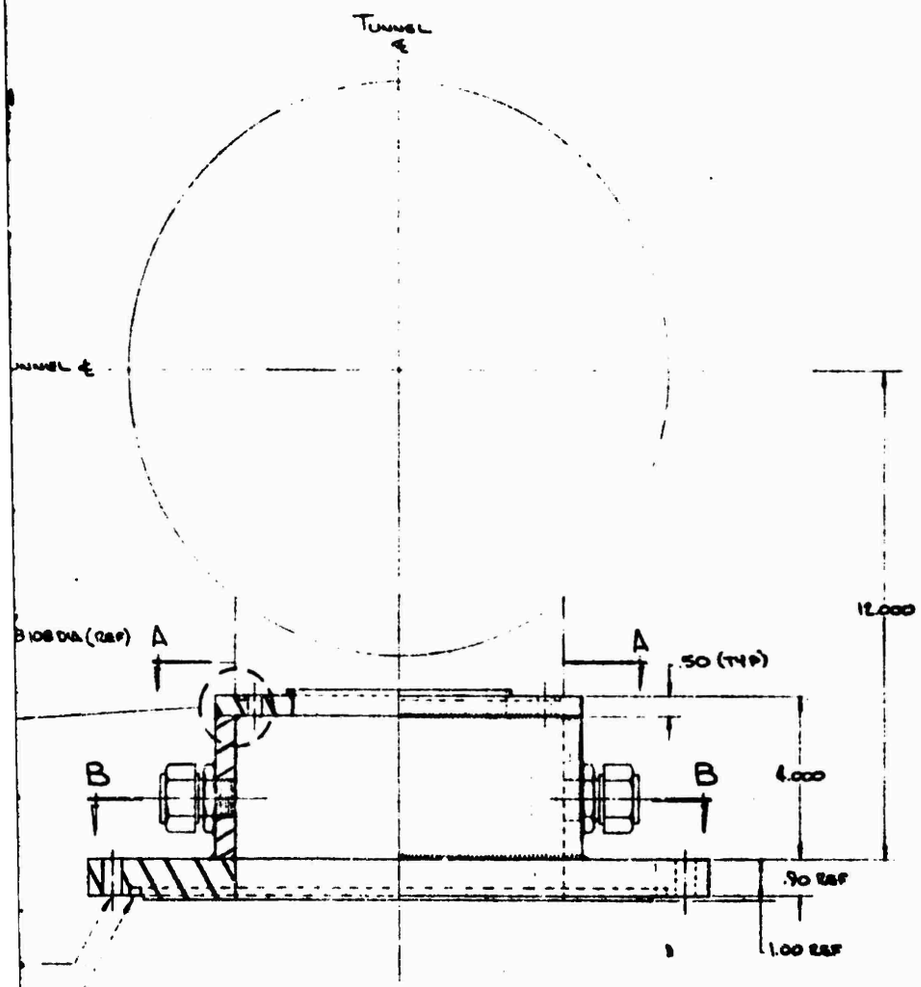

ADAPTER

B

BY P. SUNDSTT	DATE JAN 16 1978	CHECKED
ADAPTER CALTEC HI SPEED WATER TUNNEL		60IC FAB BUILDING
CONVAIR A DIVISION OF GENERAL DYNAMICS CORPORATION SAN DIEGO DIVISION	WIND TUNNEL SAN DIEGO, CALIF.	SCALE 3/4 NOTED WT-70-104701 SHEET 1 OF

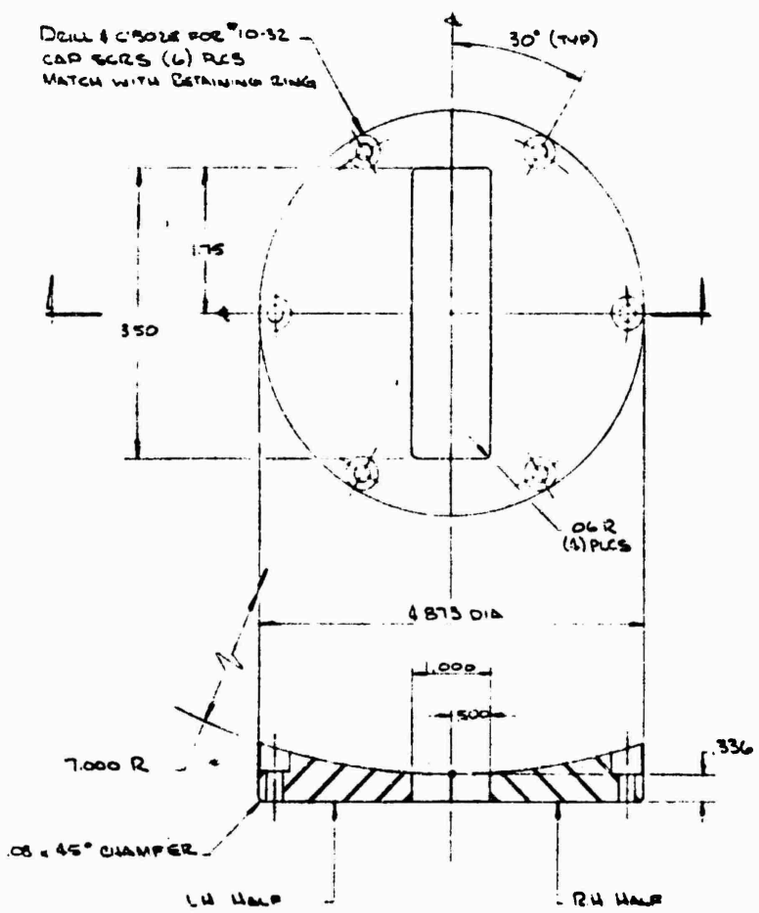

.250

DRILL & CBK FOR #10-24
FLT HD SCR (6) PLCS

#10-32 TAP THRU (6) PLCS

SHEILD SUPPORT

A

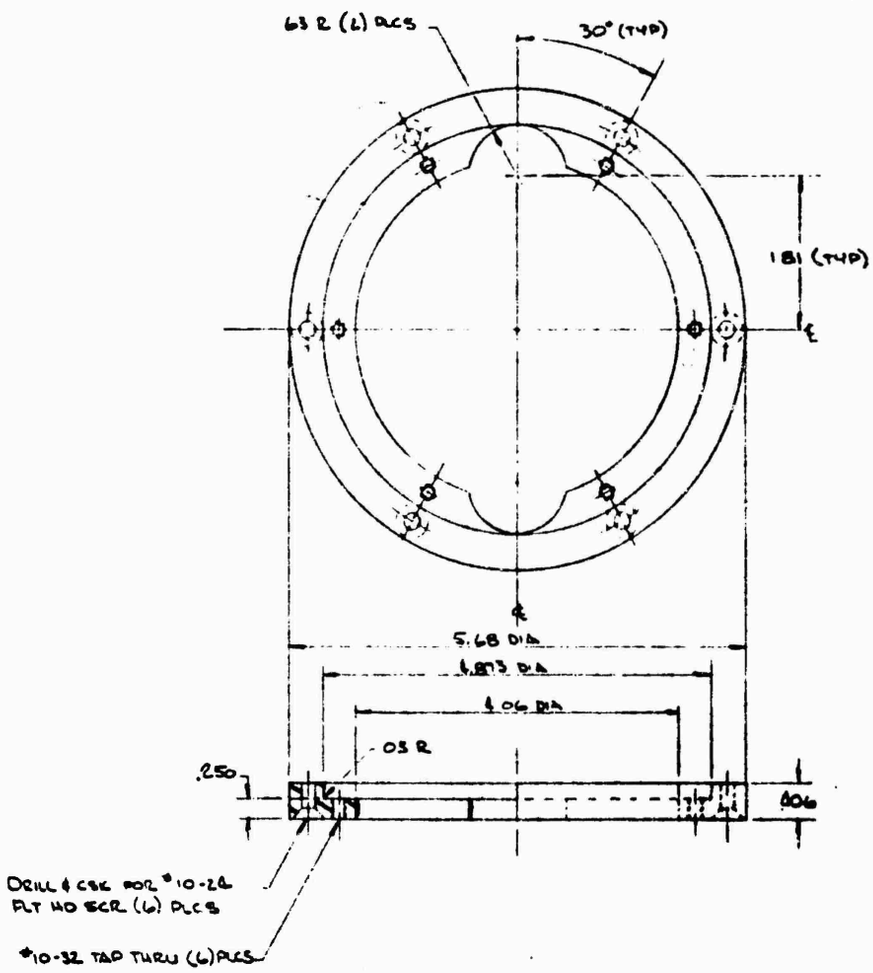

B

RETAINING RING

BY: F. Sinnett	DATE: June 10 1970	CHECKED
BALANCE SHIELD SUPPORT & RETAINING RING		
CALTEC Hi SPEED WATER TUNNEL		GD/C RUM BOILING
CONVAIR A DIVISION OF GENERAL DYNAMICS CORPORATION SAN DIEGO DIVISION	WIND TUNNEL SAN DIEGO, CALIF.	SCALE FULL WT-70-104702 SHEET 8 OF